

Mauro Sereno

INAF-OAS, Room 4E1 (Battiferro)

mauro.sereno@inaf.it

Galaxy clusters as cosmological probes

Lesson outline

Part 1: origin story

Formation and evolution of a cluster

How does a cluster look like? GL, SZE, X-ray, radio

Perturbation growth and spherical collapse

Self-similar model

Thermodynamic processes

The halo mass function

The halo bias

Part 2: the quest

Detection and calibration of large samples

Multi-wavelength surveys

Detection algorithms

Scaling relations

Mass calibration

Part 3: the final battle

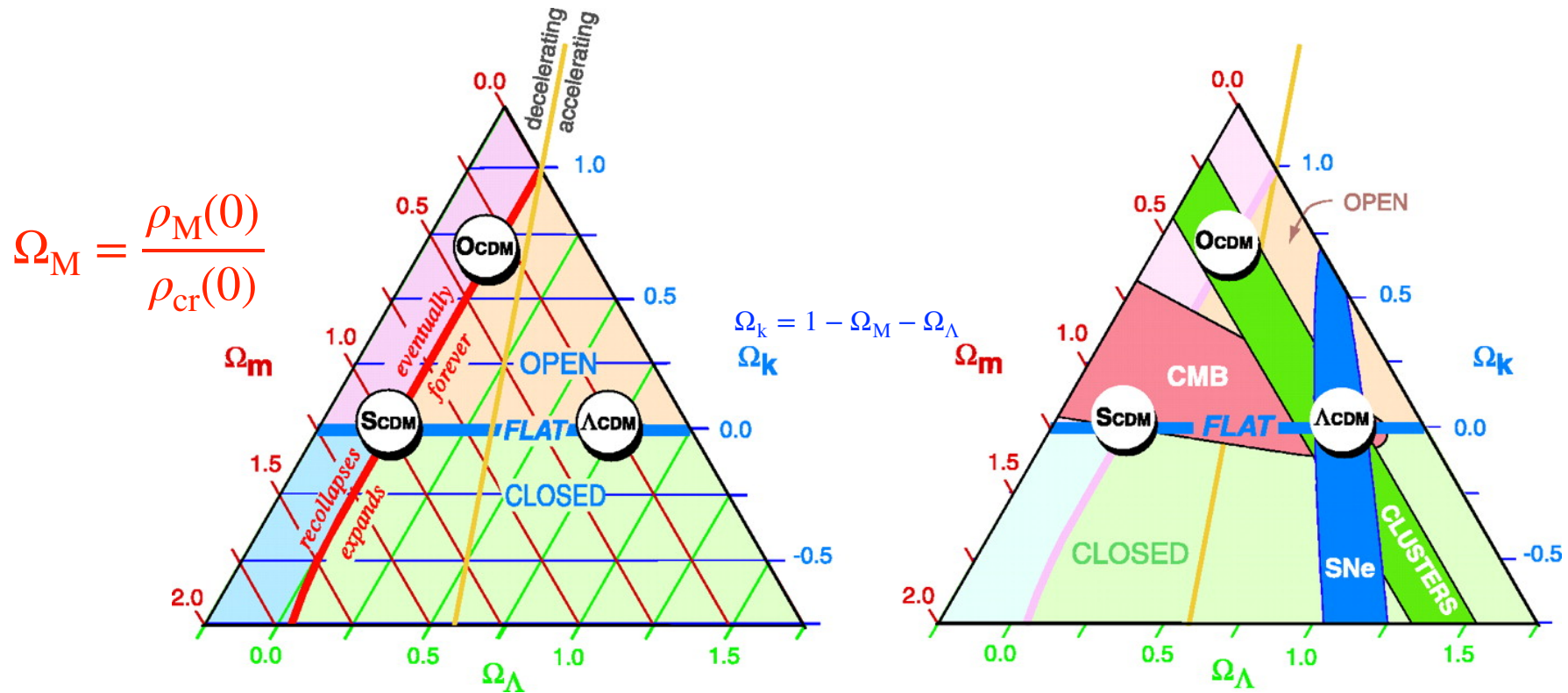
Cosmological tests with clusters

Tests with statistical samples (number counts, sparsity, clustering)

Tests with individual halos (baryonic fraction, XSZ distance, SL,)

Topics not covered in detail

The cosmic triangle



[Bahcall+1999Sci...284.1481B]

LCDM

$$\rho_{cr} = \frac{3H^2(z)}{8\pi G}$$

$$H(z) = H_0 \sqrt{\Omega_M(1+z)^3 + \Omega_\Lambda + \Omega_k(1+z)^2}$$

$$\Omega_{Mz} = \frac{\Omega_M(1+z)^3}{\Omega_M(1+z)^3 + \Omega_\Lambda + \Omega_k(1+z)^2}$$

$$\Omega_{\Lambda z} = \frac{\rho_\Lambda}{\rho_{cr}} = \frac{\Lambda}{3H^2(z)}$$

$$\Omega_{\Lambda z} = \frac{\Omega_M(1+z)^3}{\Omega_M(1+z)^3 + \Omega_\Lambda + \Omega_k(1+z)^2}$$

Virial theorem vs light: dunkle (kalte) Materie

Die Rotverschiebung von extragalaktischen Nebeln

von F. Zwicky.

(16. II. 33.)

Inhaltsangabe. Diese Arbeit gibt eine Darstellung der wesentlichsten Merkmale extragalaktischer Nebel, sowie der Methoden, welche zur Erforschung derselben gedient haben. Insbesondere wird die sog. Rotverschiebung extragalaktischer Nebel eingehend diskutiert. Verschiedene Theorien, welche zur Erklärung dieses wichtigen Phänomens aufgestellt worden sind, werden kurz besprochen. Schliesslich wird angedeutet, inwiefern die Rotverschiebung für das Studium der durchdringenden Strahlung von Wichtigkeit zu werden verspricht.

§ 1. Einleitung.

Es ist schon seit langer Zeit bekannt, dass es im Weltraum gewisse Objekte gibt, welche, wenn mit kleinen Teleskopen beobachtet, als stark verschwommene, selbstleuchtende Flecke erscheinen. Diese Objekte besitzen verschiedenartige Strukturen. Oft sind sie kugelförmig, oft elliptisch, und viele unter ihnen haben ein spiralartiges Aussehen, weshalb man sie gelegentlich als Spiralnebel bezeichnet. Dank des enormen Auflösungsvermögens der modernen Riesenteleskope gelang es, festzustellen, dass diese Nebel ausserhalb der Grenzen unseres eigenen Milchstrassensystems liegen. Aufnahmen, die mit dem Hundert-Zoll-Teleskop auf dem Mt. Wilson gemacht worden sind, offenbaren, dass diese Nebel Sternsysteme sind, ähnlich unserem eigenen Milchstrassensystem. Die extragalaktischen Nebel sind im grossen und ganzen gleichförmig über den Himmel und, wie gezeigt werden konnte, auch gleichförmig über den Weltraum verteilt. Sie treten als einzelne Individuen auf oder gruppieren sich zu Haufen. Die folgenden Zeilen beabsichtigen einen kurzen Abriss der wichtigeren Merkmale und eine Beschreibung der Methoden, welche es möglich gemacht haben, diese Merkmale zu fixieren.

§ 2. Entfernungen und allgemeine Merkmale extragalaktischer Nebel.

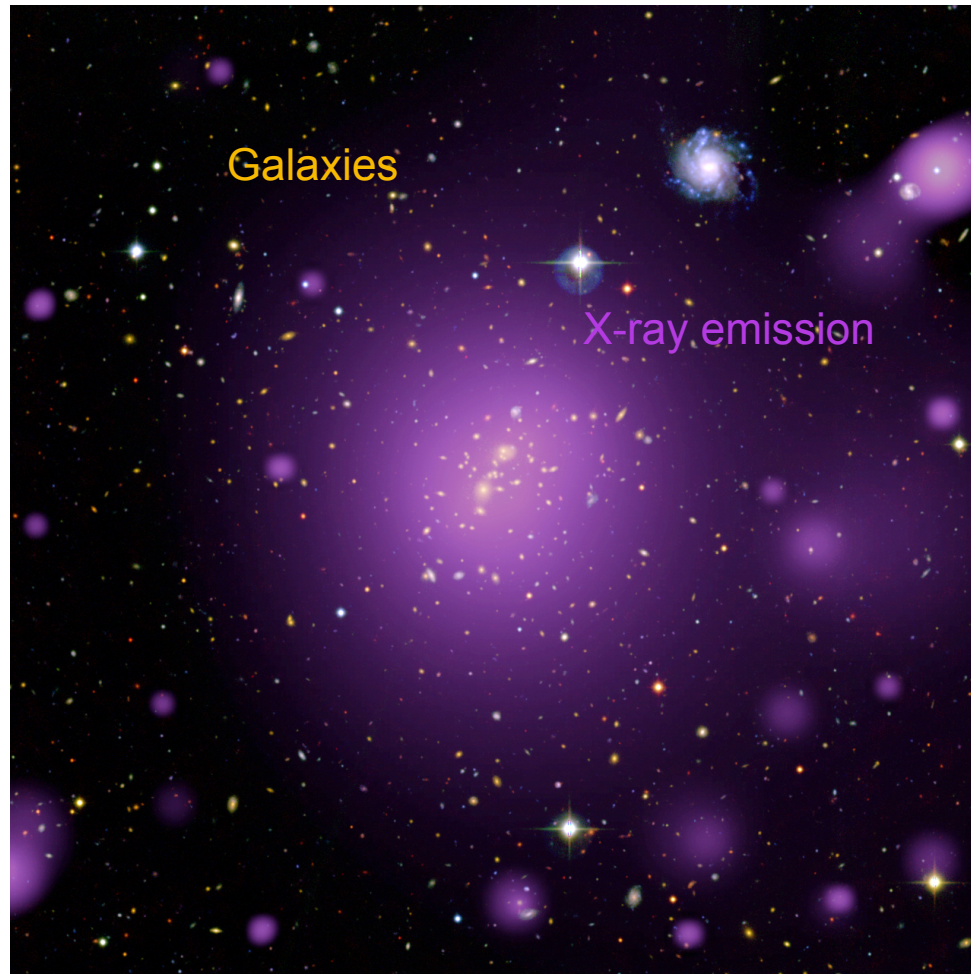
Wie schon erwähnt, gelingt es, mit Hilfe der modernen Teleskope eine ganze Anzahl von Nebeln ganz oder teilweise in einzelne Sterne aufzulösen. Im grossen Nebel in Andromeda z. B. sind eine grosse Zahl von individuellen Sternen beobachtet worden.

"From these considerations it follows that the large velocity dispersion in Coma (and in other clusters of galaxies) represents an unsolved problem."

"It is, of course, possible that luminous plus dark (cold) matter [dunkle (kalte) Materie] together yield a significantly higher density..."

[Zwicky33, translation by S. van der Bergh 99]

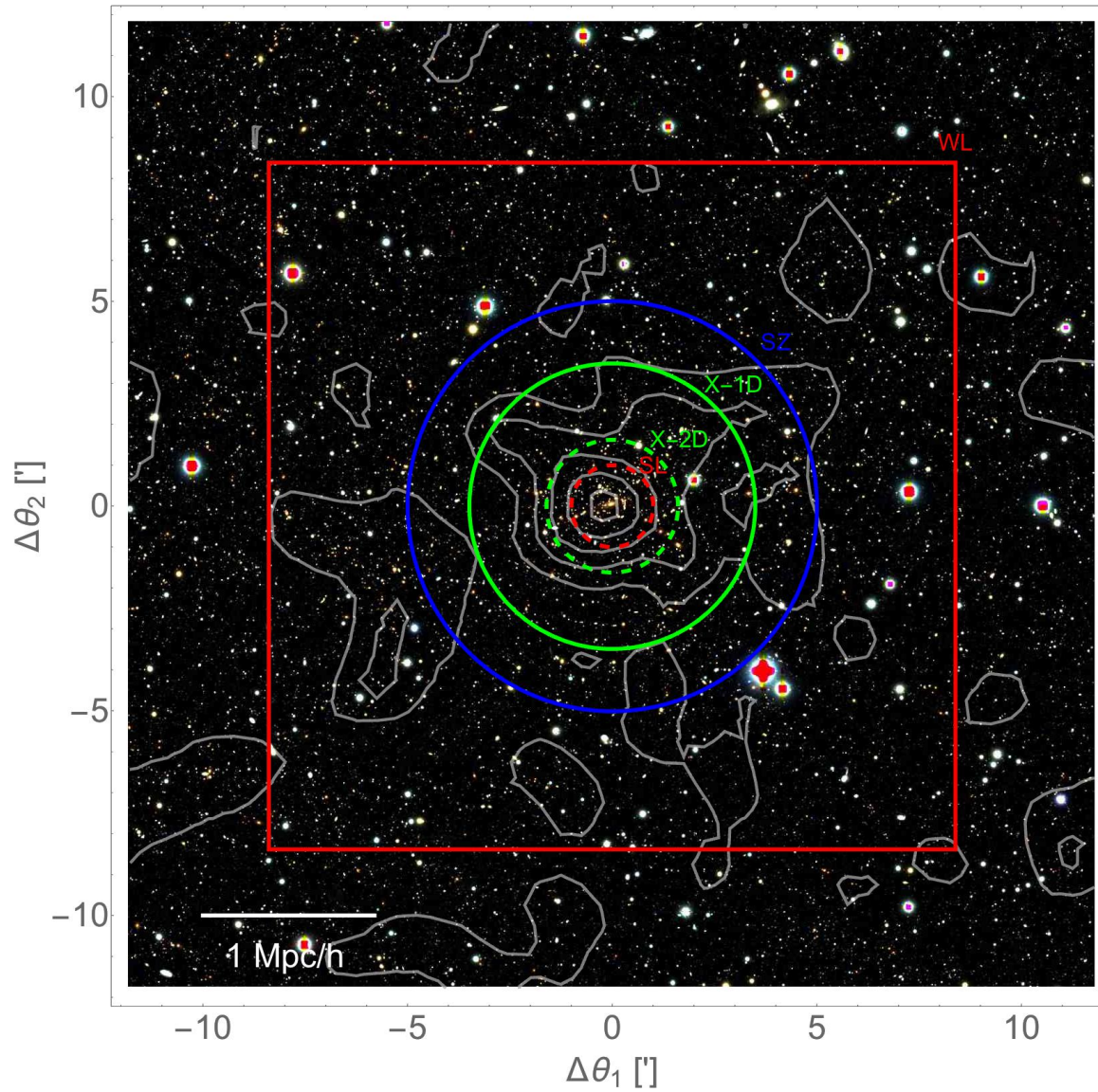
Galaxy clusters



- ~80% Dark matter
- ~18% Intra-cluster medium (thermal or non thermal)
- ~ 2% Galaxies and intra-cluster light
- ~ 0% dark energy
- ~ 0% neutrinos

Multi-wavelength view of galaxy cluster XLSSC006. Credit: ESA/XMM-Newton (X-rays); CFHT (optical); XXL Survey

Signals



MACS1206

Subaru BVRc colour image

SL: dashed red circle at 1' for SL

WL: red square of semi-size 2Mpc/h $\sim 8.39'$

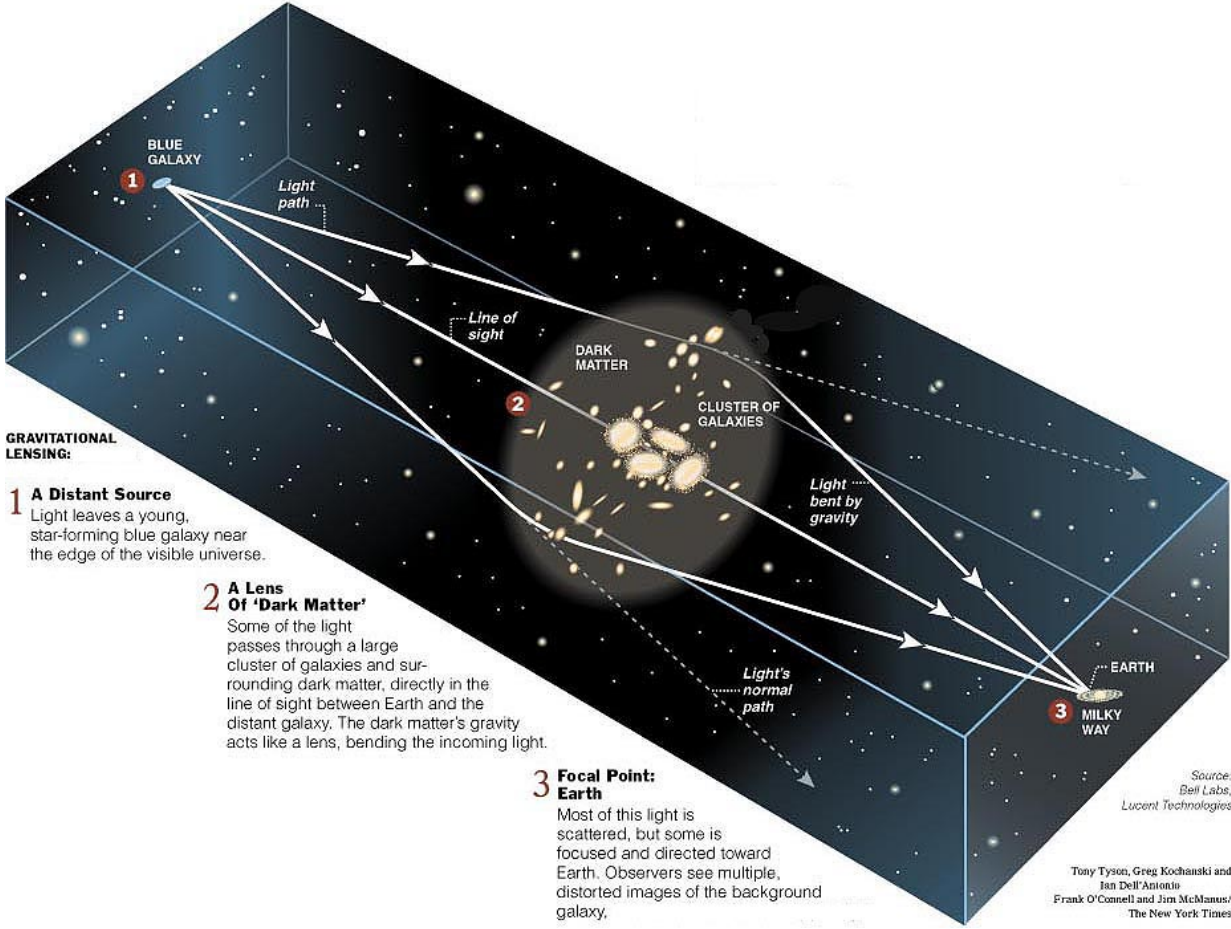
X-ray 2D, dashed green circle at $\theta_{80\%} = 1.61'$ and $3.49'$

X-ray 1D, full green circles at $3.49'$

SZe, the blue circle at $5'$

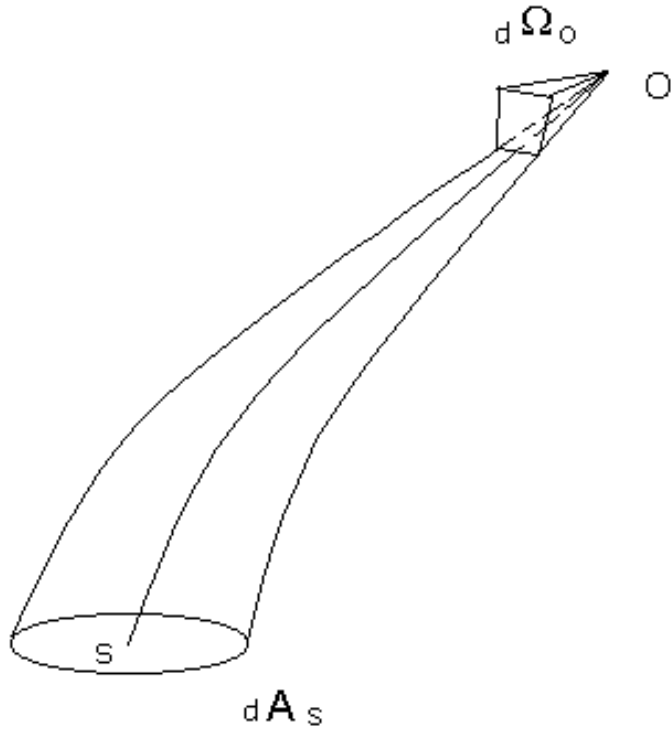
[Sereno+[2017MNRAS.467.3801+17](#)]

Gravitational lensing systems



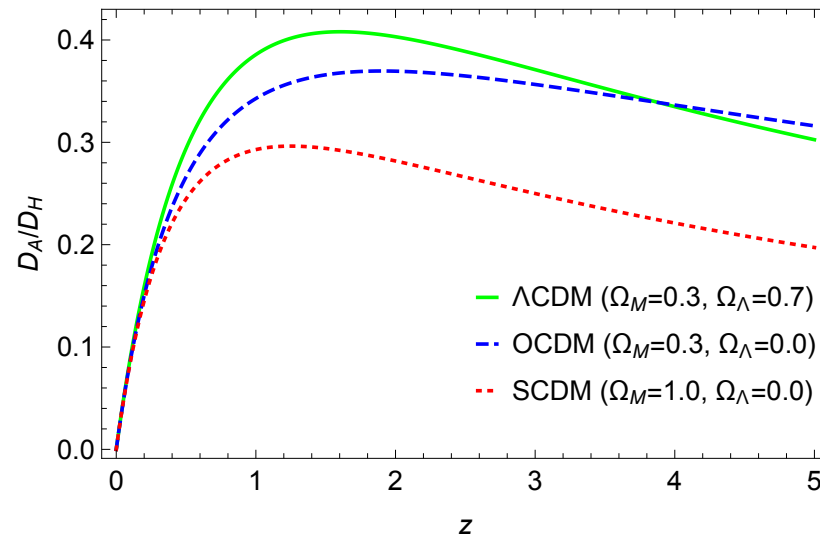
Angular diameter distance

by definition, the size of the rod over the subtended angle



$$D_A \equiv \left(\frac{dA_s}{d\Omega_O} \right)^{1/2}$$

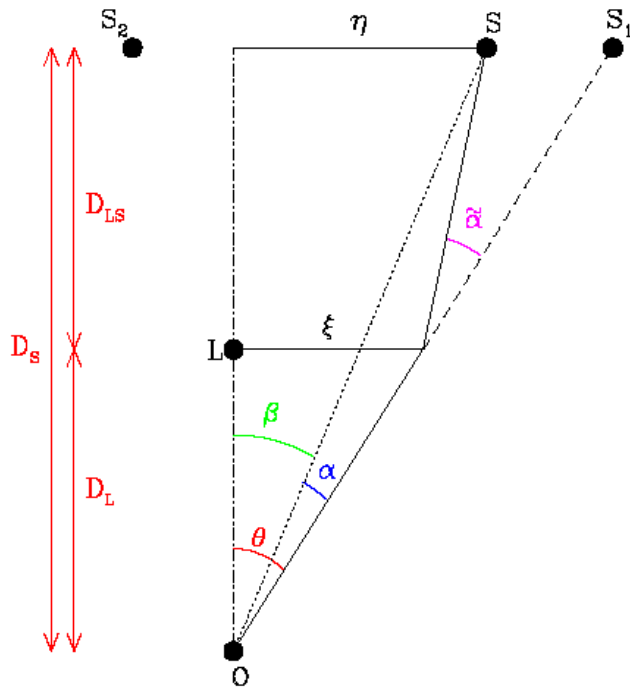
$$D_{ds} = \frac{c}{H_0} \frac{1}{1+z_s} \frac{1}{|\Omega_k|^{1/2}} \text{sinn} \left\{ |\Omega_k|^{1/2} \int_{z_d}^{z_s} \frac{H_0}{H(z)} dz \right\}$$



GL equation

GL by clusters can distort and magnify the signal from background sources

The form of the lens equation can be derived from simple geometric considerations



$$D_s \theta = D_s \beta + D_{ds} \tilde{\alpha}$$

$$\beta = \theta - \frac{D_{ds}}{D_s} \tilde{\alpha}(\theta)$$

$$\tilde{\alpha}(\theta) = \frac{4GM_{\text{cyl}}(< \theta)}{c^2 D_d \theta}$$

The expression for the deflection angle needs a theory of gravity

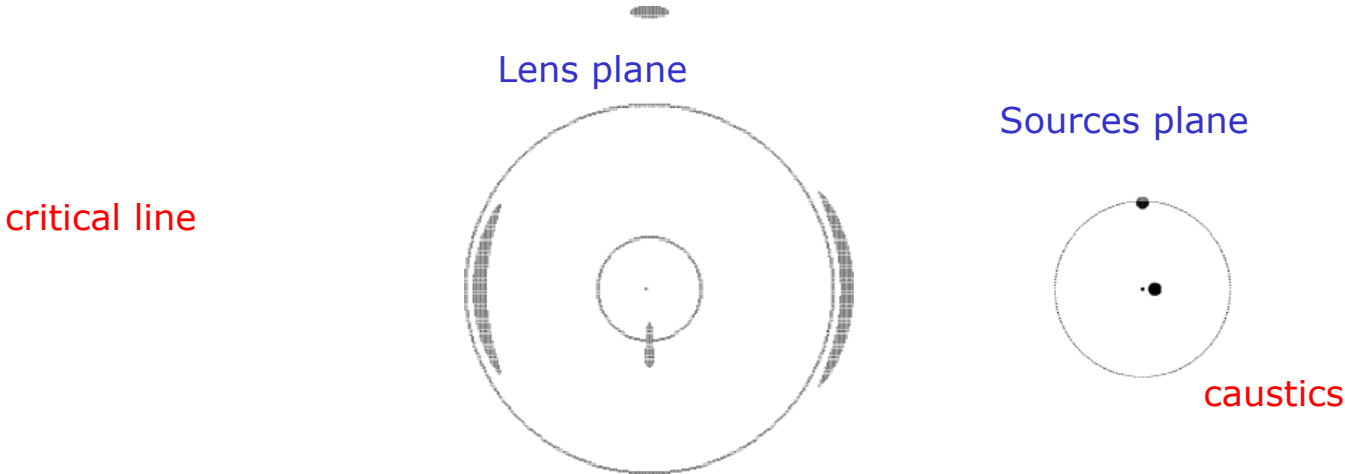
The *Einstein ring* (i.e. the tangential critical circle for $\beta = 0$, $\theta = \theta_E$) forms at

$$\theta_E = \sqrt{\frac{4GM}{c^2} \frac{D_{LS}}{D_L D_S}} \approx 2 \sqrt{M / 10^{12} M_\odot} \text{ arcsec}$$

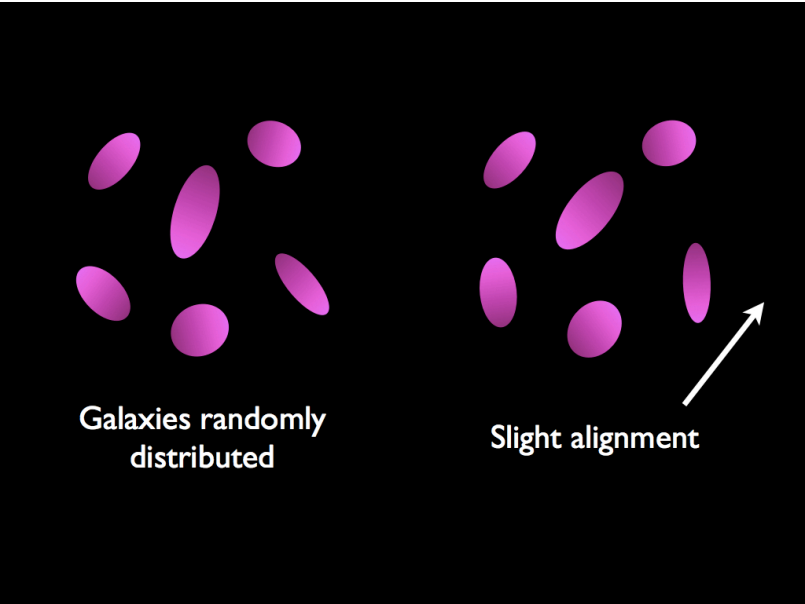
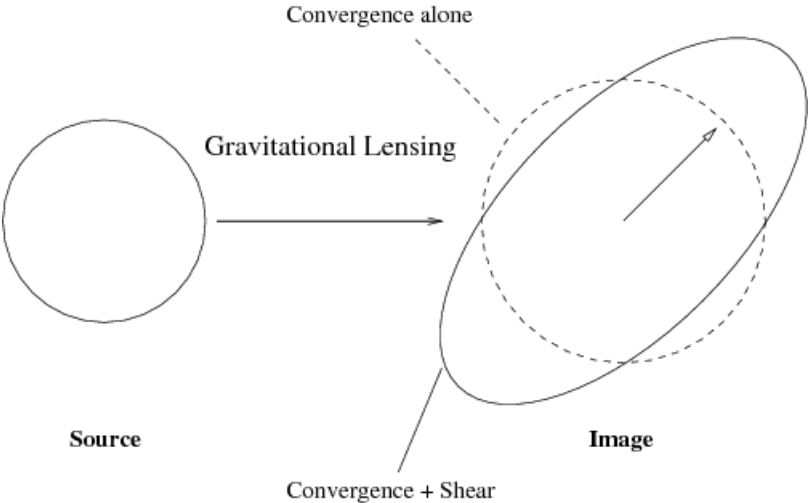
GL regimes

GL by clusters can distort and magnify the signal from background sources

Strong lensing

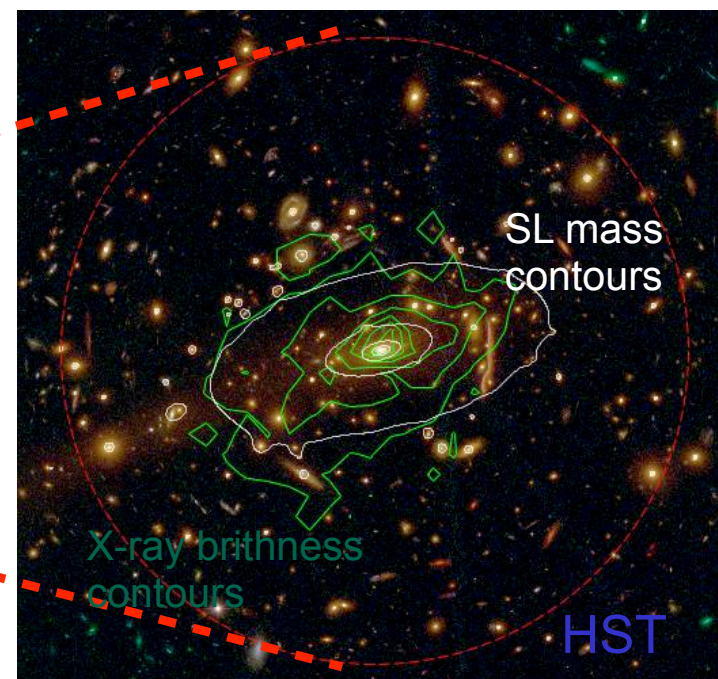
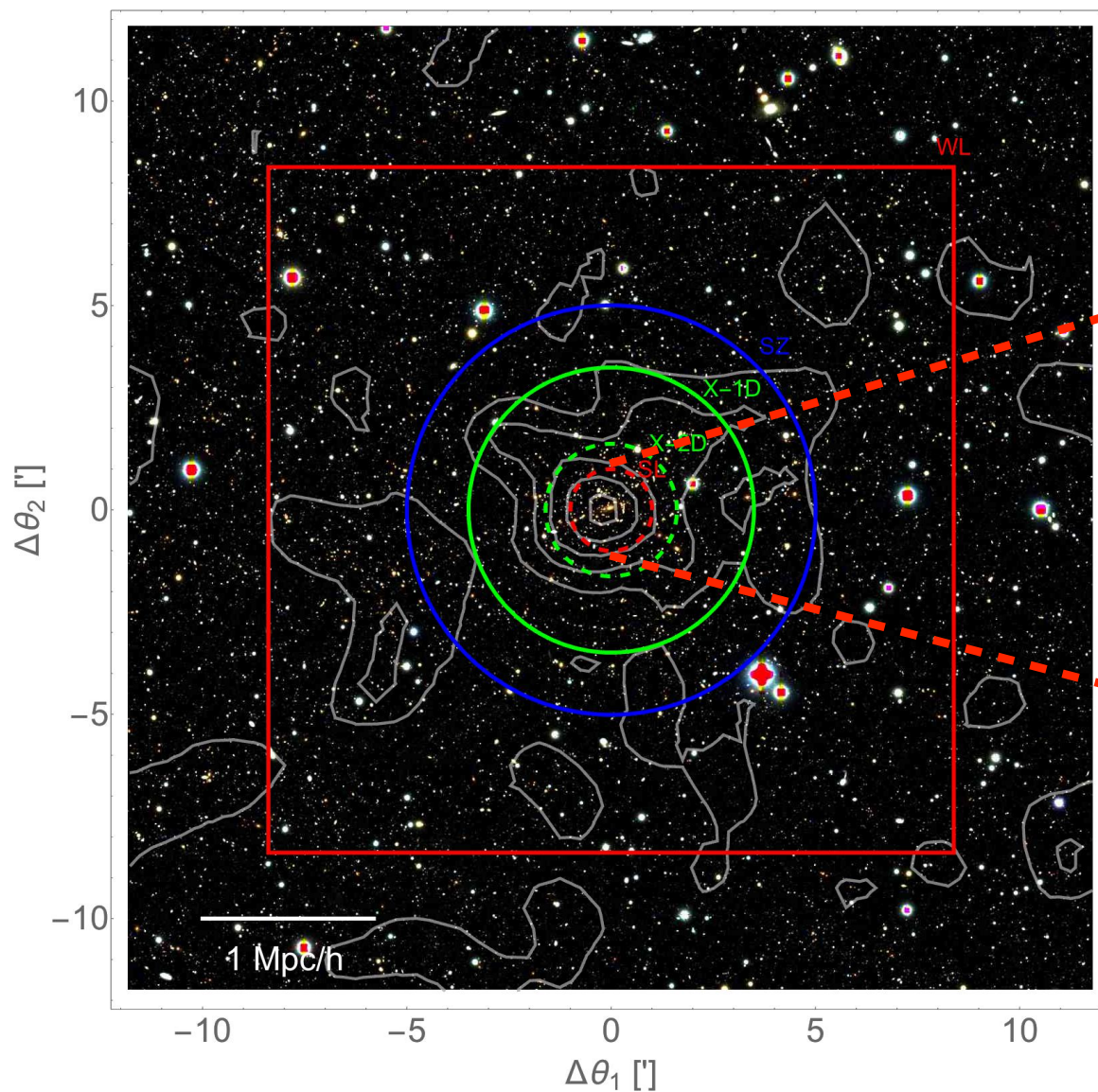


Weak lensing



Strong Lensing

Strong lensing. Halo potential distorts background galaxies. GL measures the projected mass/potential



Subaru BVRc composite colour images of MACS1206 [MS+17]

SL: dashed red circle at $1'$ for SL

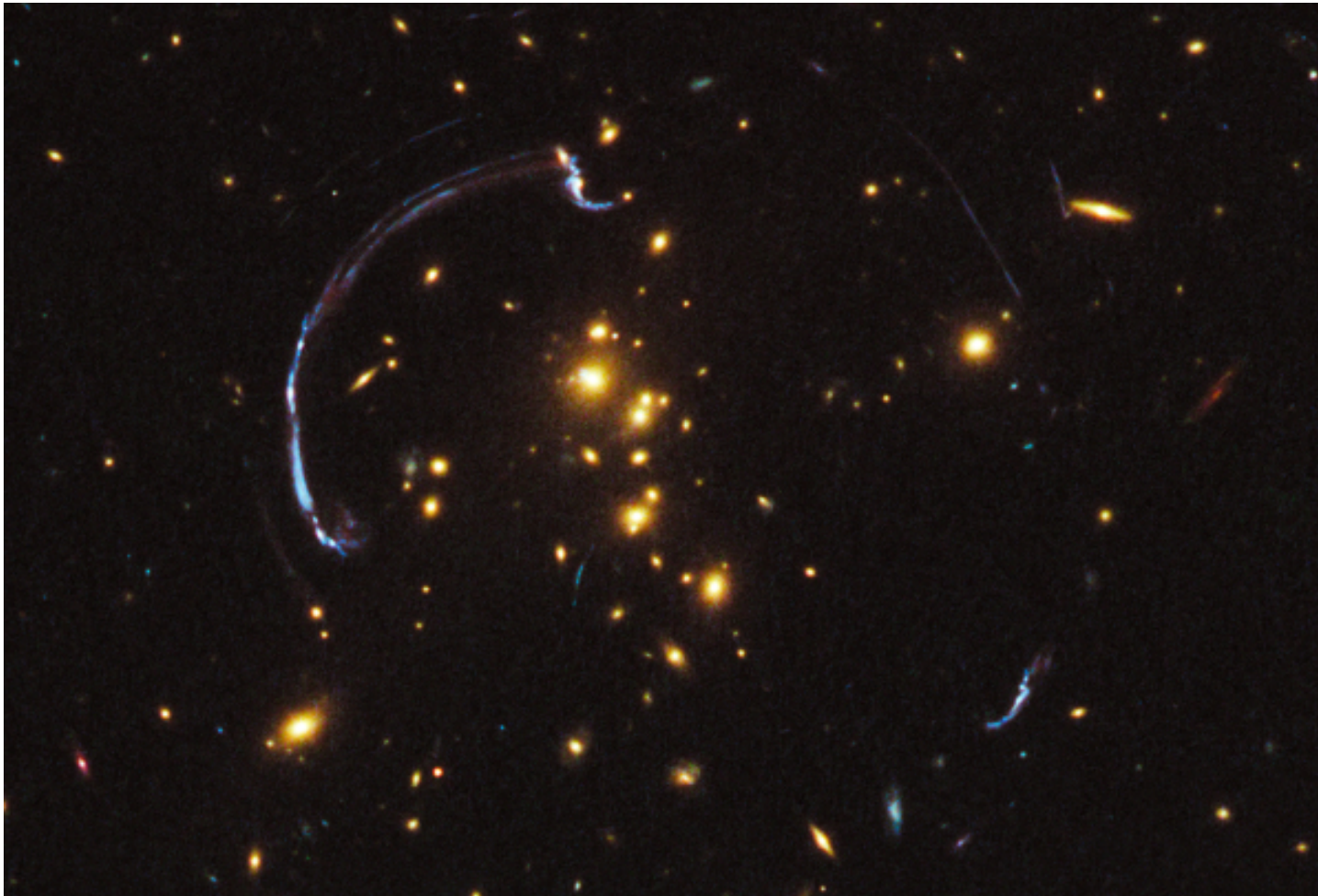
WL: red square of semi-size $2 \text{ Mpc}/h \sim 8.39'$

X-ray 2D, dashed green circle at $0.80 \times 3.49' = 1.61'$ and $3.49'$

X-ray 1D, full green circles at $3.49'$

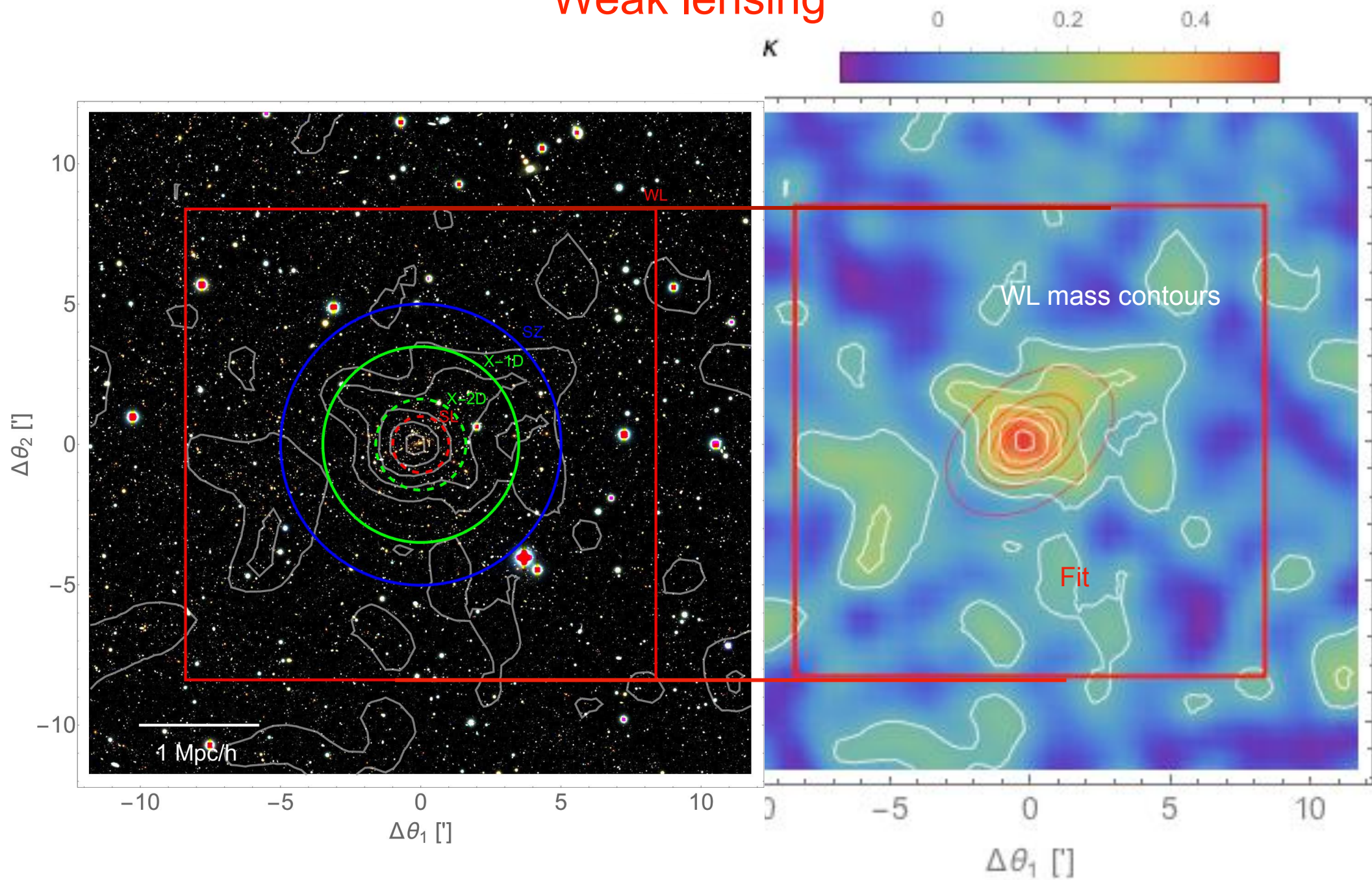
SZe, the blue circle at $5'$

Giant arcs



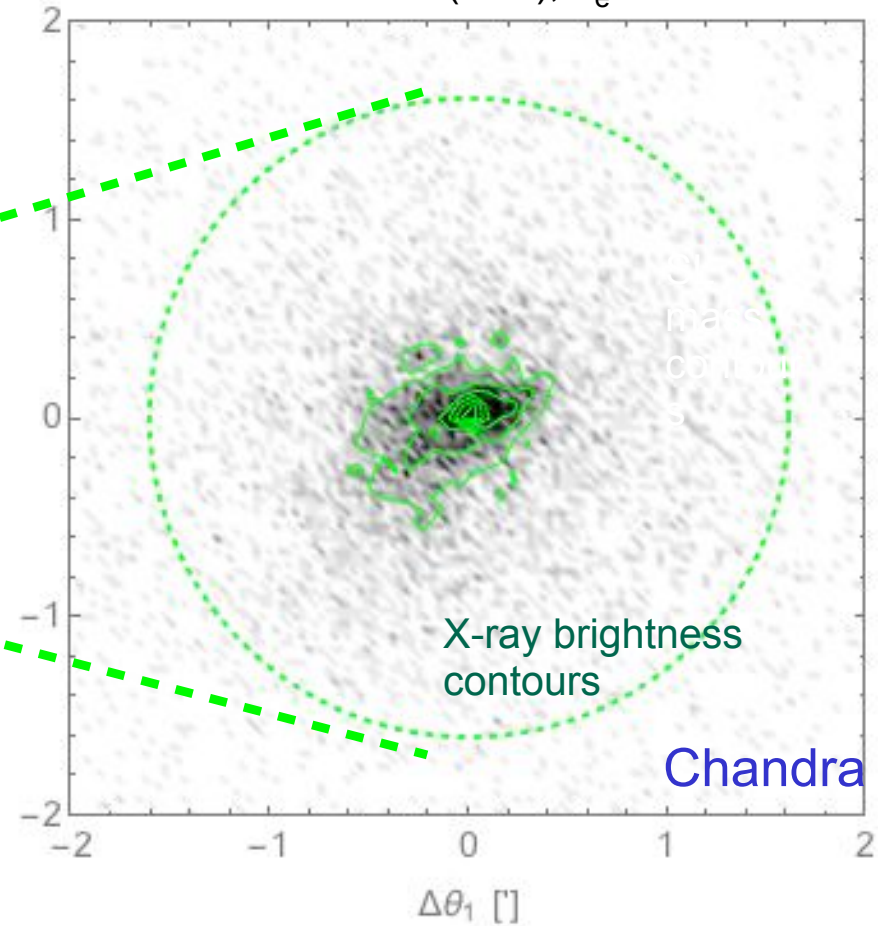
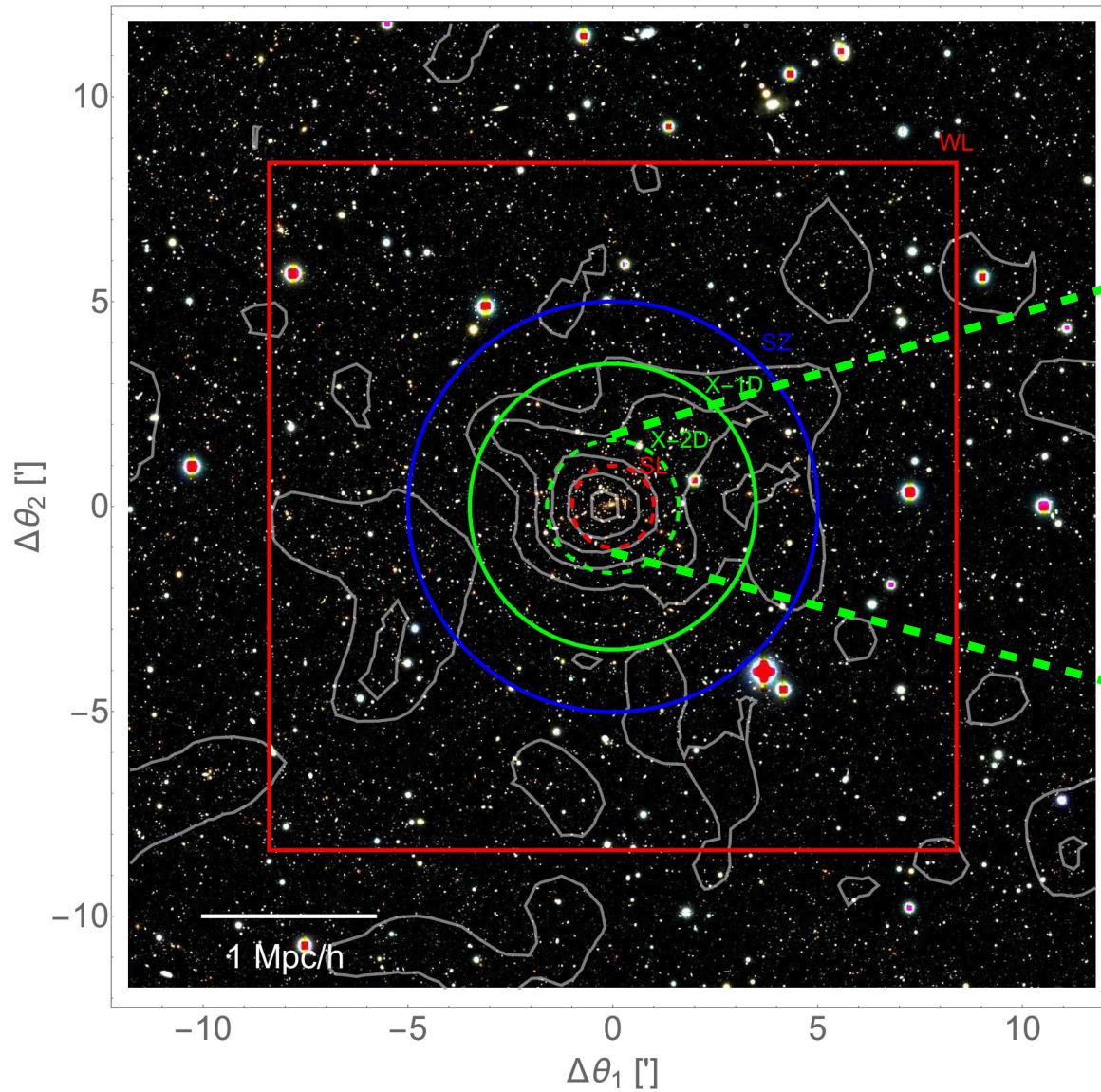
The view of a distant galaxy (nearly 10 billion light-years away) has been warped into a nearly 90-degree arc of light by the gravity of the frontier field galaxy cluster RCS2 032727-132623 (about 5 billion light-years away) [NASA, ESA, J. Rigby (NASA GSFC), K. Sharon (KICP, U Chicago), and M. Gladders and E. Wuyts (U Chicago).]

Weak lensing



X-ray observations

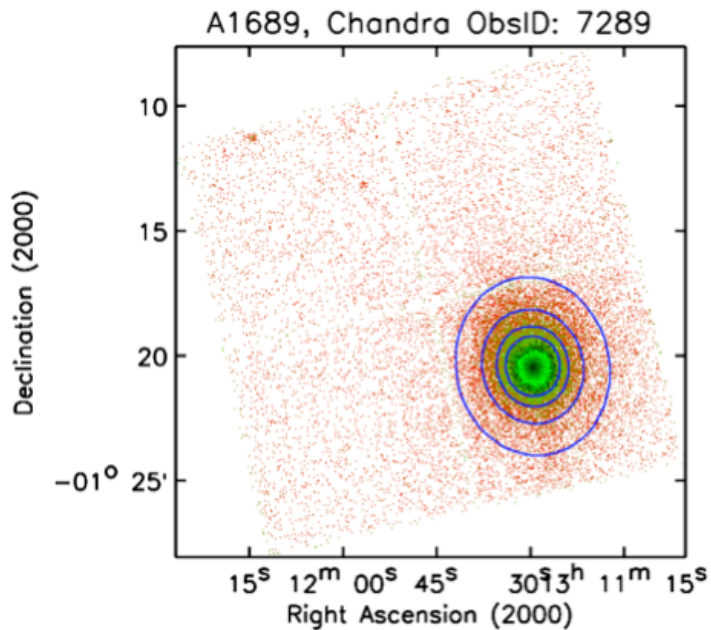
X-ray emission mainly due to bremsstrahlung from electron-ion collisions in the multimillion-degree intracluster medium (ICM), n_e .



X-ray emission

X-ray luminosity [Reese+2010ApJ...721..653R]

$$\frac{dL_X}{dE dV} = n_e^2 \lambda(E, T, Z) \quad \lambda \text{ photon emissivity at energy } E$$



Surface brightness in a given energy band [erg/s/cm²/arcmin²]

$$S_X(\Delta E) = \frac{1}{4\pi(1+z)^4} \int_{\text{l.o.s.}} n_e^2 \Lambda_{eH}(T, Z) dl$$

$\Lambda(T, z)$ is the emissivity in the considered energy band,

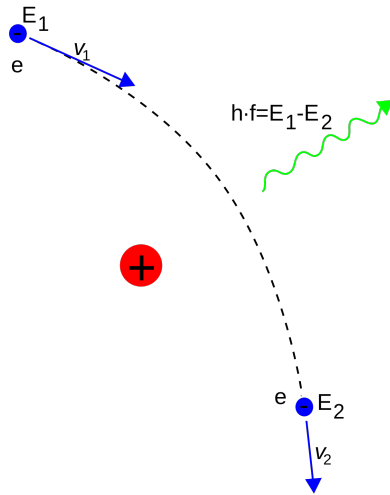
$$\Lambda_{eH}(T, Z) = \int_{\Delta E} \lambda_e(E_{\text{source}}, T, Z) dE_{\text{source}}$$

[Serenio+2012MNRAS.419.2646S]

Bremsstrahlung

Bremsstrahlung (from *bremsen* "to brake" and *Strahlung* "radiation") or **braking radiation** or "deceleration radiation", is electromagnetic radiation produced by the deceleration of a charged particle when deflected by another charged particle,

Bremsstrahlung emitted from plasma is sometimes referred to as **free-free radiation**.

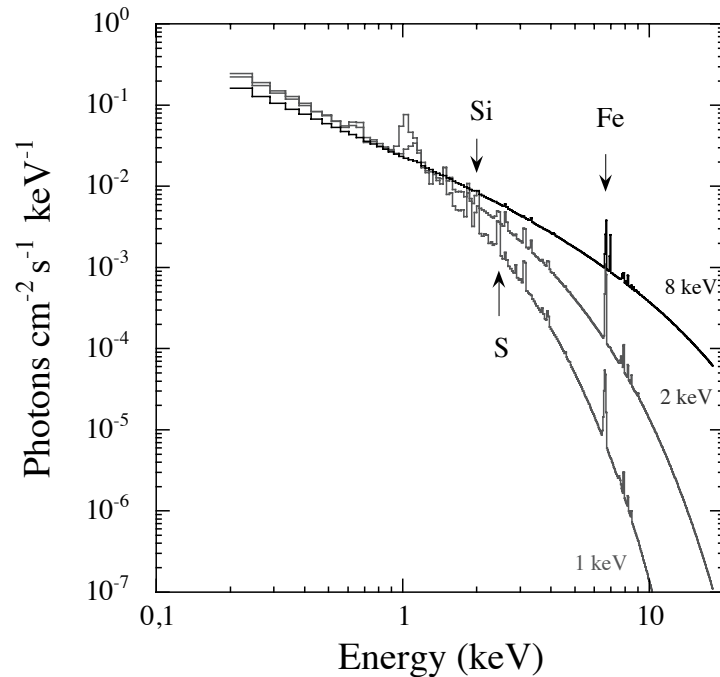


photon emissivity at energy E

$$\lambda_{\text{BR}} \propto g(E, T) T^{-1/2} \exp[-E/(k_{\text{B}}T)]$$

[wikipedia]

X-ray spectrum



$$EM(r) = \frac{4\pi(1+z)^4 S(\theta)}{\Lambda(T, Z)}$$

[Arnaud2005bmri.conf...77A]

The temperature is constrained by the position of the exponential cut-off

The gas density is estimated from the continuum:

ε is not very sensitive to kT at low energy. Counts in soft energy band ($E < 2$ keV) used to determine the gas density distribution.

Iron K line complex (~ 6.7 keV)

Line emission rapidly decreases with increasing temperature. Except for the cool clusters ($kT \leq 4$ keV) or in the cooling core present in some clusters, one cannot expect to measure the abundance of elements other than Iron because they are completely ionized.

X-ray mass

Hydrostatic equilibrium

$$\nabla P_{\text{Tot}} = -\rho_{\text{ICM}} \nabla \phi_{\text{Mat}}$$

HE + spherical symmetry

$$\frac{dP}{dr} = -\frac{GM_{\text{tot}}(< r)\rho_{\text{gas}}}{r^2}$$

equation of state for a perfect gas

$$P = \frac{\rho_{\text{gas}} k_B T_{\text{gas}}}{\mu m_p}$$

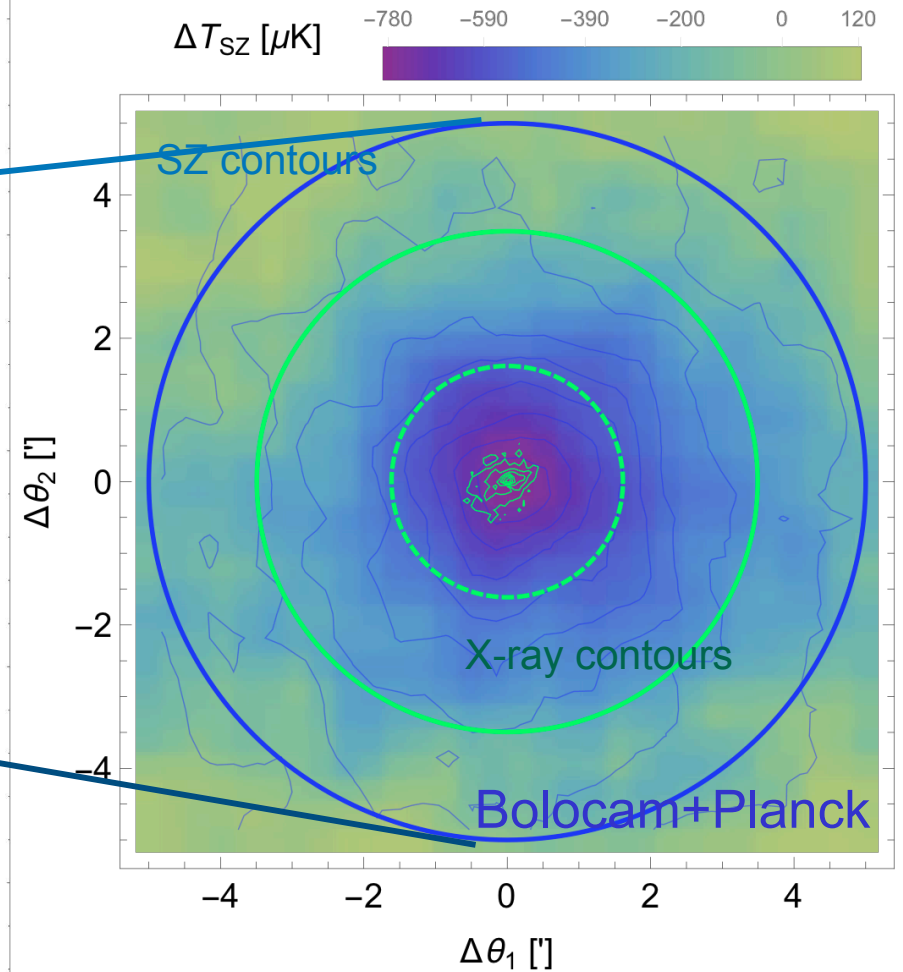
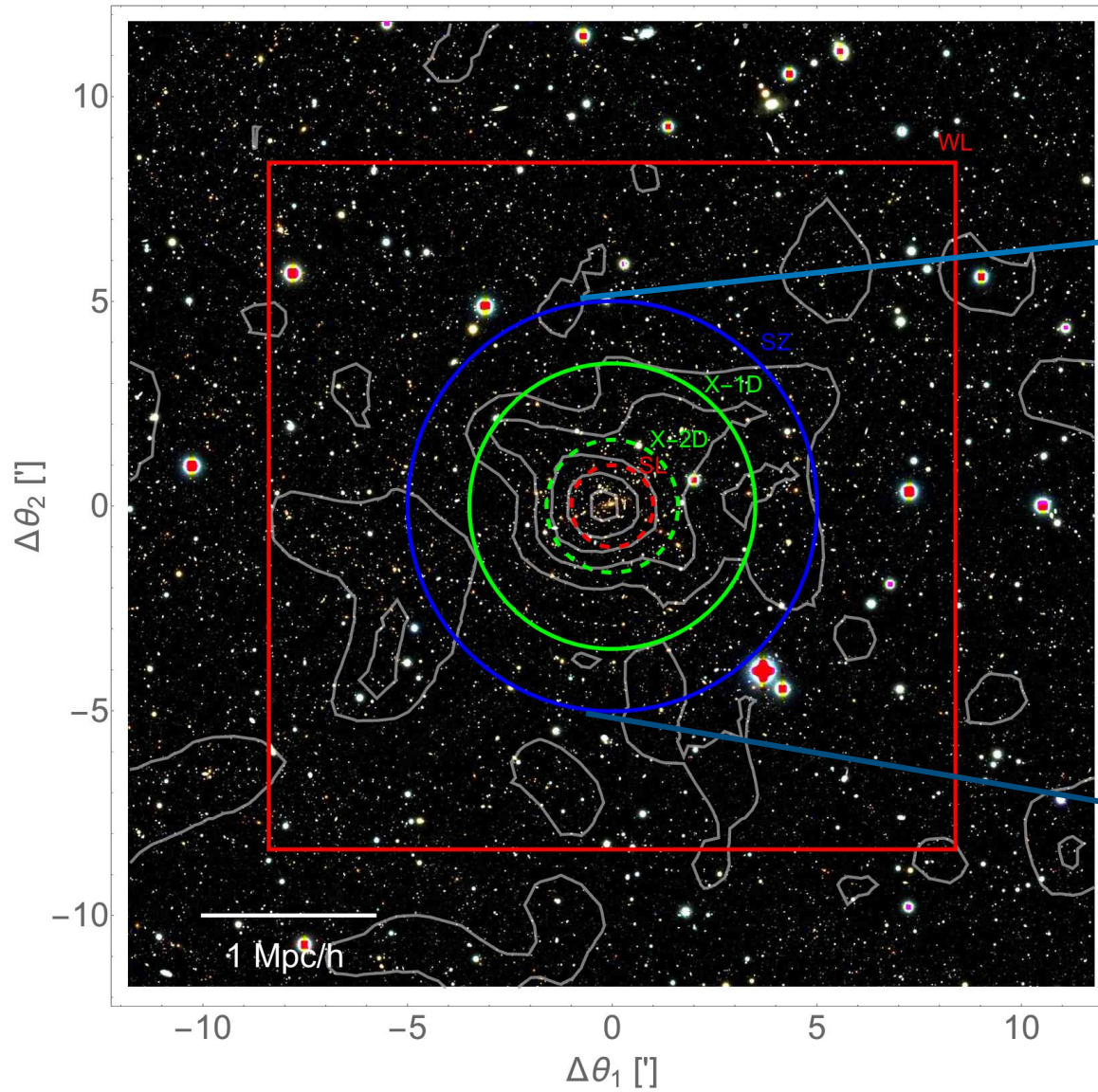
$$M_{\text{tot}}(< r) = -\frac{T_{\text{gas}} r}{G\mu m_p} \left(\frac{\delta \ln \rho_{\text{gas}}}{\delta \ln r} + \frac{\delta \ln T_{\text{gas}}}{\delta \ln r} \right)$$

HE bias of the other of 10-20%

◇ significant contribution from non-thermal pressure $P_{\text{Tot}} = P_{\text{Th}} + P_{\text{nTh}}$

Sunyaev-Zeldovich Effect (SZE)

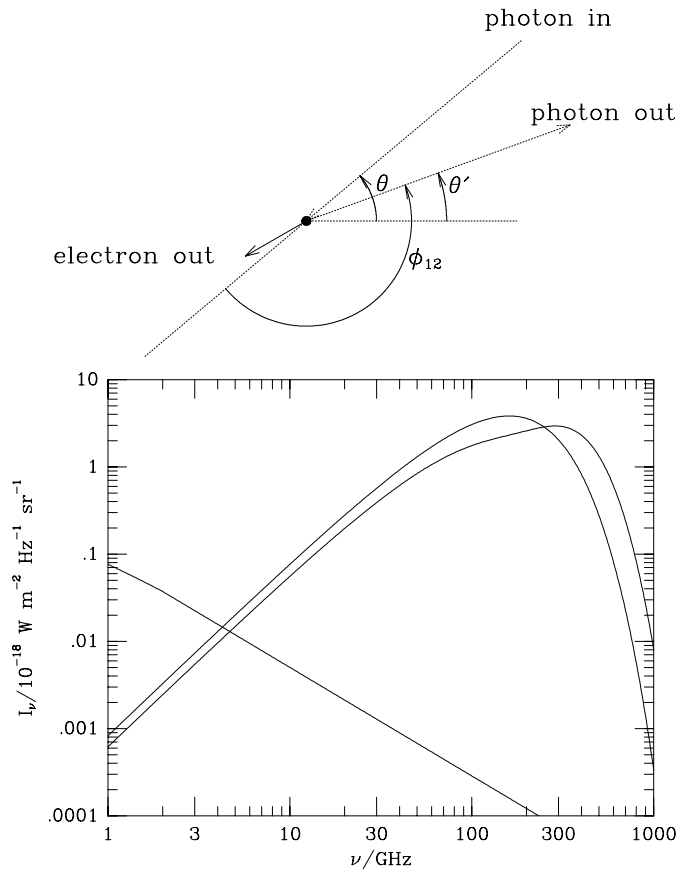
ICM distorts the CMBR with a typical temperature decrement at $\lambda \sim 1$ cm:



$$\frac{\Delta T_{SZ}}{T_{CMB}} = f(\nu, T_e) \frac{\sigma_T k_B}{m_e c^2} \int_{\text{l.o.s.}} n_e T_e dl$$

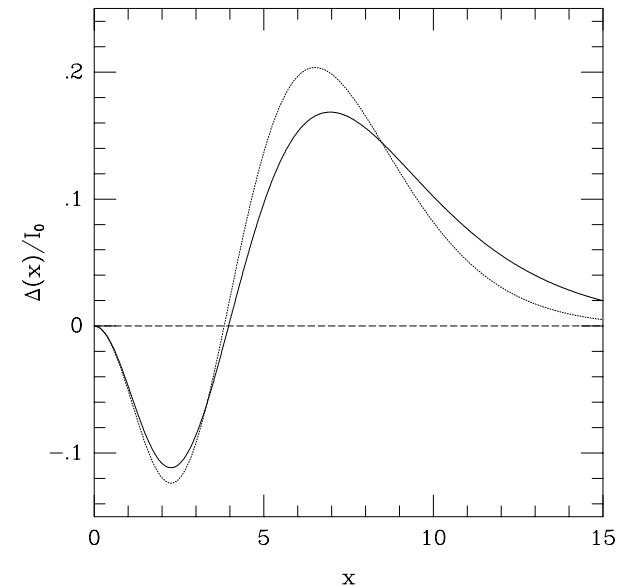
Inverse Compton scattering

Photons from the CMB passing through a cluster find many high-speed electrons and experience Inverse-Compton scattering. The process preserves the number of photons, and the black-body spectrum of the CMB is slightly distorted and shifted to larger frequencies by an amount that depends on the temperature, and on the column density of the ICM [Birkinshaw1999PhR...310...97B]



CMB spectrum after passage through an (exaggerated) scattering atmosphere with $y = 0.1$ compared with the integrated emission from the bright radio source Cygnus A. SZE causes a fractional decrease in the low-frequency intensity of the CMB

The net effect on the CMB is the production of a cold spot at low and a hot spot at high frequencies, where the pivotal frequency is about 217 GHz



The spectral deformation after a single scattering from a thermal population of electrons as a function of dimensionless frequency $x = h\nu/kT = 0.0176(\nu/\text{GHz})$, for electrons at $k_B T_e = 15.3 \text{ keV}$. The result obtained from the Kompaneets kernel is shown as a dotted line. The shape of the distortion is independent of T_e (and the amplitude is proportional to T_e) for the Kompaneets kernel, but the relativistic expression leads to a more complicated form.

Sunyaev-Zeldovich effect

$$\Delta T_{\text{SZ}} = f_{\text{SZ}}(\nu, T) T_{\text{CMB}} y$$

Compton parameter

$$y \equiv \frac{\sigma_{\text{T}} k_{\text{B}}}{m_{\text{e}} c^2} \int_{\parallel} n_{\text{e}} T_{\text{e}} dl,$$

Integrated Compton parameter

$$Y_{\Omega} = \int_{\Omega} y(\theta) d\theta$$

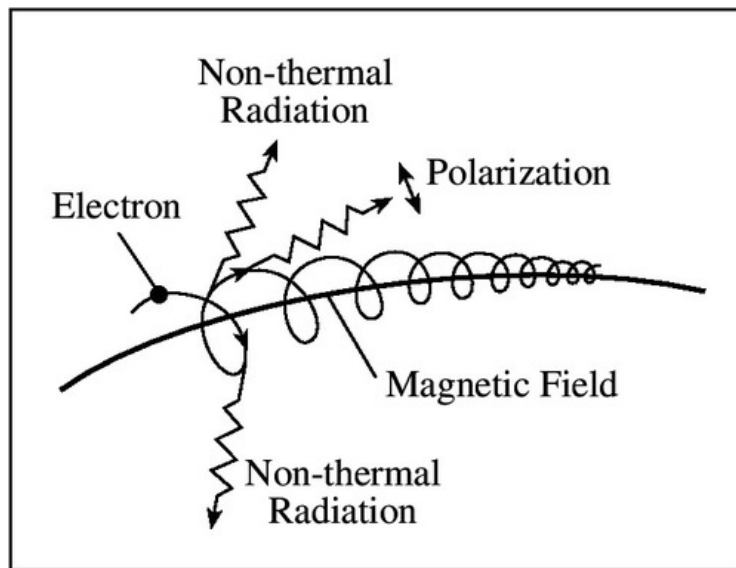
Radio [not covered]

Two proposed mechanisms for synchrotron radiation [Brunetti&2014IJMPD..2330007B]:

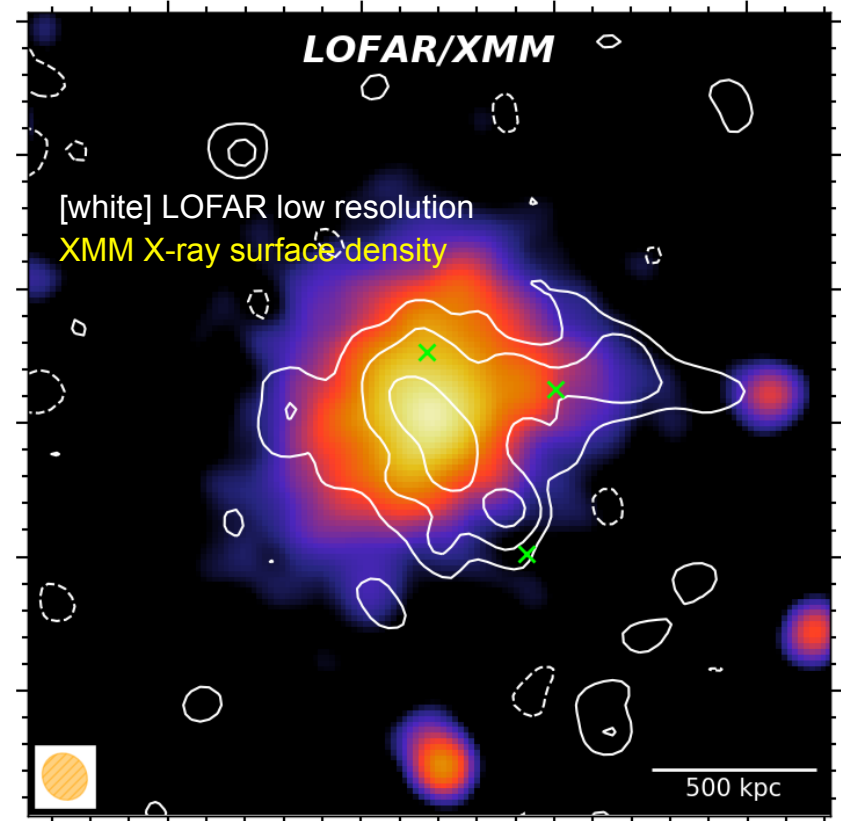
relativistic electrons are re-accelerated in the intracluster medium by turbulence driven by energetic mergers

diffusive shock acceleration

Synchrotron radiation (or magnetobremstrahlung radiation) is the electromagnetic radiation emitted when charged particles are accelerated radially, e.g., when they are subject to an acceleration perpendicular to their velocity in presence of a magnetic field



https://ase.tufts.edu/cosmos/view_picture.asp?id=1424



PSZ2 G099.86+58.45: one of the most distant radio halos discovered so far. Detection at 120-168 MHz with LOFAR Two-meter Sky Survey (LoTSS) [Cassano+19]

Mass measurements

X-ray and/or SZE

Assuming hydrostatic equilibrium

$$M_{\text{tot}}(< r) = -\frac{T_{\text{gas}} r}{G \mu m_{\text{p}}} \left(\frac{\delta \ln \rho_{\text{gas}}}{\delta \ln r} + \frac{\delta \ln T_{\text{gas}}}{\delta \ln r} \right)$$

Galaxy kinematics

➤ Optical spectroscopic measurements. **Dynamical masses** can be calculated from velocity dispersions via the Jeans equation (or by studying **caustics**)

$$M_{\text{tot}}(< r) = -\frac{\sigma_r^2 r}{G} \left[\frac{\delta \ln \sigma_r^2}{\delta \ln r} + \frac{\delta \ln n_{\text{gal}}(r)}{\delta \ln r} + 2\beta \right]$$

Gravitational Lensing

➤ GL does not require assumptions regarding the dynamical state.

$$M_{\text{cyl}}(< r_{\text{E}}) = \frac{c^2}{4G} \frac{D_{\text{s}}}{D_{\text{ds}} D_{\text{d}}} r_{\text{E}}^2$$

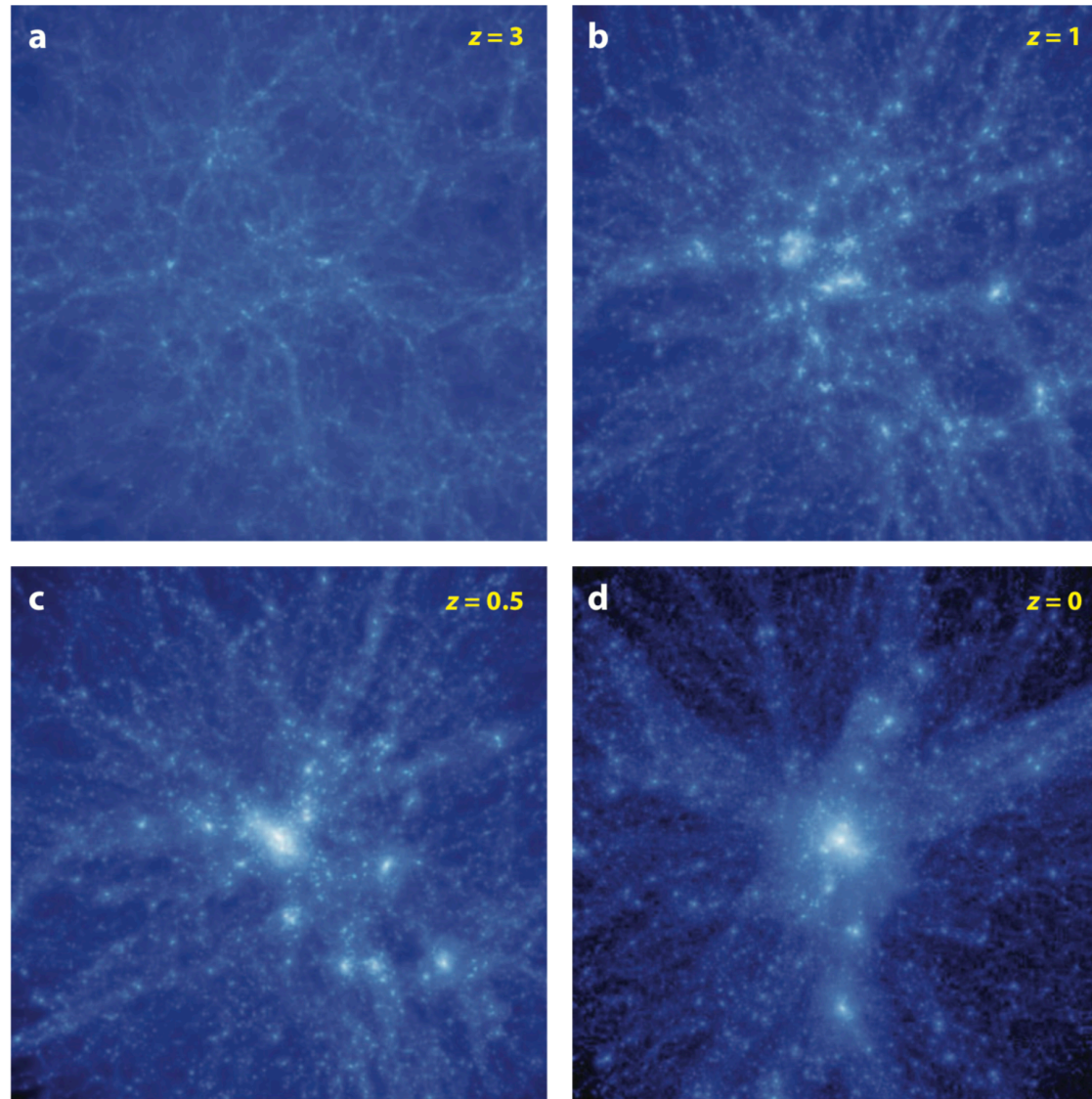
Direct mass measurements

	GL	X-ray	sigma
cost	<input type="checkbox"/> <input checked="" type="checkbox"/>	<input type="checkbox"/>	<input type="checkbox"/>
3D	<input type="checkbox"/> <input checked="" type="checkbox"/>	<input checked="" type="checkbox"/>	<input checked="" type="checkbox"/>
equilibrium	<input checked="" type="checkbox"/>	<input type="checkbox"/>	<input type="checkbox"/>
bias	<input type="checkbox"/> <input checked="" type="checkbox"/>	<input type="checkbox"/>	<input type="checkbox"/> <input checked="" type="checkbox"/>
scatter	<input type="checkbox"/>	<input type="checkbox"/>	<input type="checkbox"/>

Scatters with respect to the “true” mass [Sereno&152015MNRAS.450.3633S.]

- WL ~ 15-20%
- HE ~ 10-20%
- Caustics ~ 30%

Evolution of density fields



Evolution of a DM density field in a comoving region of $15h^{-1}$ Mpc on a side around cluster mass density peak in the initial perturbation field. The panels show (a) $z = 3$, (b) $z = 1$, (c) $z = 0.5$, and (d) $z = 0$. The cluster has $M_{200} \approx 1.2 \times 10^{15} h^{-1} M_{\odot}$ at $z = 0$. The collapse of real density peaks is complex: strong deviations from spherical symmetry, accretion of matter along filaments, presence of smaller-scale structure within the collapsing cluster-scale mass peak [Kravtsov&2012ARA&A..50..353K]

Density perturbations

$$\delta(x) = \frac{\rho(x) - \rho_0}{\rho_0}$$

If perturbations are Gaussian, power spectrum characterizes all features

Correlation function $\xi(r) \equiv \langle \delta(x)\delta(x+r) \rangle$

Fourier transform $\xi(\mathbf{r}) = \frac{V}{(2\pi)^3} \int |\delta_{\mathbf{k}}|^2 e^{-i\mathbf{k}\mathbf{r}} d^3k$

Power spectrum $P(x) = \langle |\delta_k^2| \rangle$

σ is the filtered linear rms $\sigma^2 = \int P(k) \hat{W}(kR) k^2 dk$

A mass corresponds to a filter scale radius $M = 4\pi/3 \bar{\rho}_m R^3$

$\sigma_8 \equiv \sigma(R = 8 \text{ Mpc}/h, z = 0)$

Power-law spectrum

$$\langle |\delta_k^2| \rangle \propto k^n$$

the index n governs the balance between large. and small scale power

Filter the density field with a box of comoving size k

This filters out waves with $k' > 1/k$, i.e. masses $< k^3$

$$\langle \delta^2 \rangle = \int_0^{1/k} k'^n 4\pi k'^2 dk' \propto k^{-(n+3)}$$

$$M \propto R^3 \propto k^{-3}$$

$$\delta_{\text{rms}} \propto M^{-(n+3)/6}$$

Primordial index $n \sim 1$

Today index at cluster scale $n \sim -1$

Spherical collapse: Hubble flow

Equation of motion for the radius r of a spherical shell containing a constant mass M
In a matter only universe, with the Birkhoff theorem,

$$\frac{d^2r}{dt^2} = -\frac{GM}{r^2} \longleftrightarrow \frac{1}{2}\dot{r}^2 - \frac{GM}{r} = E_0$$

If the energy is null, i.e. the shell moves at the escape velocity $r(0) = 0$, $E_0 = 0$

$$r_{\text{back}}(t) = \frac{1}{2} (GMt)^{2/3}$$

Density

$$\rho = M/V = M/(4/3\pi r^3)$$

expansion factor in an EdS universe

$$a = \frac{1}{1+z} \propto t^{2/3}$$

Spherical collapse: perturbation growth

Cycloid solution ($E_0 > 0$) $\frac{d^2 r}{dt^2} = -\frac{GM}{r^2}$

$$r(\theta) = A(1 - \cos \theta)$$

$$t(\theta) = B(\theta - \cos \theta)$$

$$A = \frac{GM}{2E_0} \quad B = \frac{GM}{(2E_0)^{3/2}}$$

Up to order θ^5

$$r \sim r_{\text{back}}(1 - \delta_{\text{lin}}/3)$$

$$\rho \sim \rho_{\text{back}}(1 - \delta_{\text{lin}})$$

$$\delta_{\text{lin}} = \frac{3}{20} \left(\frac{6t}{B} \right)^{2/3}$$

at early times, the sphere expands with the Hubble flow ($a \propto t^{2/3}$)
density perturbations grow proportional to flow

Details

$$r_\epsilon \sim r_{\text{back}}(1 - \epsilon f_1[t]) \quad \longrightarrow \quad \frac{d^2 r_\epsilon}{dt^2} = -\frac{GM}{r_\epsilon^2} + O(\epsilon^2) \quad \longrightarrow \quad f_1(t) = c_2 t^{2/3}$$

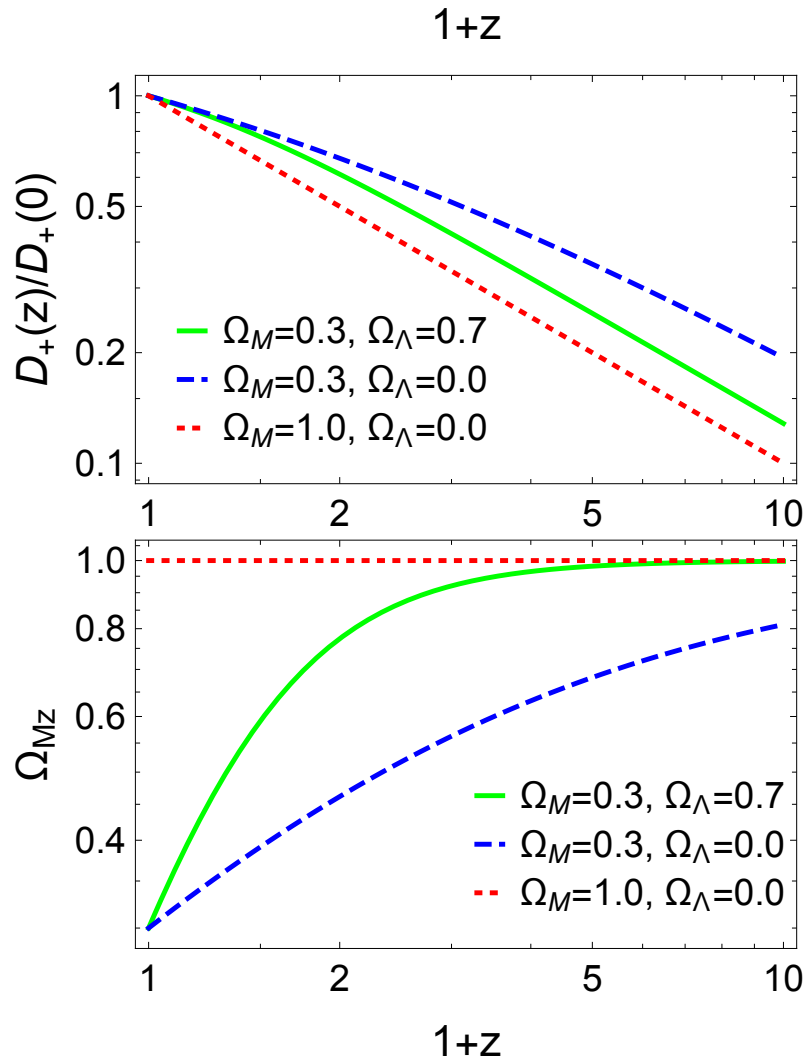
$$r(\theta) - r_\epsilon(t(\theta)) = O(\theta^5) \quad \longrightarrow \quad c_2 = -\frac{1}{20} \left(\frac{6}{B} \right)^{2/3}$$

Use $\frac{d}{dt} = \left(\frac{dt}{d\theta} \right)^{-1} \frac{d}{d\theta}$

Perturbation growth: LCDM

In a general LCDM universe

$$\sigma \propto D_+(a)$$



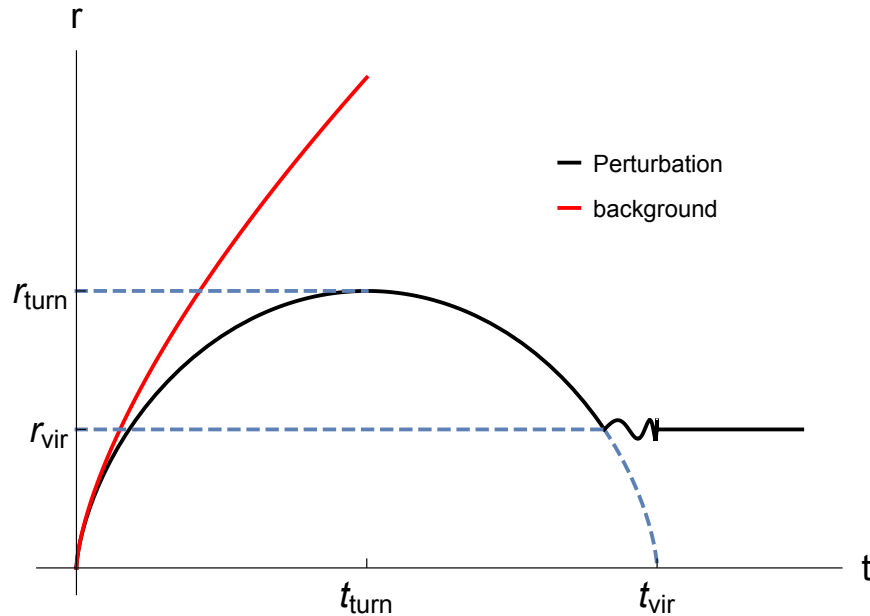
$$D(a) \propto \frac{d\rho}{\rho} \propto \frac{\dot{a}}{a} \int_0^a \frac{da'}{\dot{a}'^3}$$

Growth enhanced when background is DM dominated $\Omega_M \sim 1$

For a given Ω_M , evolution in OCDM ($\Omega_M < 1, \Omega_\Lambda = 0$) suppressed w.r.t. LCDM ($\Omega_M + \Omega_\Lambda = 1$), where Λ keeps up pcr

For $\Omega_\Lambda = 0$, the larger Ω_M the more pronounced the growth

Spherical collapse: epochs



$$E_K = \frac{1}{2} \dot{r}^2$$

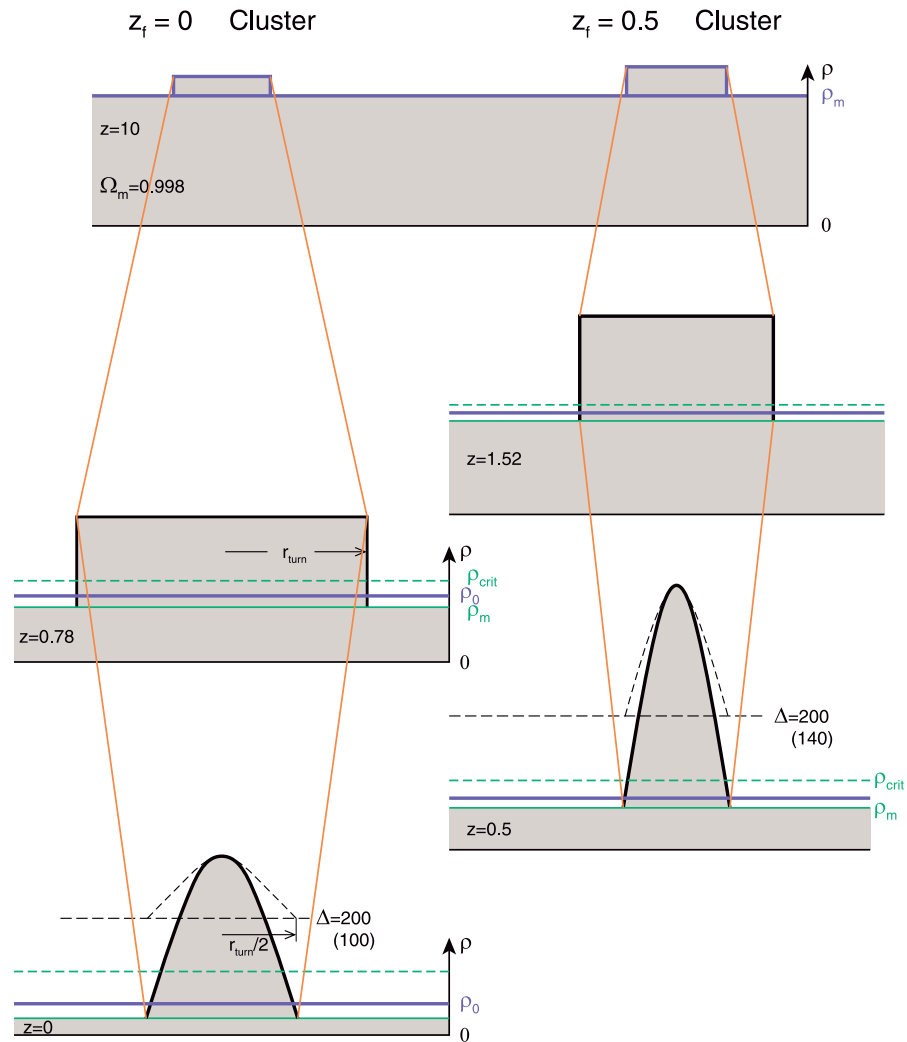
$$E_V = - \frac{GM}{r}$$

density enhancement with respect to the background

$$\Delta = \rho / \rho_{\text{back}}$$

- The sphere breaks away from the general expansion
- **Turnaround.** Maximum radius $r = r_{\text{max}}$ at $\theta = \pi$, $\Delta = 5.55$, $\delta_{\text{lin}} \approx 1.06$
- **Collapse.** If only gravity operates, the sphere will collapse to a singularity at $\theta = 2\pi$, $\delta_{\text{lin}} \approx 1.69$
- **Virialization.** Dissipative physics prevent collapse. Kinetic energy of collapse is converted into random motions. At $\theta = 3\pi/2$, $V = -2K$, the condition for virial equilibrium determines the final radius $r_{\text{vir}} = r_{\text{max}}/2$
- If virialization achieved only at time corresponding to collapse, $t_{\text{vir}} = t_{\text{collapse}}$ ($\theta = 2\pi$), $\Delta = (6\pi)^2/2 \approx 178$

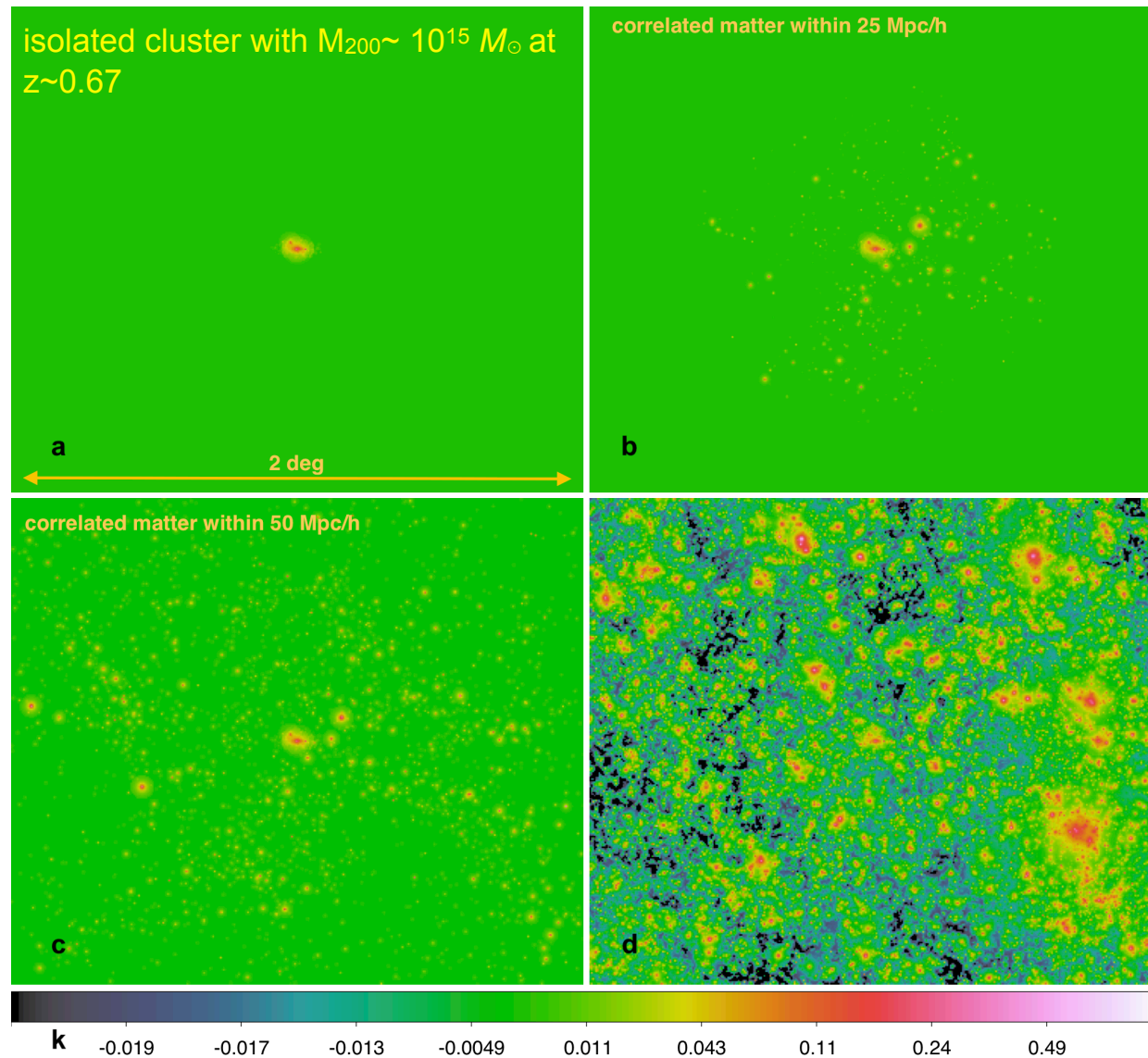
Collapse



More prominent peaks collapse earlier

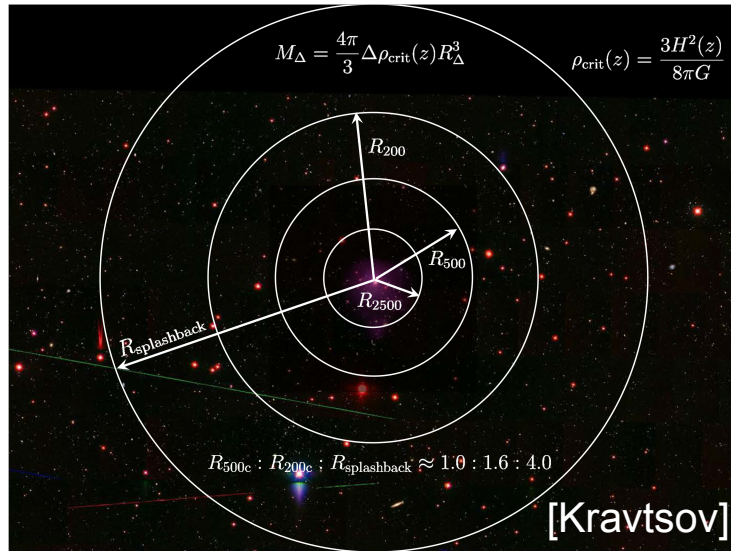
Illustration of how the galaxy cluster structure scaling depends on the formation epoch of the cluster and on the critical density of the universe in an Einstein-de Sitter (densities are blue) and in a concordance cosmological model (green). The *left panel* provides a sketch of cluster collapse for a cluster with a formation redshift of $z = 0$, and the *right panel* shows a cluster forming at $z = 0.5$ [Böhlinger+2012A&A...539A.120B.]

Galaxy clusters, correlated and uncorrelated matter

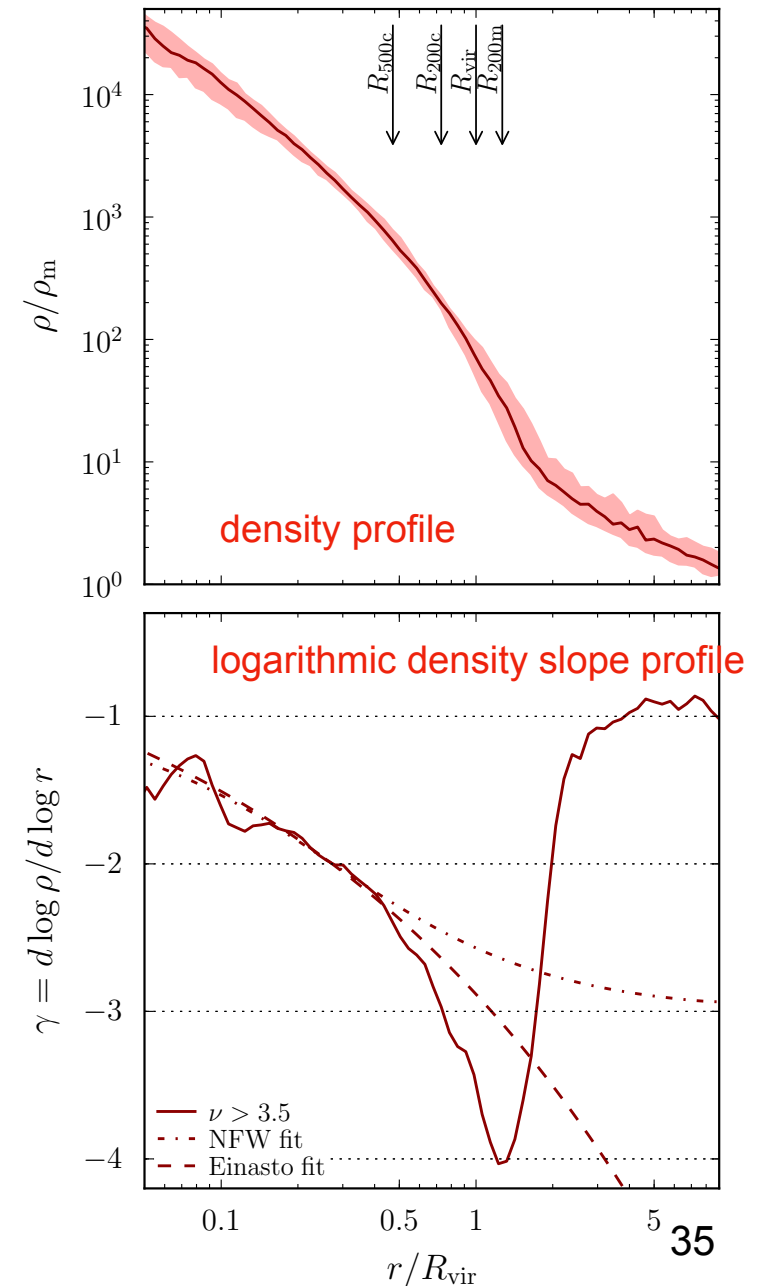


a massive cluster at $z \sim 0.6$ and the projected mass density [Serenio+2018NatAs...2..744S]

Galaxy clusters and correlated matter



Density profiles of simulated massive halos at $z = 0$
 [Diemer&2014ApJ...789....1D]



Infalling material is still in the process of falling towards the halo
 Collapsed material has experienced at least one orbital pericenter passage and it is orbiting the halo

Truncation

The slope of the profile steepens sharply at $r > 0.5 r_{\text{vir}}$.
 Minimum slope at $r_t \sim 1-2 r_{200m}$ ($r_{200m} \sim 1.4 r_{200c}$)

Splashback

apocenter of the most recently accreted particles that have passed through the pericenter of their orbit once since their infall, $r_{\text{sb}} \sim r_t$

Turnaround

The turnaround radius at $\sim 2-3 r_{200m}$ can be defined as the outermost radius where the radial velocity becomes zero

Density profile

Numerical simulations suggest that the shape of the virialized objects is universal

$$\rho_M \propto r^{-p}(r + r_s)^{p-q}$$

Singular Isothermal $p=2, q=p$

$$\rho_{\text{SIS}} = \frac{\sigma^2}{2\pi Gr^2} = \frac{\Delta \rho_{\text{cr}}}{3(r/r_\Delta)^2}$$

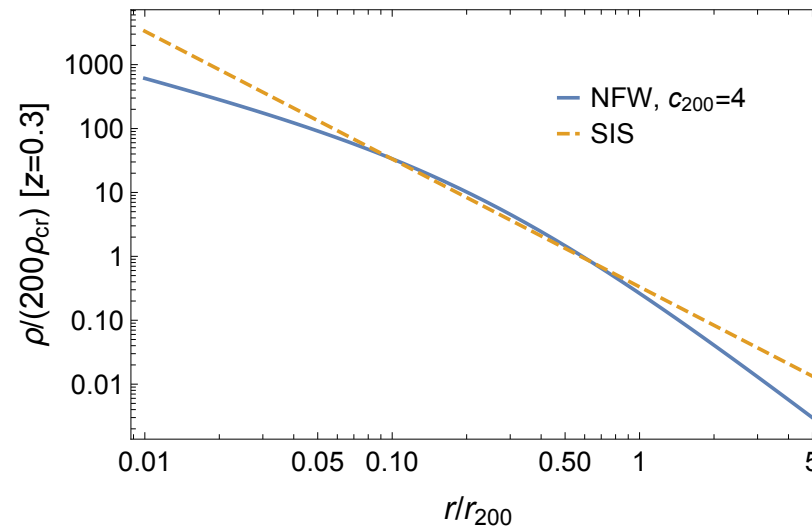
Navarro-Frenk-White $p=1, q=3$

Two parameter profiles: mass and concentration

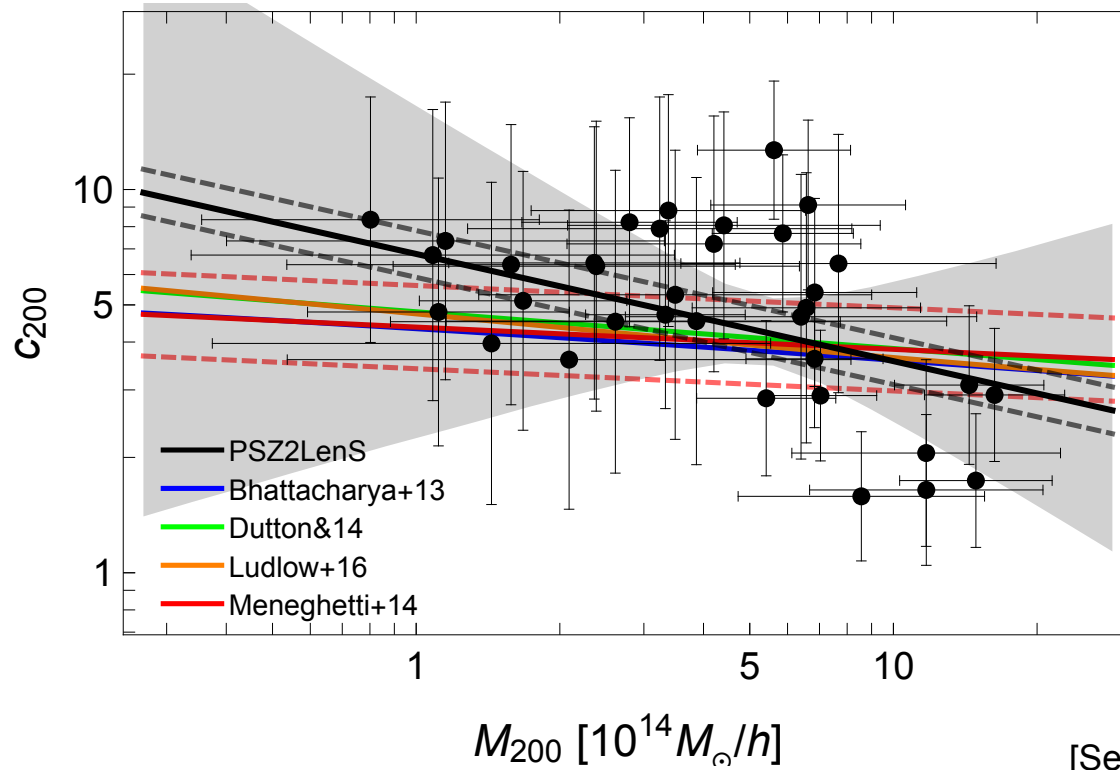
$$\rho_{\text{NFW}} = \frac{\rho_{\text{cr}} \delta_c}{(c_\Delta r/r_\Delta)(1 + (c_\Delta r/r_\Delta)^2)}$$

$$c_\Delta = r_\Delta / r_s$$

$$\delta_c = \frac{\Delta c_\Delta^3}{3 \left(\ln(1 + c_\Delta) - \frac{c_\Delta}{1 + c_\Delta} \right)}$$



Mass - concentration relation



concentrations are smaller for larger mass haloes and at early times

$$c_{200} \sim 3.7 \left(\frac{M_{200}}{10^{14} M_{\odot}} \right)^{-0.08} \left(\frac{1+z}{1+0.3} \right)^{-0.5}$$

[Duffy+2008MNRAS.390L..64D]

Self-similarity

Spherical collapse suggests that cluster properties are universal at a given density contrast.

When generalized to non flat LCDM models, spherical collapse (SC) shows that Δ is z dependent

SC does not account for triaxial structures, continuous accretion, environment

N-Body simulations can prefer universality in terms of fixed, constant contrast:

» $\Delta_c=500$ or 200 of the critical density

» $\Delta_m=200$ of the mean matter density

We assume that properties are self-similar at a given, well suited Δ

By definition, the relation between mass and radius

$$M_{\Delta_z} \equiv \frac{4\pi}{3} \Delta_z \rho_{cr} R_{\Delta_z}^3$$

Any redshift dependence is expressed in terms of

$$F_z \equiv E_z \Delta_z^{1/2}$$

The final state of any dimensionless statistical property of the perturbations, e.g. correlation function or number density, is self-similar

$$S[\Delta(r, t_1)] = S[\Delta(\alpha r, t_2)]$$

Closed box

The matter budget of the clusters resembles the universal value

$$M_{\text{gas},\Delta_z} \propto M_{\Delta_z} \quad \rho_{\text{gas},\Delta_z} \propto M_{\Delta_z}/R_{\Delta_z}^3 \propto F_z^2$$
$$f_{\text{gas},\Delta_z} \sim \text{constant}$$

Light traces mass: optical richness proportional to mass

$$\lambda \propto M_{\Delta_z}$$

Virial equilibrium

Galaxy clusters are nearly dynamically relaxed in the inner regions. The crossing time

$$t_{\text{crossing}} = \frac{R}{\sigma_v} \sim \left(\frac{R}{1\text{Mpc}} \right) \left(\frac{10^3 \text{km s}^{-1}}{\sigma_v} \right)$$

For a cluster, $t_{\text{crossing}} \sim 1 \text{ Gyr} < t_{\text{Hubble}} \sim 10 \text{ Gyr}$

The virial theorem is assumed to be satisfied $E_G + 2E_K = 0$

$$E_G \propto -\frac{GM_{\Delta_z}}{r_{\Delta_z}} \quad E_K \propto \frac{M_{\Delta_z} \sigma_v^2}{2}$$

Relation between mass and velocity dispersion $\sigma_v \propto F_z^{1/3} M_{\Delta_z}^{1/3}$

Relation between temperature and velocity dispersion

$$\mu m_p \sigma_v^2 \sim k_B T_{\text{gas}} \rightarrow T_{\text{gas}} \propto -\frac{GM_{\Delta_z}}{r_{\Delta_z}} \rightarrow T_{\text{gas}} \propto F_z^{2/3} M_{\Delta_z}^{2/3}$$

These relations can be verified for the SIS

LX-M

Relation between X-ray luminosity and mass

$$L_X \propto \epsilon_X R_{\Delta,z}^3$$

Assuming bremsstrahlung radiation

Bolometric luminosity

$$\epsilon_{X,\text{Bol}} \propto \rho_{\text{gas}}^2 T_{\text{gas}}^{1/2}$$



$$L_{X,\text{Bol}} \propto F_z^{7/3} M_{\Delta_z}^{4/3}$$

Soft band luminosity

$$\epsilon_{X,\text{soft}} \propto \rho_{\text{gas}}^2$$



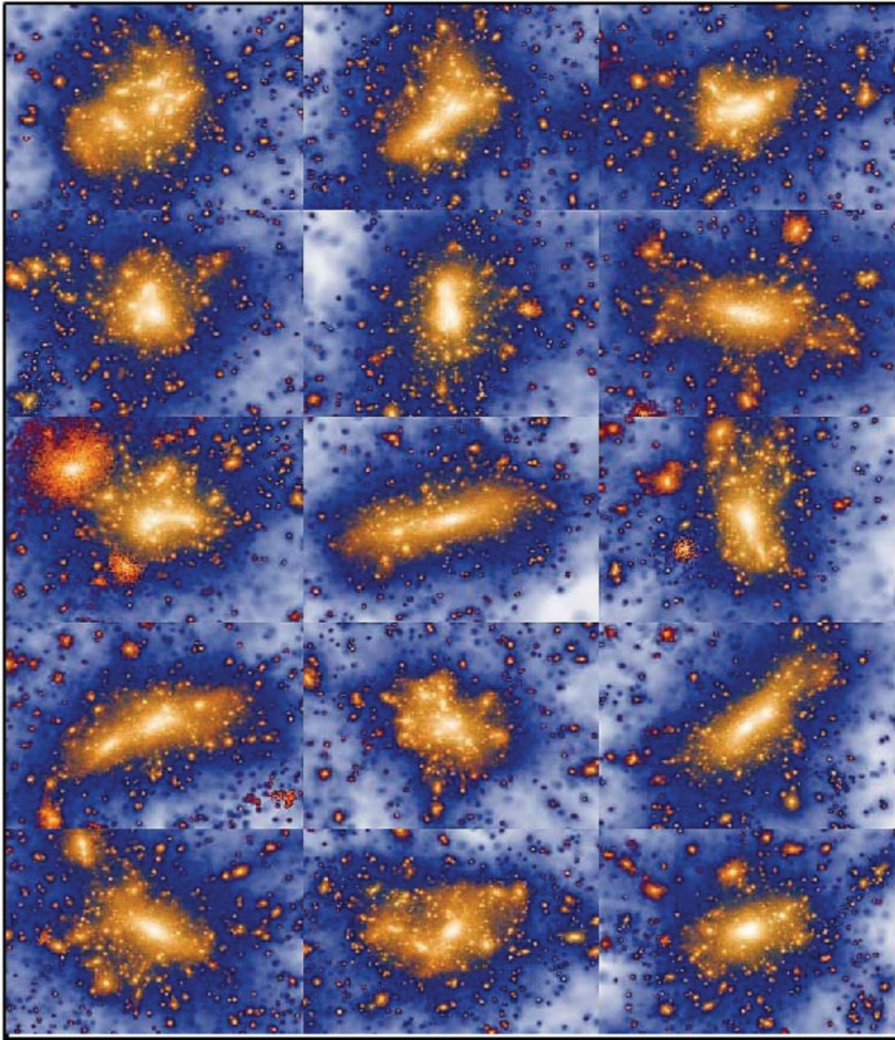
$$L_{X,\text{soft}} \propto F_z^2 M_{\Delta_z}$$

SZE-M

relation for the Compton parameter

$$D_{\text{A}}^2 Y_{\Delta_z} \propto T_{\text{gas}} M_{\text{gas}} \longrightarrow D_{\text{A}}^2 Y_{\Delta_z} \propto F_z^{2/3} M_{\Delta_z}^{5/3}$$

Intrinsic scatter



Large variety in shape and internal structure.

Scatter due to:

- Profile variation
- Internal structure/substructures
- Triaxiality
- Orientation
- Environment
- Line-of-sight projections
- Non gravitational, baryonic physics (injections, feedbacks,...)
- Deviations from equilibrium

The 15 most massive MXXL haloes (sorted by M_{200} at $z = 0.25$).

Each image corresponds to a region of dimensions $6 \times 3.7 h^{-1}$

Mpc wide and $20 h^{-1}$ Mpc deep [Angulo+12].

Scale of non linearity

Power-law spectrum: perturbations are scale free

$$\sigma(M, t) \sim D_+(t) M^{-(n+3)/6}$$

In EdS, the universe is scale-free, $D_+ \sim t^{2/3}$

$$\sigma(M, t) \sim t^{2/3} M^{-(n+3)/6}$$

Non linearity occur when $\delta \sim 1$

$$\sigma(M_{\text{NL}}, t) \sim 1 \longrightarrow M_{\text{NL}} \propto t^{4/(3+n)} \quad \text{i.e.} \quad M_{\text{NL}} \propto (1+z)^{-6/(n+3)}$$

Any dimensionless statistical property of the perturbations, e.g. correlation function or number density, is a function of M/M_{NL} and the final state is self-similar

$$S[\Delta(r, t_1)] = S[\Delta(\alpha r, t_2)]$$

$$\alpha = \left(\frac{M_{\text{NL}}(t_2)}{M_{\text{NL}}(t_1)} \right)^{1/3} = \left(\frac{t_2}{t_1} \right)^{4/(3n+9)}$$

Thermodynamics of the gas

Gravitational collapse. The diffuse gas infalling onto the DM-dominated potential wells of clusters converts the kinetic energy acquired during the collapse into thermal energy via adiabatic compression and shocks. The shocks arising during cluster formation can be classified into two broad categories: strong external shocks surrounding filaments and the virialized regions of DM halos and weaker internal shocks, located within the cluster virial radius.

Because gravity does not have a characteristic length scale, we expect the predictions of the self-similar model to apply when gravitational gas accretion determines the thermal properties of the ICM.

Radiative cooling

ICM (and, to a lesser extent, its interstellar counterpart) is optically thin at most wavelengths, and radiation loss is the primary cooling mechanism for the baryonic component of halos.

Cooling introduces new scales and it can break self-similarity of the ICM even in the absence of heating. Cooling removes low-entropy gas from the hot ICM phase in the cluster cores, which is replaced by higher entropy gas from larger radii. Somewhat paradoxically, the cooling thus leads to an entropy increase of the hot, X-ray emitting ICM phase

The cooling timescale of the gas in massive halos is typically longer than a Hubble time, except for a subset of systems that exhibit cool cores. The central ~ 100 -kpc region of such systems tends to be X-ray bright and typically contains a dominant elliptical galaxy.

Stellar and active galactic nuclei feedback.

Steady heating is required to offset the ongoing radiative cooling observed in the form of strong X-ray emission. Feedback of mass, momentum, and entropy from stellar/ SMBH sources can limit cooling and star formation in low-mass halos. Feedback is driven by photoionization and supernova-driven winds

or jets propelled by accretion onto the central SMBH.

This feedback typically ties the energy input to the mass accretion rate which, in turn, is governed by the local rate of cooling and/or cold accretion.

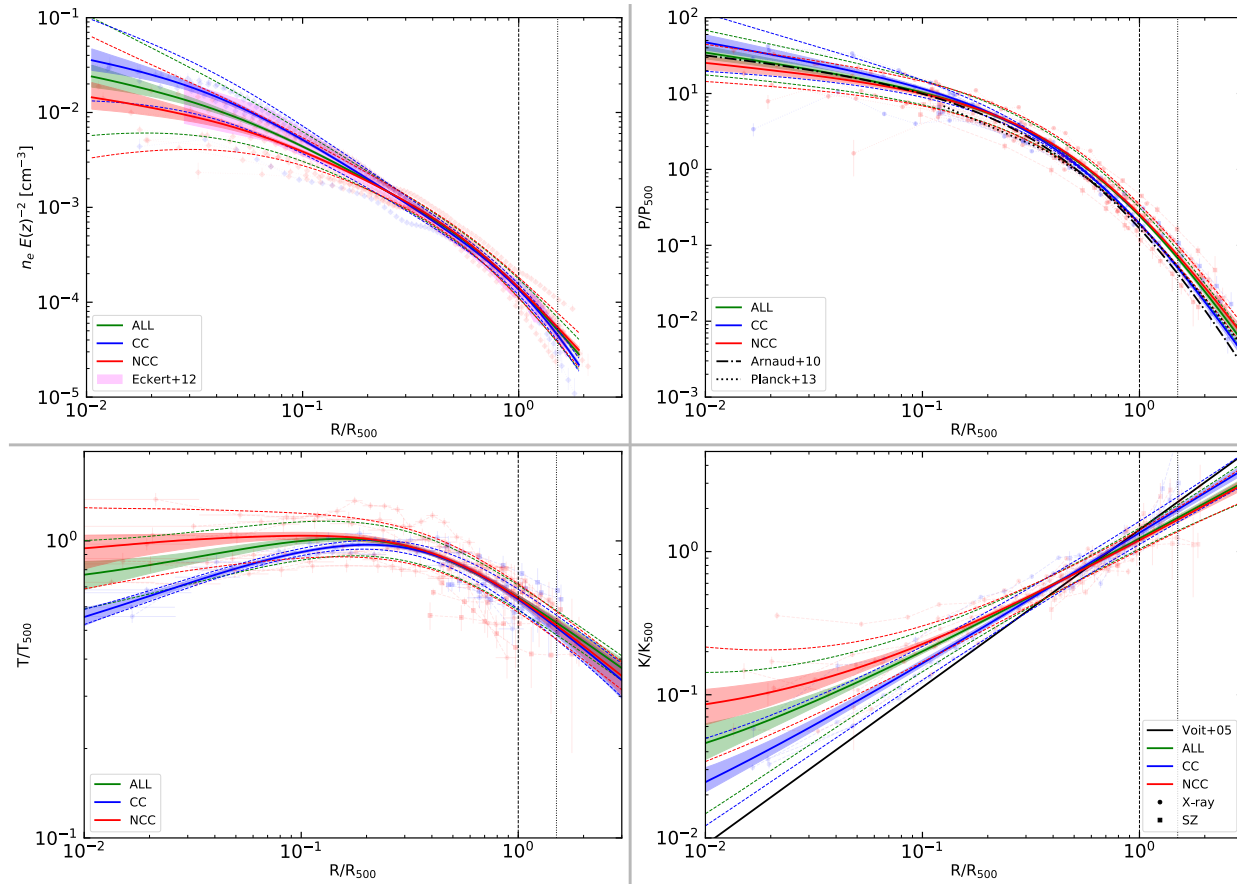
the kinetic feedback of SNe is included in the form of galactic winds carrying the kinetic energy comparable to all of the energy released by Type II SNe expected to occur according to star formation in the simulation.

energy input from the AGN in the central cluster galaxies can provide most of the energy required to offset cooling. AGN feedback can reduce star formation in massive cluster galaxies and reduce the hot gas content in the poor clusters and groups,

Phenomenological preheating. The first proposed mechanism to break self-similarity was high-redshift ($z_h \sim 3$) pre-heating by nongravitational sources of energy, presumably by a combined action of the AGN and stellar feedback. As a result, gas density is relatively lower in lower mass systems, especially at smaller radii, while their entropy is higher.

Universal thermodynamic profiles

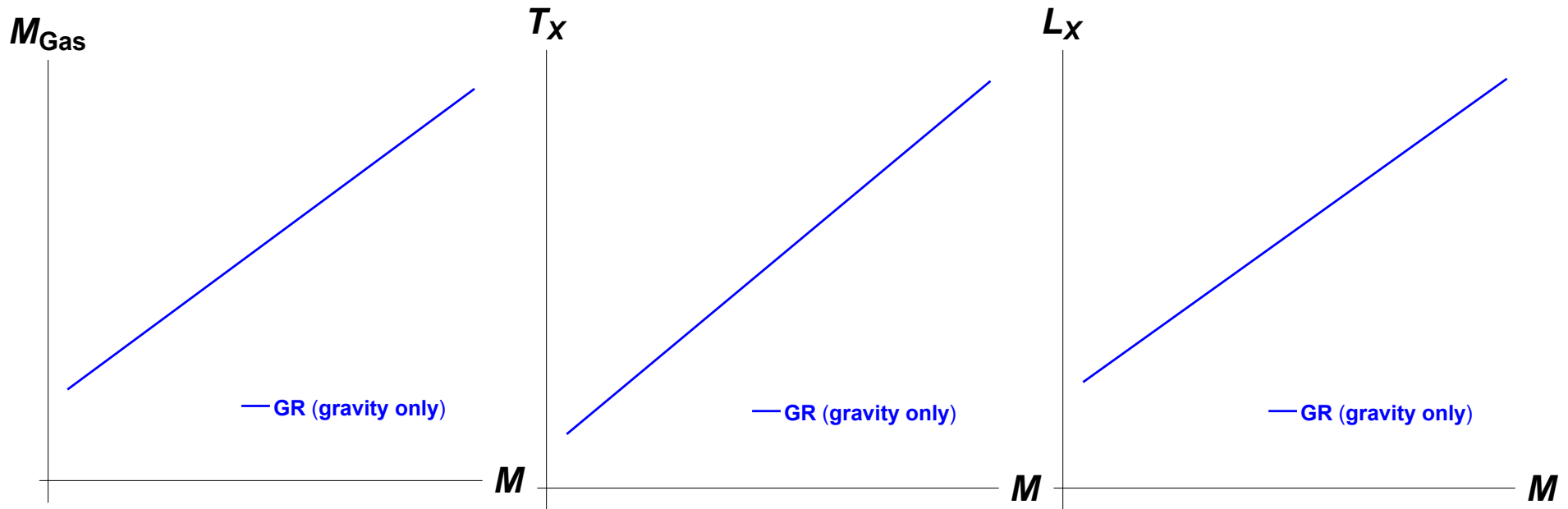
Thermodynamic profiles are remarkably similar in relaxed clusters with a cool core and a central luminosity spike. This makes the pressure less sensitive to the equilibrium status [Vikhlinin+2006ApJ...640..691V, Arnaud+2010A&A...517A..92A, Ghirardini+2019A&A...621A..41G]



$$P_{\text{th}} \propto T_{\text{gas}} n_e$$

$$K_e = k_B T_{\text{gas}} n_e^{-2/3}$$

Gravity driven scaling relations

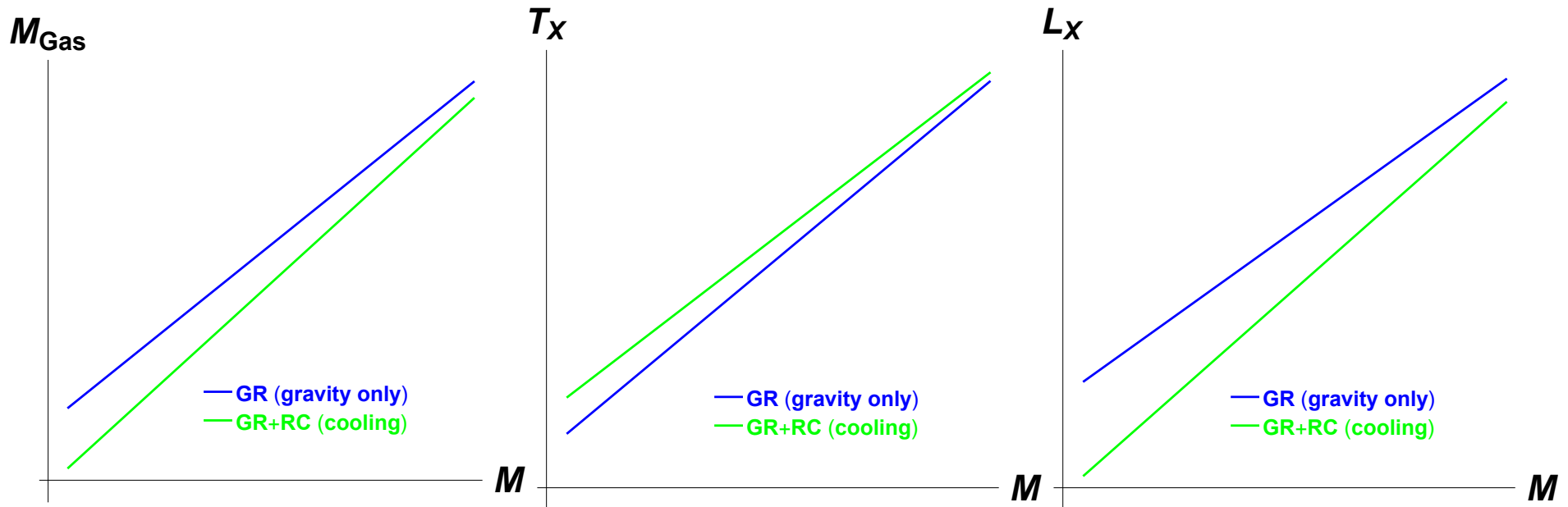


$$M_{\text{gas}} \propto M_{\Delta}$$

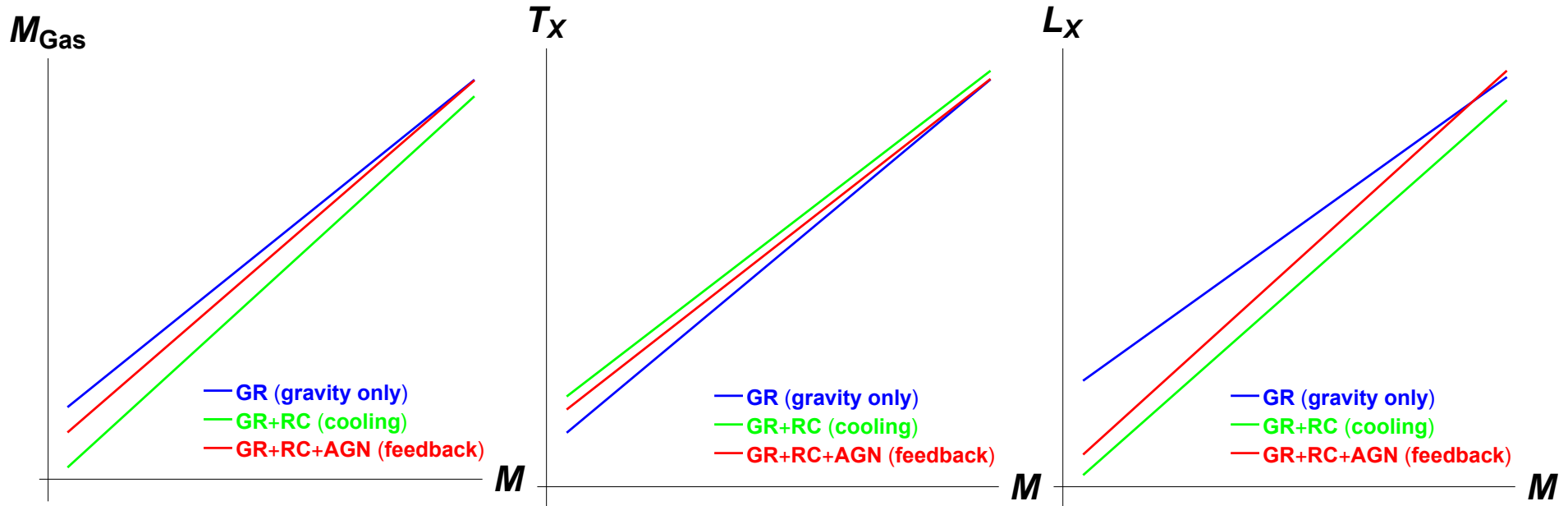
$$T_X \propto M_{\Delta}^{2/3}$$

$$L_X \propto M_{\Delta}^{4/3}$$

Star formation



AGN feedback



Halo mass function

Number of halos per mass interval dM in a comoving volume

$$\frac{dn}{dM} = \frac{\rho_0}{M} \left| \frac{dF(>M)}{dM} \right|$$

Fraction of the universe condensed into objects with mass $>M$

$$F(>M) = \frac{\int_M^\infty dM' M' dn(M')/dM'}{\rho_0}$$

$M^2 f(M)/\rho_0$ gives the fraction of the mass of the universe contained in haloes of a unit range in $\ln M$

Gaussian perturbations

If the density field δ is Gaussian, the probability that a given point lies in a region with $\delta > \delta_c$

$$p(\delta > \delta_c | M_f) = \frac{1}{2} \text{erfc} \left(\frac{\delta_c}{\sqrt{2}\sigma(M_f)} \right)$$

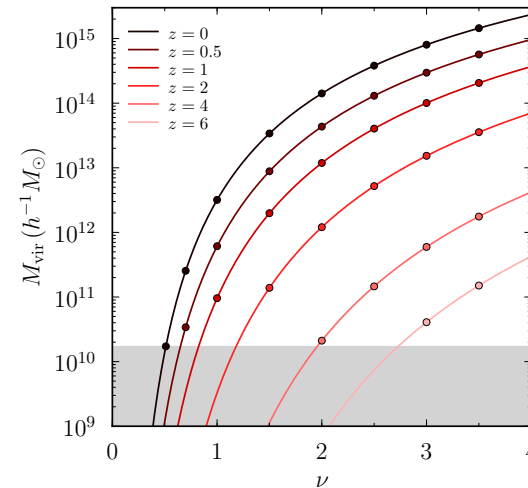
σ is the filtered linear rms

$$\text{erfc}(x/\sqrt{2})/2 = \int_x^\infty N(t) dt$$

Peak height

$$\nu = \delta_c / \sigma(M)$$

threshold in units of the rms density fluctuation



Virial mass of halos as a function of their peak height at different redshifts [Diemer&2014ApJ...789....1D]

Press - Schechter

- ★ Collapse to a virialized object occurs where linear-theory δ averaged over a box containing mass M reaches some critical value δ_c . From spherical collapse, $\delta_c=1.686$
- ★ Objects exist if they reached the collapse threshold. Objects counted as objects of the larger scale (if $\delta > \delta_c$ for a given M_f , then $\delta = \delta_c$ on some larger scale)
- ★ Factor 2 for the half of the mass which is unaccounted for (negative perturbations $\delta < 0$ not considered)

Fraction of the universe condensed into objects with mass $>M$

$$F(>M) = 2p(\delta > \delta_c | M) = \text{erfc} \left(\nu / \sqrt{2} \right)$$

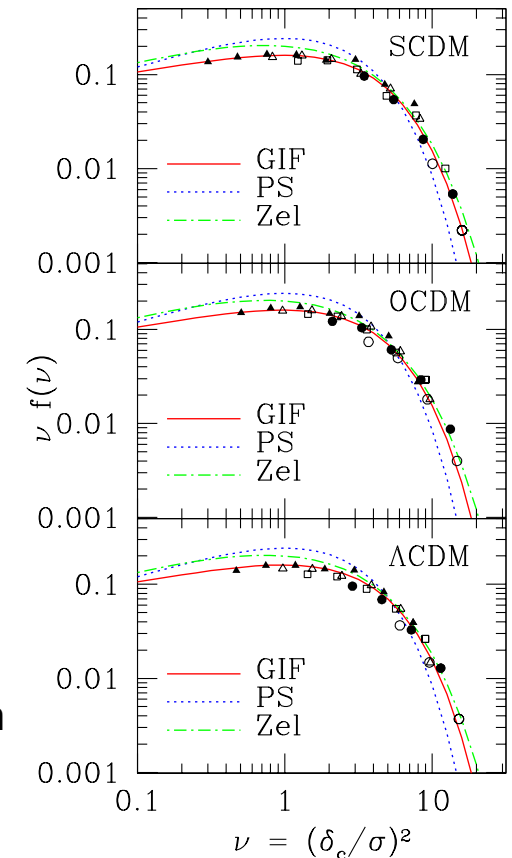
comoving number density of objects in the range dM

$$\frac{dn}{dM} = \frac{\rho_0}{M} \left| \frac{dF(>M)}{dM} \right|$$

$$\frac{dn}{dM} = f(\sigma) \frac{\rho_m}{M} \frac{d\sigma^{-1}}{dM} \quad f_{\text{PS}}(\sigma) = \sqrt{\frac{2}{\pi}} \nu \exp \left[-\frac{\nu^2}{2} \right]$$

For a power law power spectrum, it is a generalized Gamma (Schechter) function

$$\frac{dn}{dM} = \frac{1}{\sqrt{\pi}} \left(1 + \frac{n}{3} \right) \frac{\rho_m}{M^2} \left(\frac{M}{M_*} \right)^{(3+n)/6} \exp \left[- \left(\frac{M}{M_*} \right)^{(3+n)/3} \right]$$



[Sheth&1999MNRAS.308..119S]

N-body HMF

Alternative results from numerical simulations

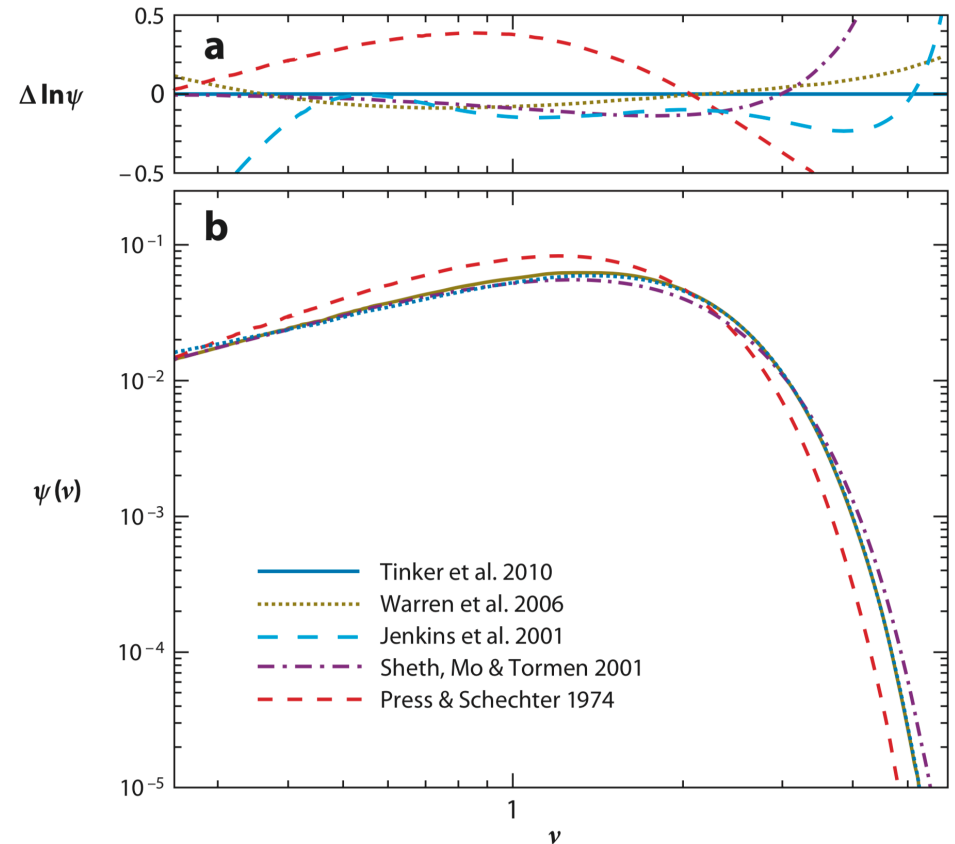
$$\frac{dn}{dM} = f(\sigma) \frac{\rho_m}{M} \frac{d\sigma^{-1}}{dM}$$

$$f_{\text{PS}}(\sigma) = \sqrt{\frac{2}{\pi}} \nu \exp\left[-\frac{\nu^2}{2}\right]$$

$$f_{\text{ST}}(\sigma) = A \sqrt{\frac{2a}{\pi}} \left(1 + \frac{1}{a\nu^{2p}}\right) \nu \exp\left[-\frac{a\nu^2}{2}\right]$$

$$f_{\text{Tinker}}(\sigma) = A \left(1 + \left(\frac{\sigma}{b}\right)^{-a}\right) \exp\left[-\frac{c}{\sigma^2}\right]$$

$$\frac{dn}{d \ln M} = \frac{\rho_m}{M} \psi(\nu)$$



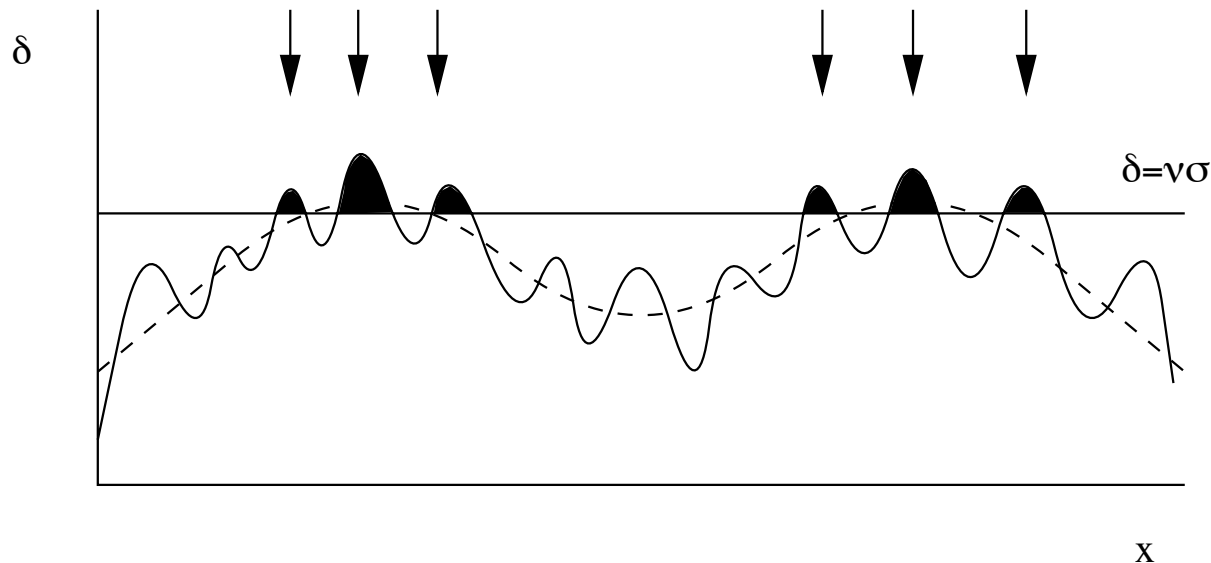
The function $\psi(\nu)$ defining the comoving abundance of collapsed halos for $z = 0$. Panel *a* shows deviations of specific models and calibrations from Tinker+10 [Kravtsov&2012ARA&A..50..353K]

Halo bias

Halos are biased mass tracers. A rare high density fluctuation, corresponding to a massive object, collapses sooner if it lies in a region of large-scale overdensity.

Overdense regions contain an enhanced abundance of massive objects with respect to the mean, so that these systems display enhanced clustering.

$$\left(\frac{\delta\rho}{\rho}\right)_{\text{halos}} = b \left(\frac{\delta\rho}{\rho}\right)_{\text{mass}}$$



The high-peak bias model. If we decompose a density field into a fluctuating component on galaxy scales, together with a long-wavelength 'swell' (shown dashed), regions of density that lie above a threshold in density of v times the rms will be strongly clustered. If proto-objects form at the sites of these high peaks (shaded, and indicated by arrows), then this is a population with Lagrangian bias - i.e. a non-uniform spatial distribution even prior to dynamical evolution of the density field [Peacock2003astro.ph..9240P].

The peak-background split

#1 dynamical effect: the large-scale disturbance move haloes closer together where $\langle \delta_m \rangle > 0$, giving a density contrast of $1 + \langle \delta_m \rangle$.

#2 statistical effect: if a constant shift $\langle \delta_m \rangle$ is added to the density perturbations over some large region, fluctuations only need to reach the threshold $\delta > \delta_c - \langle \delta_m \rangle$ to achieve collapse. This gives a bias in the number density of haloes in Lagrangian space: $\delta f/f = b_L \delta b$

$$\delta_h = \langle \delta_m \rangle + \frac{\delta f}{f} \langle \delta_m \rangle \quad f = dn/dM$$

$$\langle \delta_m \rangle = \left(\frac{\delta \rho}{\rho} \right)_m$$

$$\delta f = \frac{df}{d\langle \delta_m \rangle} \langle \delta_m \rangle = - \frac{df}{d\delta_c} \langle \delta_m \rangle$$

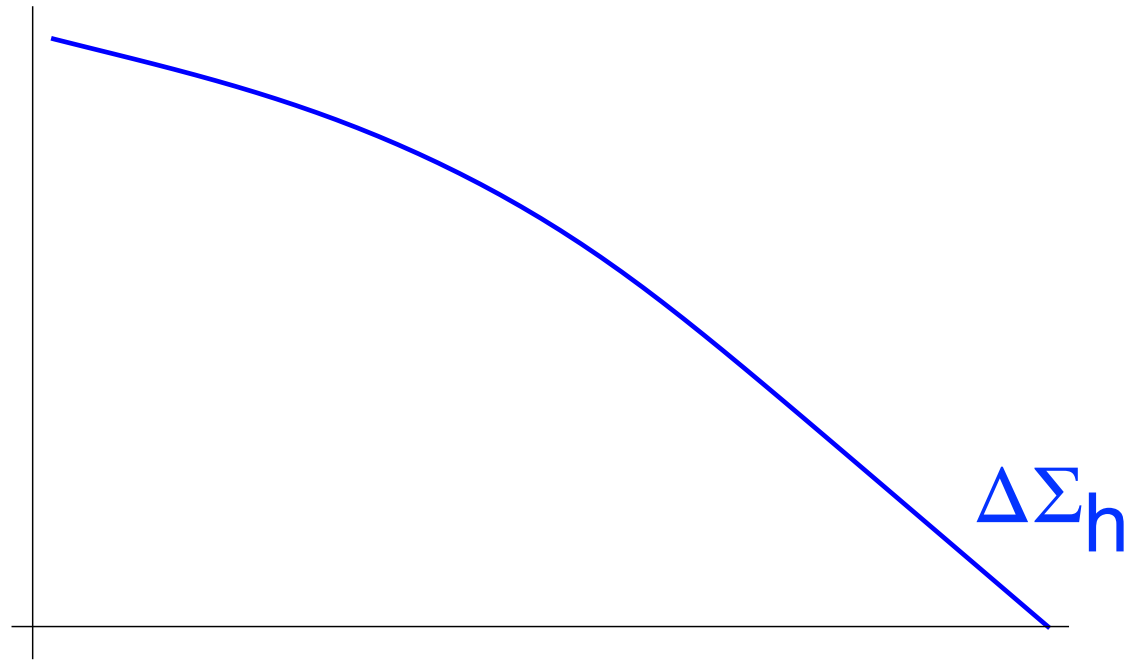
$$b = \delta_h / \delta_m$$

$$b = 1 - \frac{\delta \ln f}{d\delta_c}$$

$d/d\delta_c = \sigma(M)^{-1} (d/dv) = (v/\delta_c)(d/dv)$, since M is not affected by the threshold change,

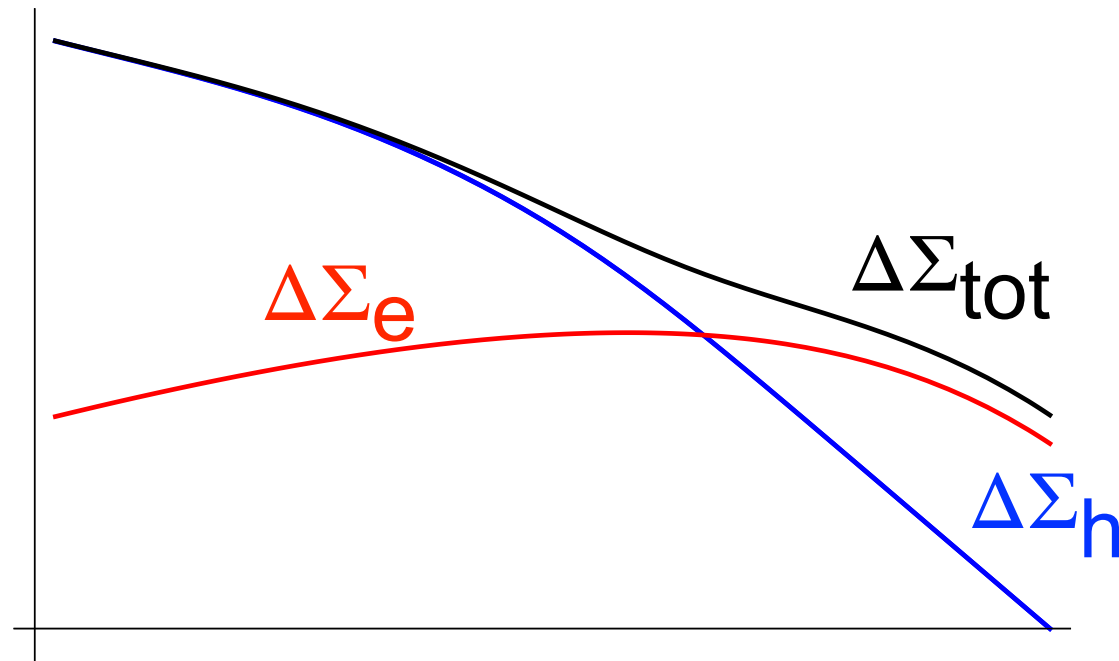
$$b_{PS} = 1 + \frac{v^2 - 1}{\delta_c}$$

Shear signal



Shear signal from the main halo

Shear signal



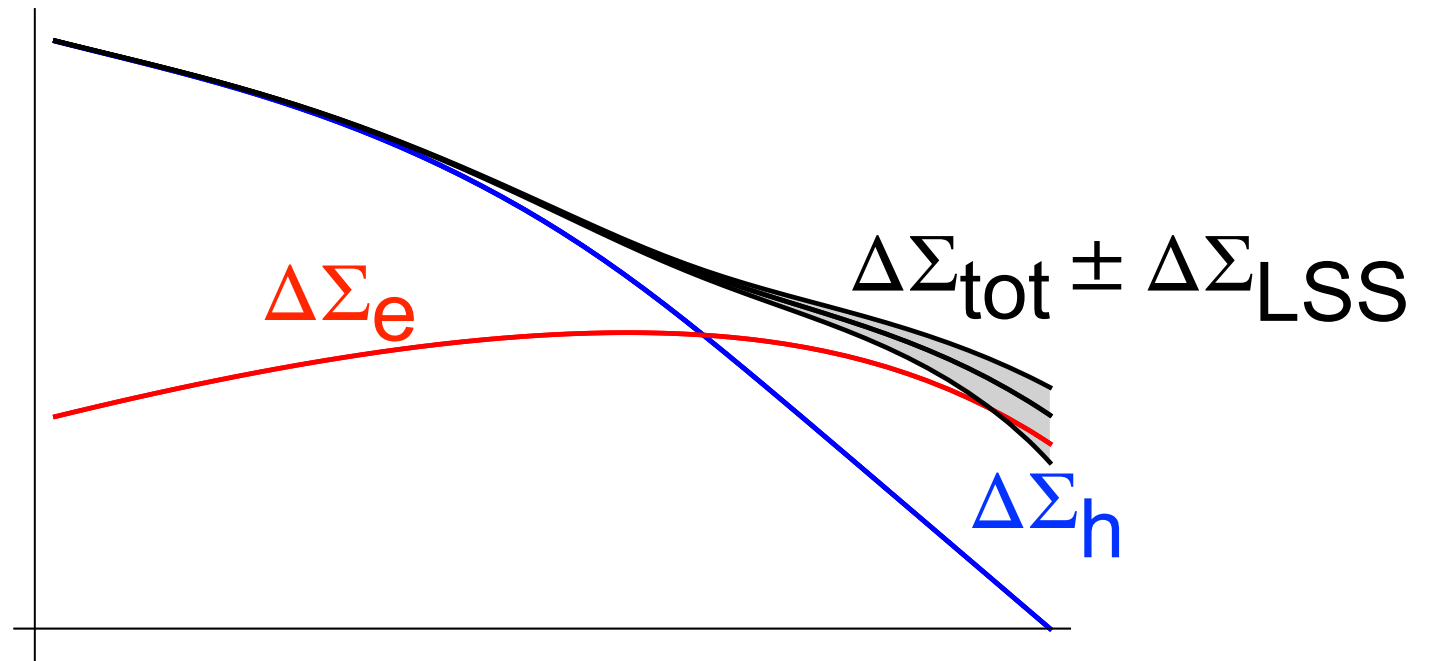
The contribution of correlated matter can be seen as a bump in the lensing signal

$$\Delta\Sigma_e(\theta; M, z) = b_e \frac{\bar{\rho}_M(z)}{(1+z)^3 D_d^2} \int \frac{l dl}{2\pi} J_2(l\theta) P_m(k_l; z)$$

halo bias: how much the cluster environment is overdense

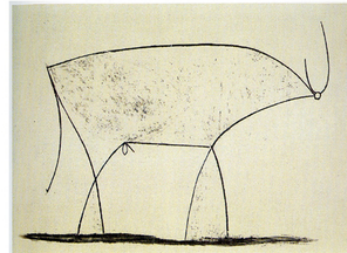
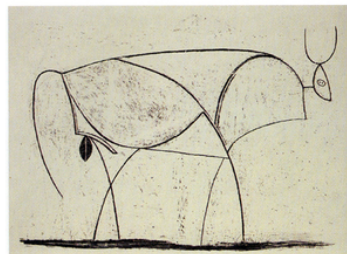
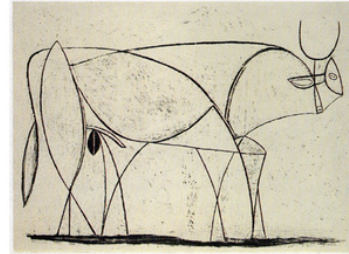
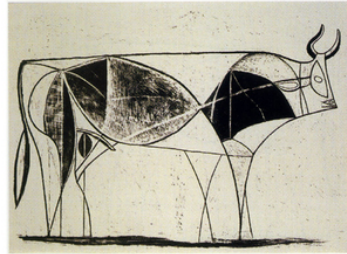
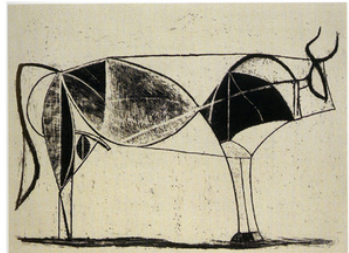
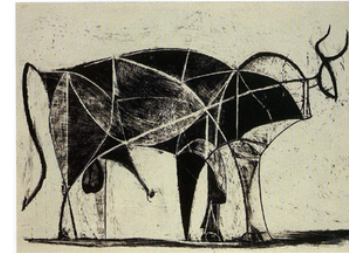
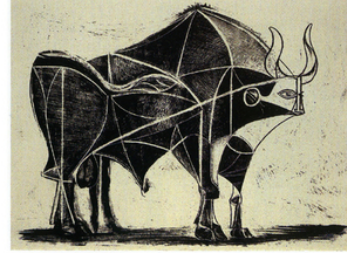
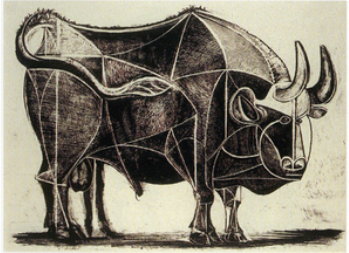
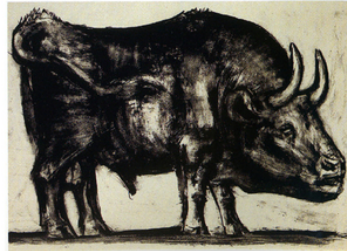
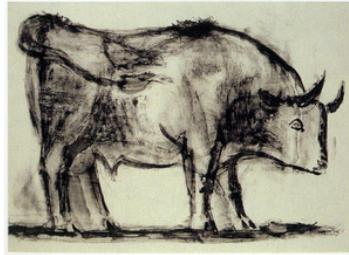
Power spectrum $\sim \sigma_8^2$

Shear signal



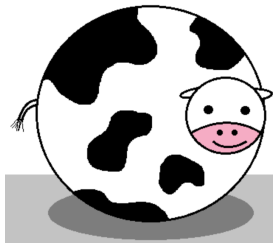
Large scale structure brings a positive or negative signal

$$\Delta\Sigma_{\text{tot}} = \Delta\Sigma_h + \Delta\Sigma_e \pm \Delta\Sigma_{\text{LSS}} \pm \delta\Delta\Sigma_{\text{Stat}}$$



[Picasso]

Part 2



<https://abstrusegoose.com/406>

Requirements for cosmology

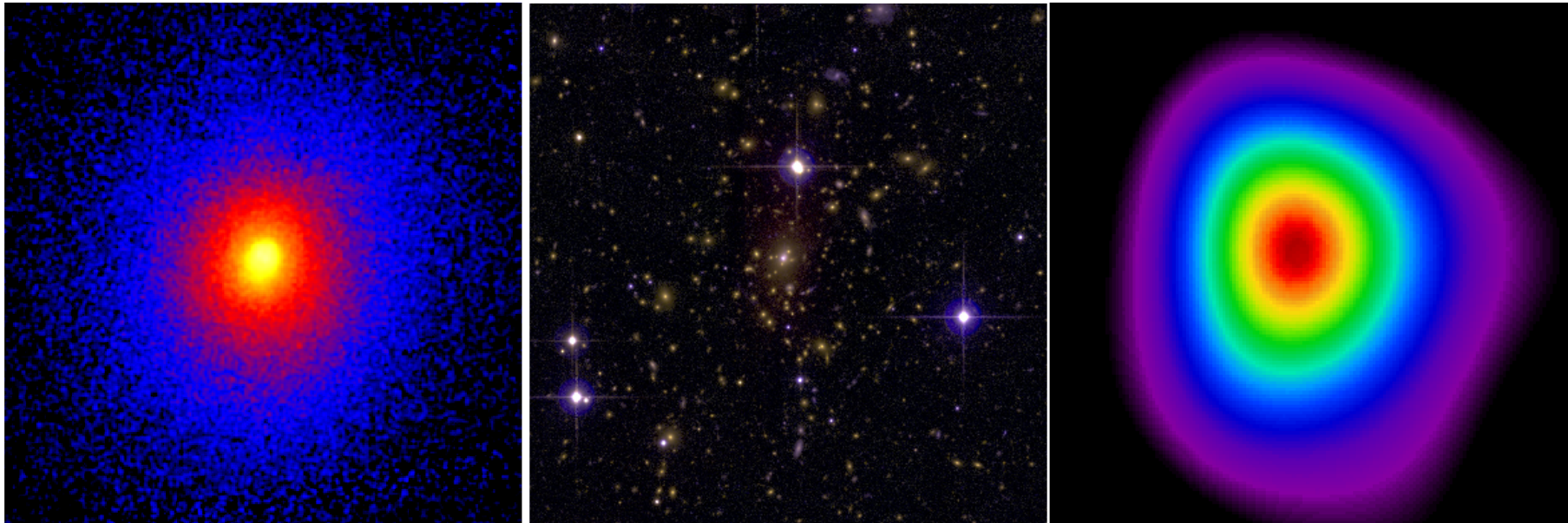
Large, statistically complete samples are needed for unbiased cosmological analyses

Direct mass measurements are available only for a small, not representative number of clusters

Mass can be based on proxies (luminosity, richness), this needs accurate scaling relations for calibration

Cluster detection

Clusters look very different at different wave-lengths

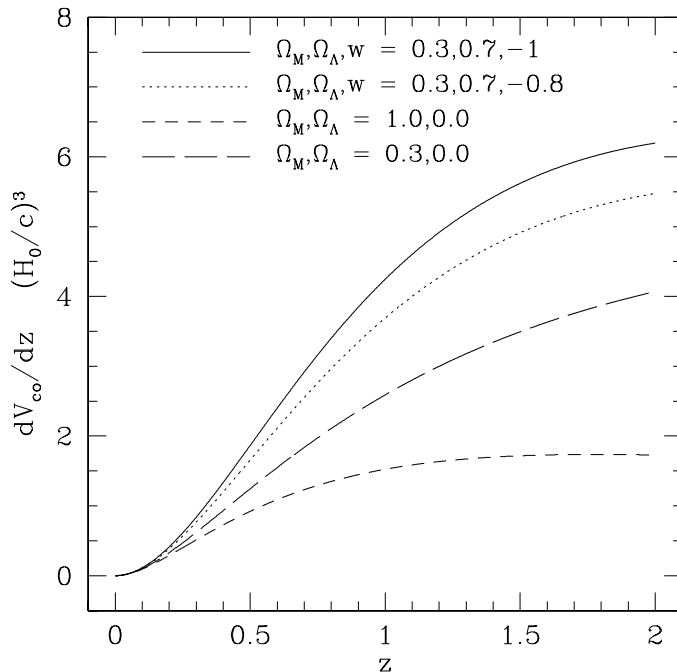


Images of Abell 1835 ($z = 0.25$) at (a) X-ray, (b) optical, and (c) millimeter wavelengths, exemplifying the regular multi-wavelength morphology of a massive, dynamically relaxed cluster. All three images are centered on the X-ray peak position and have the same spatial scale, 5.2 arcmin or ~ 1.2 Mpc on a side (extending out to $\sim r_{2,500}$). Figure credits: (left) X-ray: *Chandra X-ray Observatory*/A. Mantz; (middle) optical: Canada-France-Hawaii Telescope; (right) millimeter: Sunyaev Zel'dovich Array [Allen+2011ARA&A..49..409A]

Volume vs flux

There are not many clusters in the local universe. The comoving volume is small at low z

$$\frac{dV_C}{dzd\Omega} = D_H \frac{(1+z)^2 D_A^2}{E(z)}$$



Redshift dependence of comoving volume in various cosmologies. The quantity dV_{co}/dz is the comoving volume of the entire sky between redshift z and $z + dz$, divided by the interval dz . If clusters were a non-evolving population of objects, one could distinguish between these cosmologies simply by counting the number of clusters on the sky in each redshift interval. [Voit2005RvMP...77..207V]

The more distant the cluster, the more difficult to detect

If we select only clusters above a limiting flux, f_{th} , the threshold luminosity evolves as

$$L_{th}(z) = f_{th} D_L^2$$

Optical detection

Clusters are identified as galaxy overdensities in

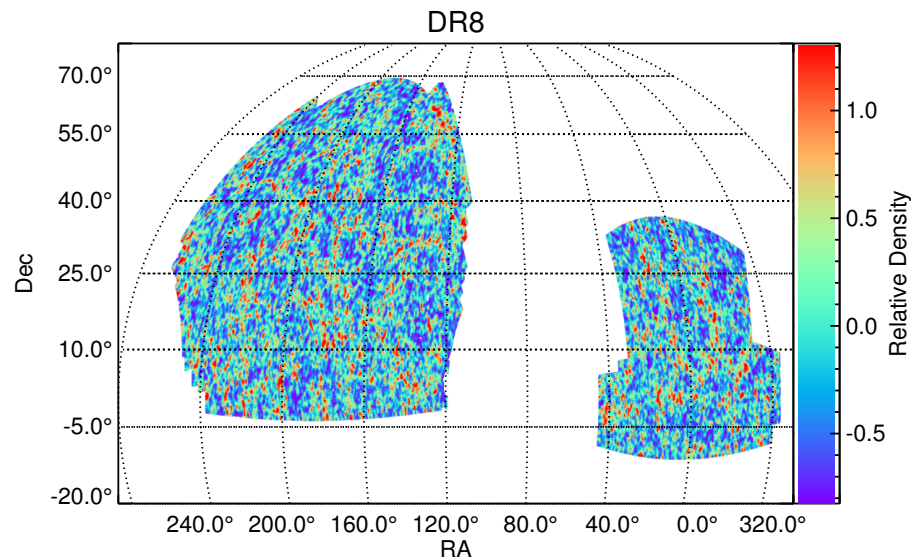
- ◆ space (2D or 3D if redshift available)
- ◆ magnitude
- ◆ colors
- ◆ around BCG

- ✓ Up to high z
- ✓ Down to low mass
- ✓ Methods can be optimized with astrophysics priors (CRS, MaxBCG)
- ✓ Optical surveys are WL surveys too

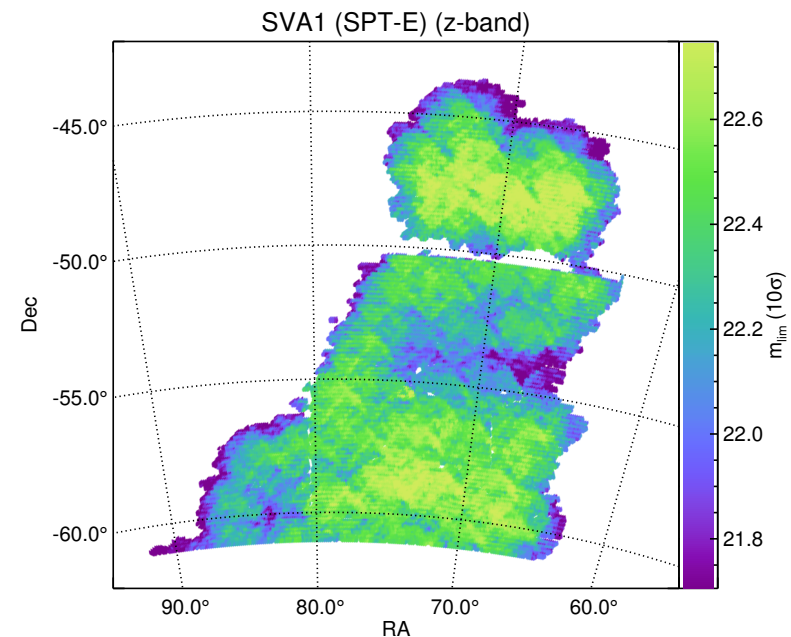
- Severe contamination and projection effects

Recent surveys

Catalog	Survey	deg ²	z	#clusters	reference
RedMapper	SDSS-DR8	10134	0.1-0.6	26111	2014ApJ...785..104R
RedMapper	DES-YR1	~1500	0.2-0.65	6504	2020arXiv200211124D
AMICO	KiDS-DR3	414	0.1-0.8	7988	2019MNRAS.485..498M
CAMIRA	HSC-S16A	232	0.1-1.1	1921	2018PASJ...70S..200



Angular cluster density contrast for the SDSS DR8 redMaPPer catalog in the redshift range [0.1, 0.3], averaged on a 30' scale. [Rykoff+16]
Total: 26111 clusters in 10134deg² in 0.1<z<0.6



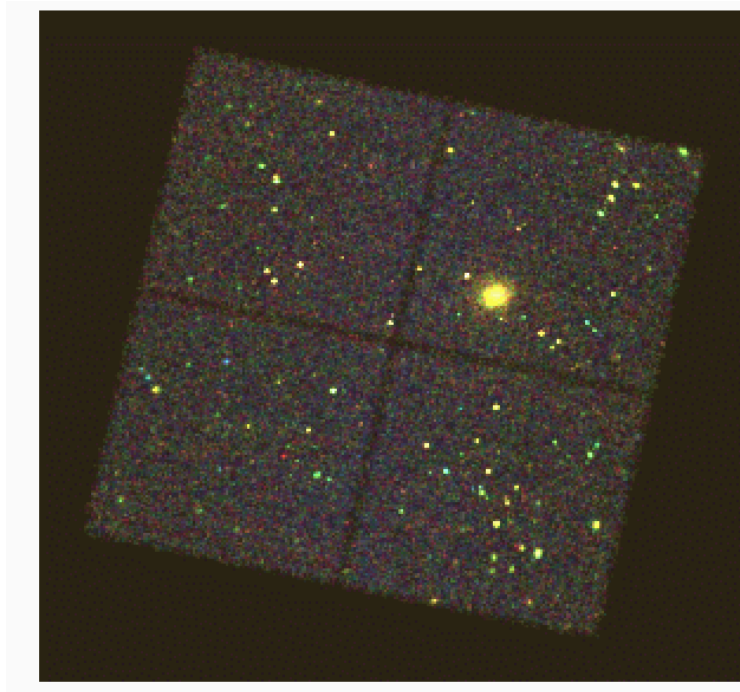
Angular cluster density contrast for the DES SVA1 redMaPPer catalog in the redshift range [0.2, 0.8], averaged on a 30' scale.

X-ray detection

Clusters appear as strong–contrast sources in the X-ray sky up to high redshifts, thanks to the dependence of the X-ray emission on the square of the gas density.

Given the relatively small number of sources, X-ray images of clusters are virtually free from contamination from foreground and background structures.

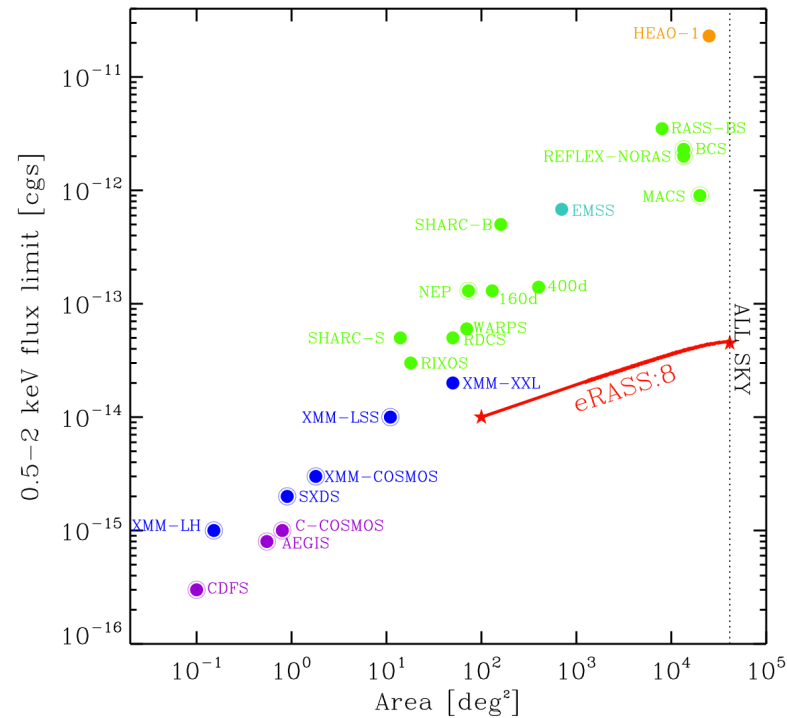
Clusters are the second most prominent sources in the X-ray sky (after AGN), at striking difference with the optical and millimetric bands where they have to struggle to emerge above other strong signals



The cluster MS1137, $z = 0.79$, in a $16' \times 16'$ field observed for 116 ks with the X-ray telescope Chandra ACIS–I detector. The cluster is the bright extended source in the center, while most of the remaining sources are AGN [Tozzi 06]

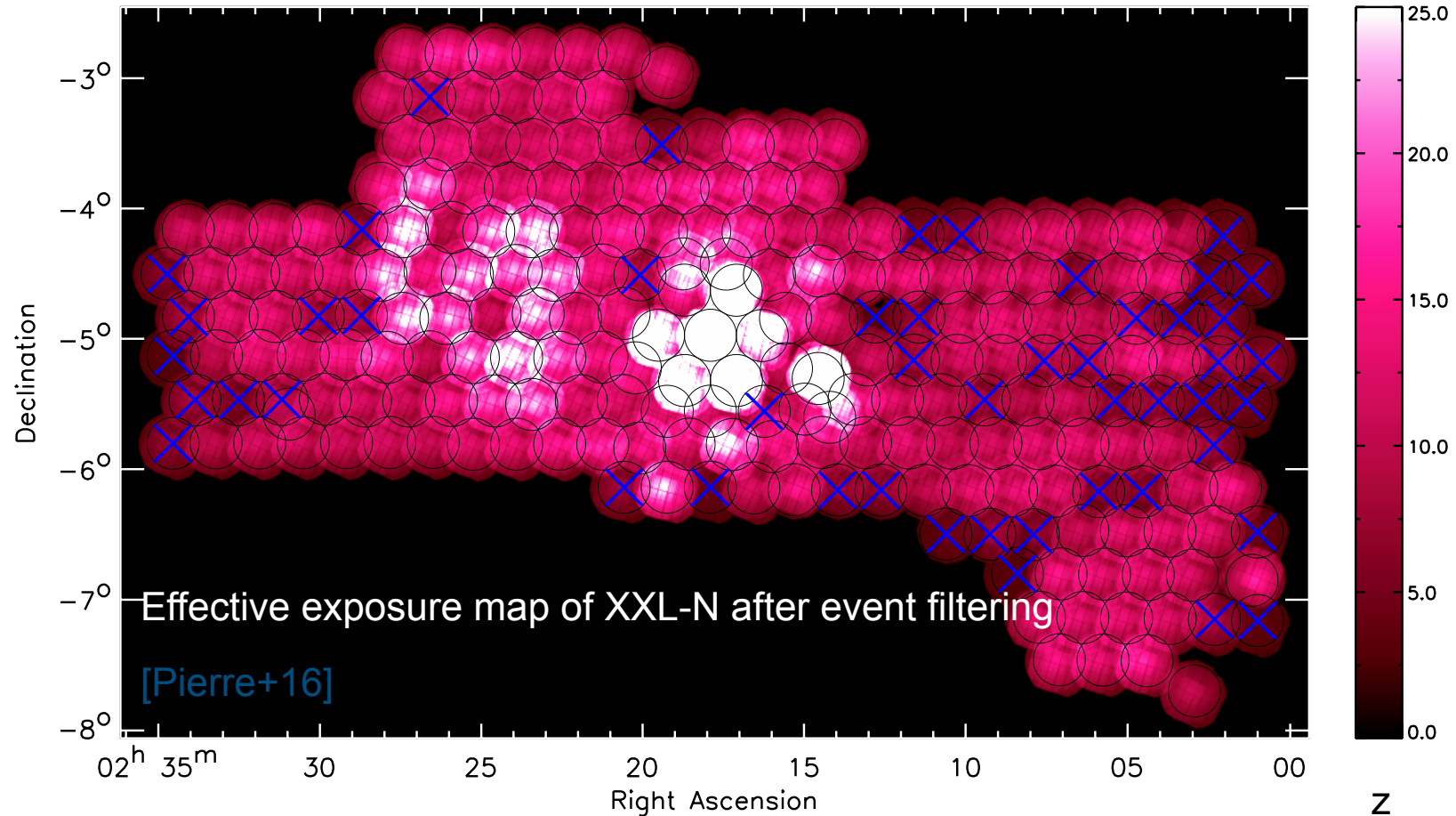
Recent and future X-ray surveys

MCXC [2011A&A...534A.109P]: meta-catalogue of X-ray detected clusters of galaxies based on publicly available ROSAT All Sky Survey-based (NORAS, REFLEX, BCS, SGP, NEP, MACS, and CIZA) and serendipitous (160SD, 400SD, SHARC, WARPS, and EMSS) cluster catalogues. The MCXC comprises 1743 clusters



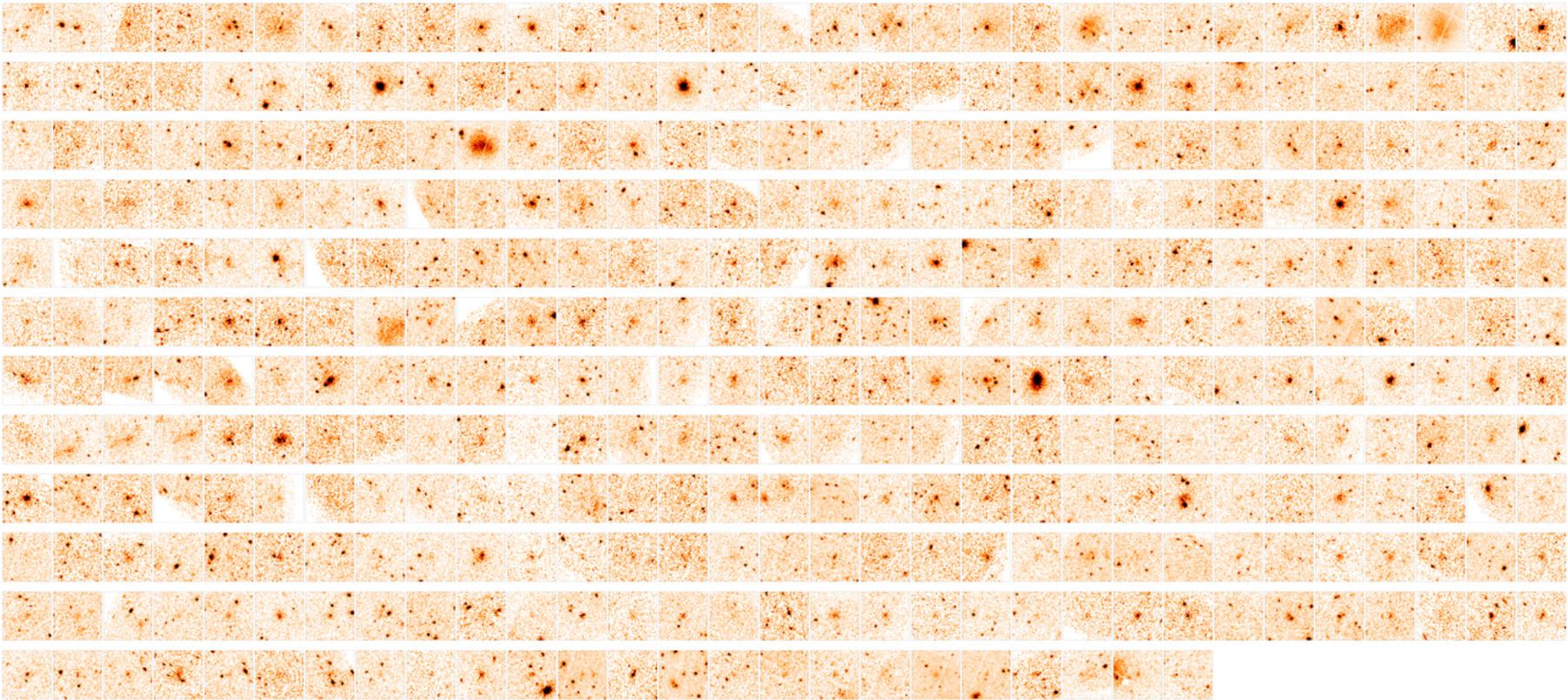
eRosita planned survey area versus flux in comparison to existing cluster surveys
[\[https://www.mpe.mpg.de/eROSITA\]](https://www.mpe.mpg.de/eROSITA)

XXL survey



- ❖ XMM Very Large Programme (6.9 Ms) surveying two 25 deg² fields
- ❖ depth of $\sim 6 \times 10^{-15}$ erg s⁻¹cm⁻² in [0.5-2] keV for point-like sources
- ❖ completeness limit of $\sim 1.3 \times 10^{-14}$ erg s⁻¹cm⁻² in [0.5-2.0] keV for extended sources
- ❖ 365 confirmed clusters

Clusters in XXL-DR2

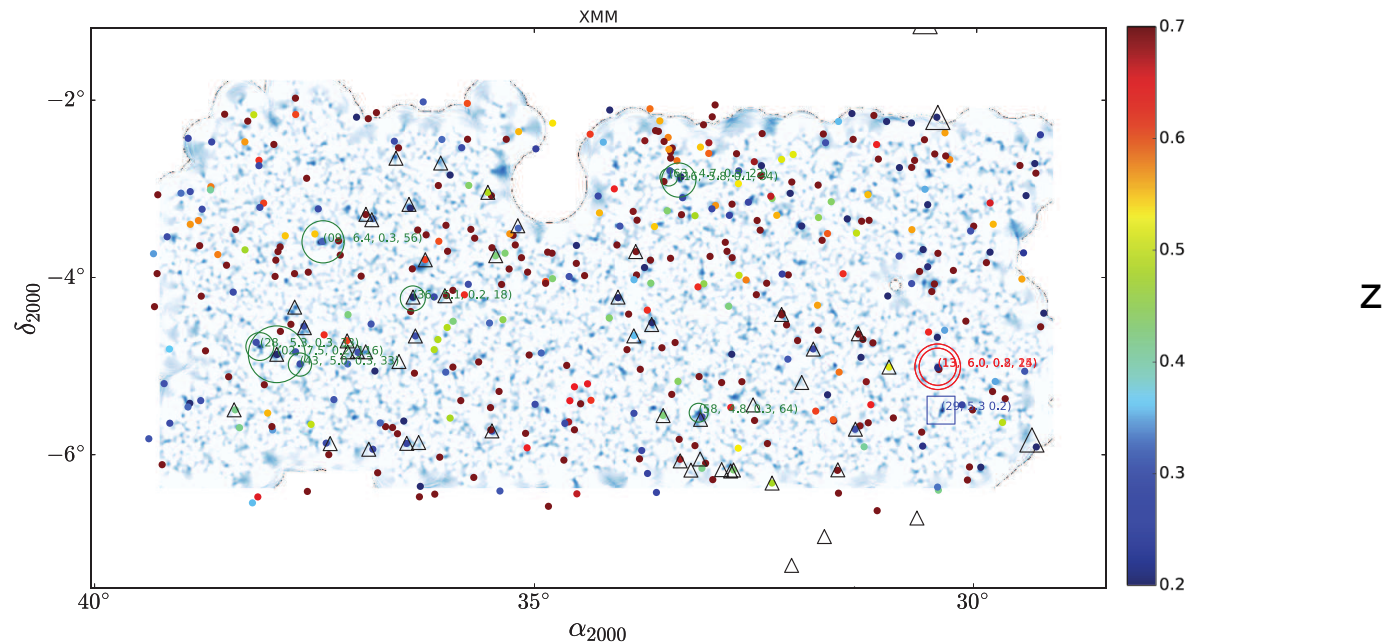


The 365 galaxy clusters of the XXL Survey DR2. *Credit: ESA/XMM-Newton/XXL Survey*

WL surveys

Identification of peaks in convergence (i.e. surface mass) maps

- ✓ mass selected sample
- ✓ Sensitive to sub-luminous clusters
- Severe contamination and projection effects
- Bias towards clusters elongated towards observer
- To date, only ~700 clusters (independently of the selection method) with measured WL mass [2015MNRAS.450.3665S]

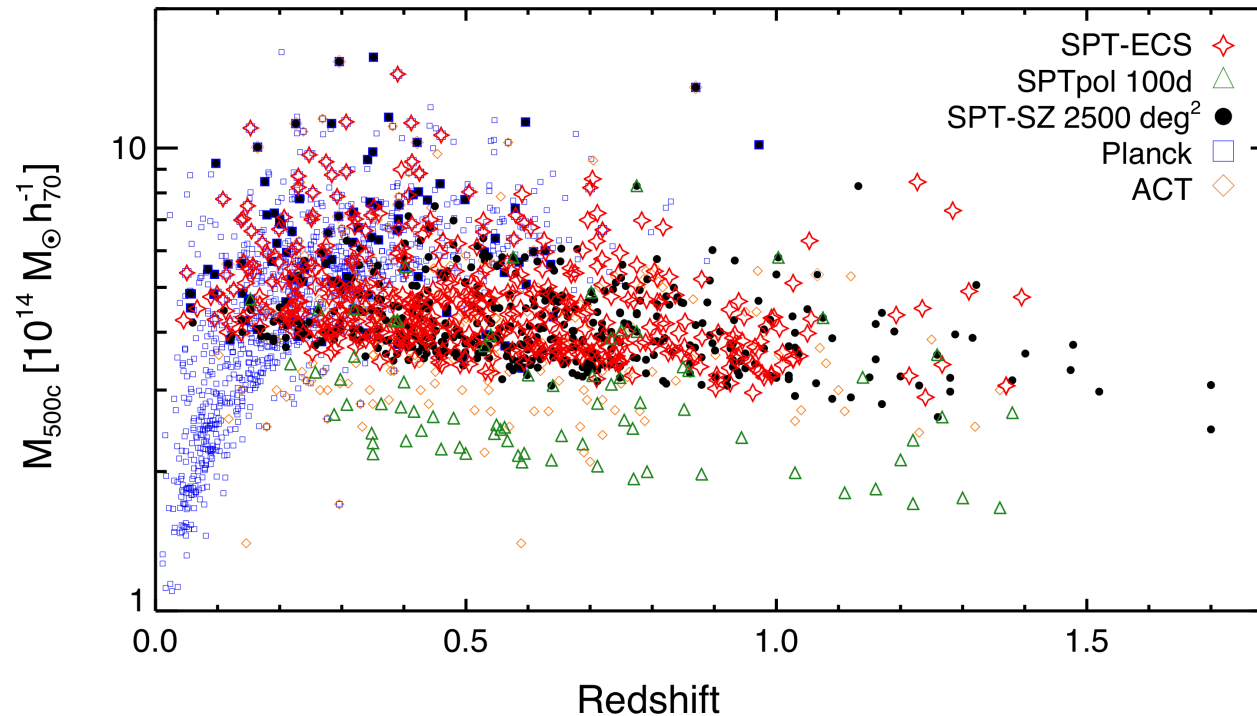


- ❖ WL mass aperture SN map for the XXL-N field [Miyazaki+2018PASJ...70S..27M].
- ❖ Hyper-Suprime-Cam is an optical 1.77 deg² wide-field imager. Optical imaging survey in five broad bands (*grizy*)
- ❖ to be observed 1400 deg² (Wide)
- ❖ limiting magnitude of *i* ~26 ABmag (5 σ for point sources)
- ❖ ~24 gal/arcmin² with measured shear

SZe surveys

Identification of shadows in millimeter maps

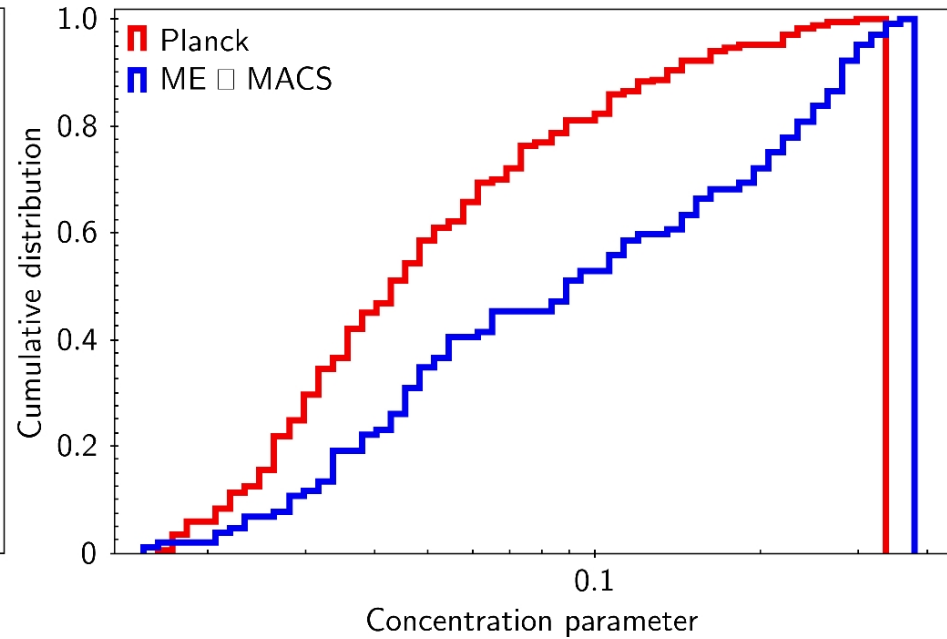
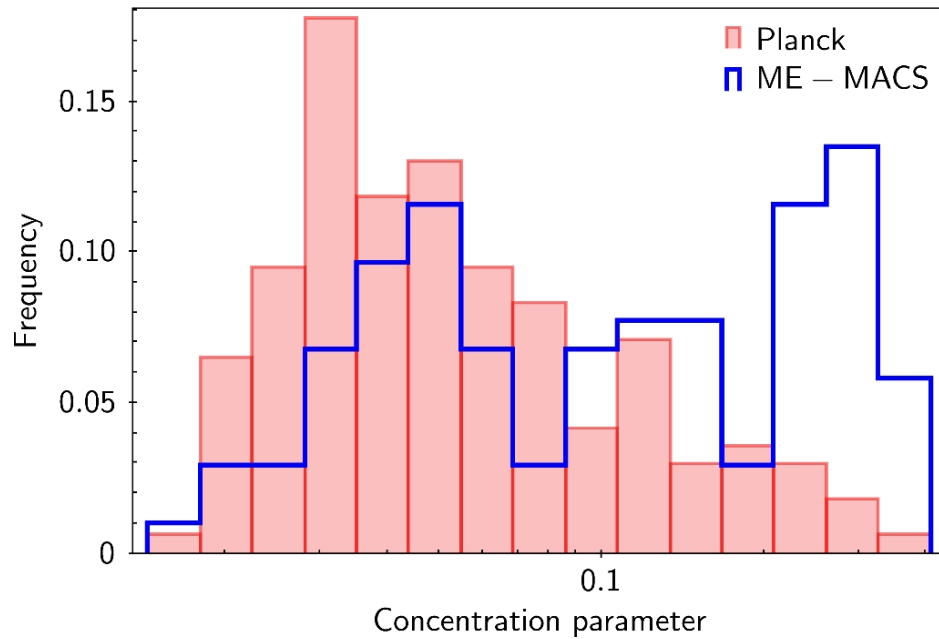
- ✓ Absence of the redshift dimming allows one to identify clusters virtually up to high z
- ✓ The selection criteria are nearly mass-like (pressure profile is nearly universal)
- Severe contamination and projection effects



Mass-Redshift Distribution of the SPT-SZ, the SPTpol 100d, and the SPT-ECS cluster samples: comparison of the 2500 deg² SPT-SZ cluster catalog [539 optically-confirmed clusters], the SPTpol 100d [79 clusters], and the SPT-ECS cluster sample [448 clusters] to other SZ-selected cluster samples, 220 clusters from the ACT survey, and 1094 SZ-selected clusters from the Planck survey with $M_{500c} > 1 \times 10^{14} M_{\text{sun}} h^{-1}$. [<https://pole.uchicago.edu/public/data/sptsz-clusters/>]

X-ray follow up of Planck clusters

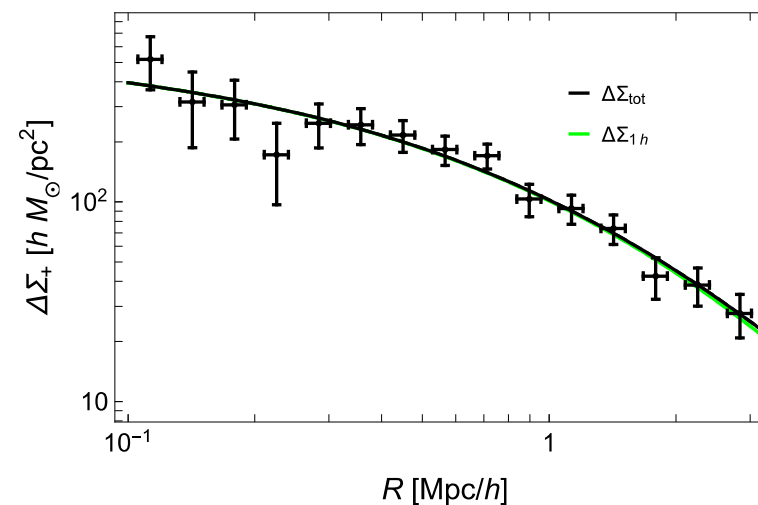
The cool core state of Planck SZ-selected clusters (PSZ1-cosmo) versus X-ray selected samples (e.g., MACS): no evidence for cool core bias [Rossetti+2017MNRAS.468.1917R]



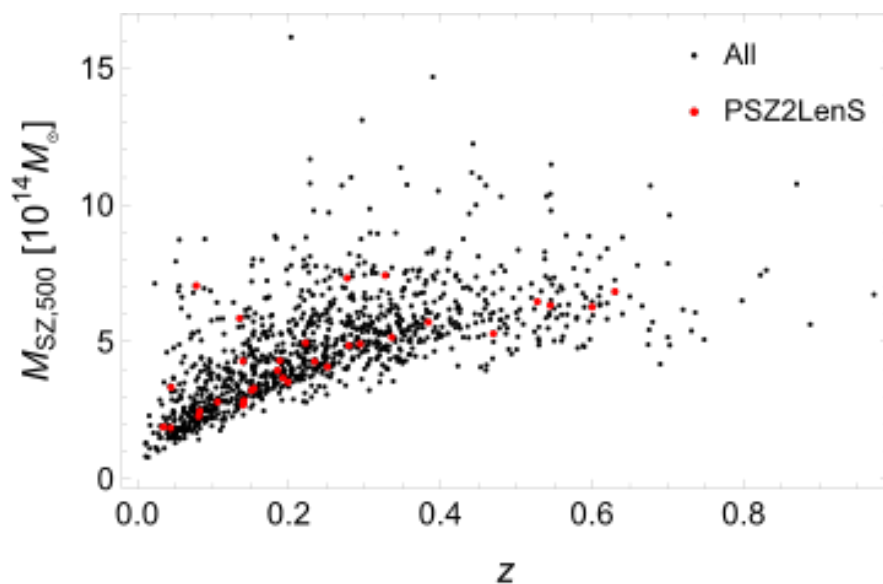
GL follow up of Planck clusters: PSZ2LenS

GL analysis of all (35) PSZ2 confirmed clusters in the field of the CFHTLenS/RCS2LenS.
Unbiased subsample of PSZ2
[Serenio+2017MNRAS.472.1946S]:

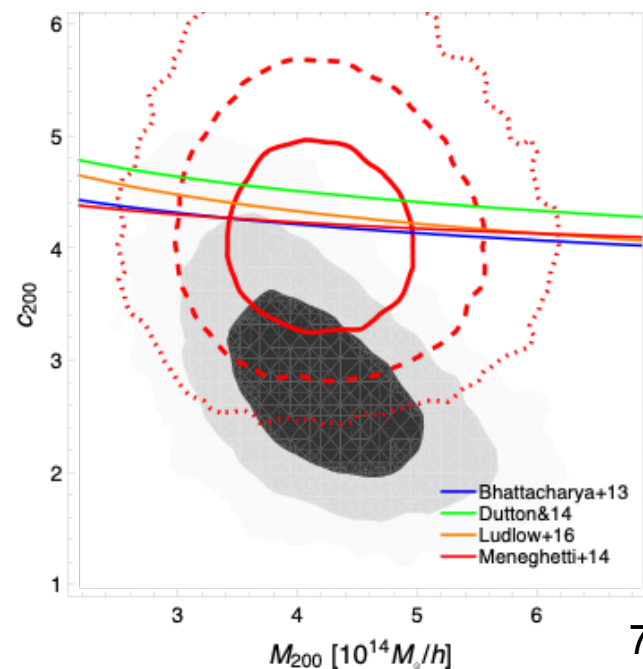
GL profile agrees with cuspy LCDM profiles



mass-concentration relation as in LCDM



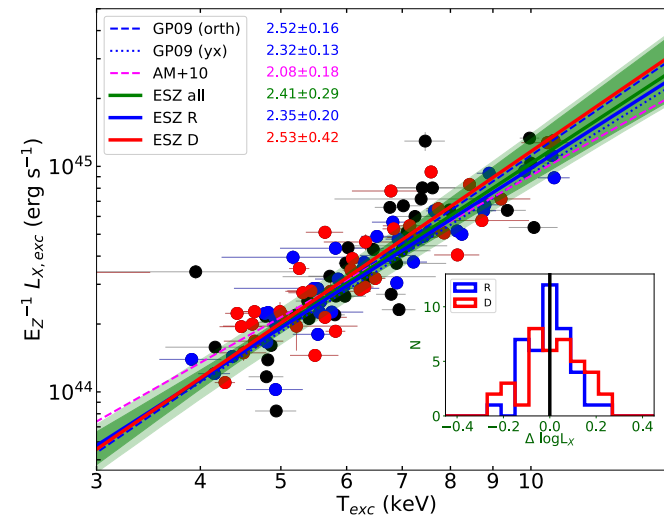
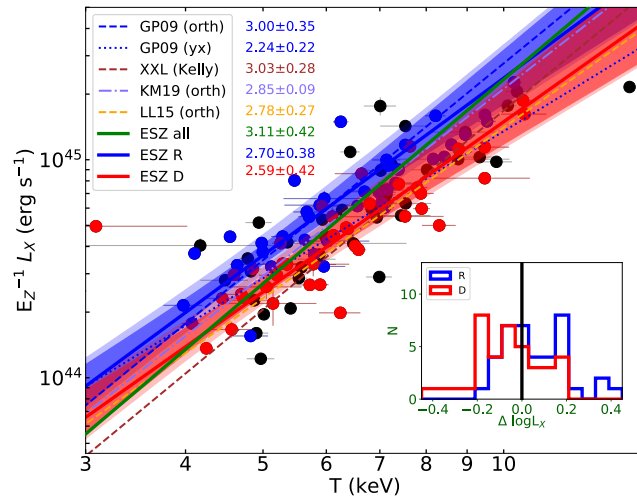
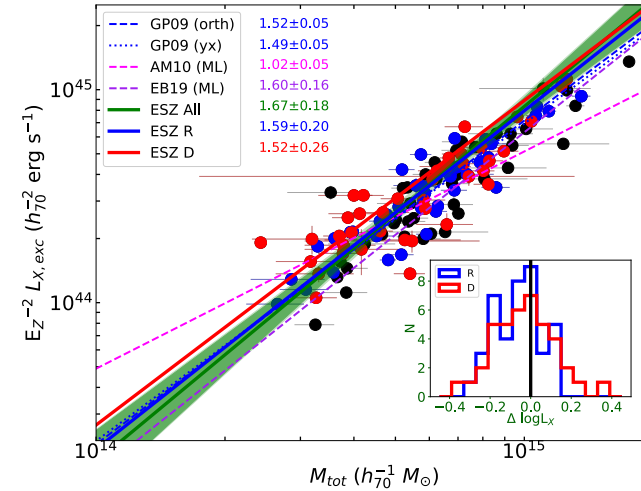
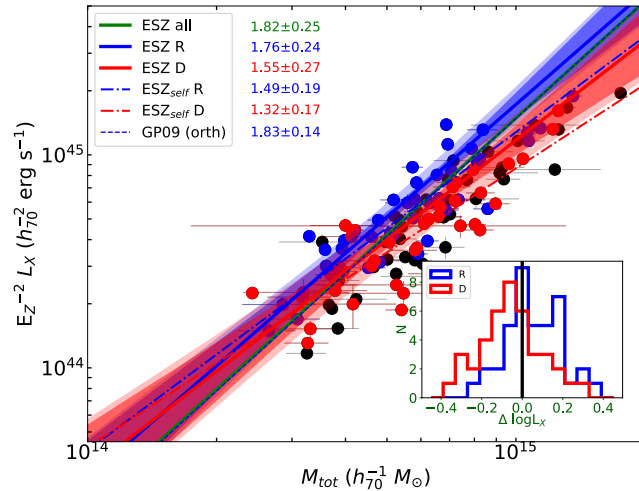
✓ PSZ clusters are a likely unbiased sample of the massive cosmological haloes



Relaxed vs disturbed

Relaxed clusters have on average ~30% higher X-ray luminosity than disturbed clusters at a given mass.

Using the core-excised cluster luminosities reduces the scatter and brings into better agreement the L– M_{tot} and L–T relations determined for different samples



X-ray scaling relations derived of 120 galaxy clusters in the Planck Early Sunyaev–Zel’dovich (SZ) sample spanning the redshift range of $0.059 < z < 0.546$ [Lovisari+2020ApJ...892..102L]

Detection algorithms

Clusters re very rare peaks

there are only ~2000 clusters with $M > 10^{15} M_{\text{sun}}$

Most detections techniques can be used at different wave-lengths

Some algorithms relies on specific feature in a given wave-length

Matched Filter

The spatial and luminosity distribution of observed galaxies in a given field is modeled as the sum of two contributions, one from the field, another from the cluster. Clusters are identified by scanning a map with a filter (i.e. moving box of given size centered on each pixel) and searching for peaks

$$D(\theta, \mathbf{m}, z) = A(\theta_c, z_c) \times M_c(\theta - \theta_c, \mathbf{m}, z) + N(\mathbf{m}, z)$$

D: Data, e.g. galaxy density

N: noise

A Signal Amplitude

M_c : model for a cluster centered in θ_c, z_c , e.g. the product of the projected radial profile of the cluster galaxies as a function of the projected radial distance from the cluster center and the differential cluster luminosity function

Optimal filtering

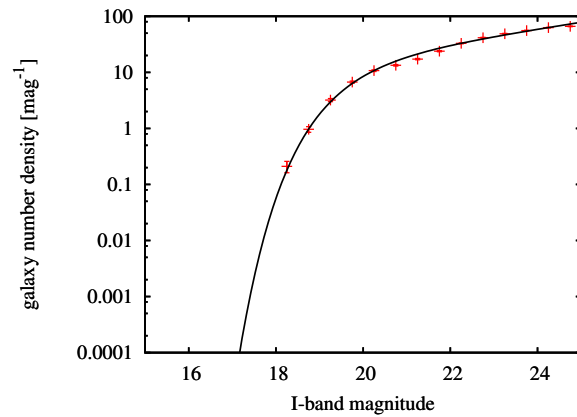
$$A(\theta_c, z_c) = \frac{\int \psi_c(\theta_c, \mathbf{m}, z_c) D(\theta, \mathbf{m}, z) d^2\theta dm dz}{\int \psi_c^2(\theta_c, \mathbf{m}, z_c) N(\mathbf{m}, z) d^2\theta dm dz} - B(z)_c$$

$$\psi_c = M_c(\theta - \theta_c, \mathbf{m}, z) / N(\mathbf{m}, z)$$

Filters

$$D(\theta, \mathbf{m}, z) = A(\theta_c, z_c) \times M_c(\theta - \theta_c, \mathbf{m}, z) + N(\mathbf{m}, z)$$

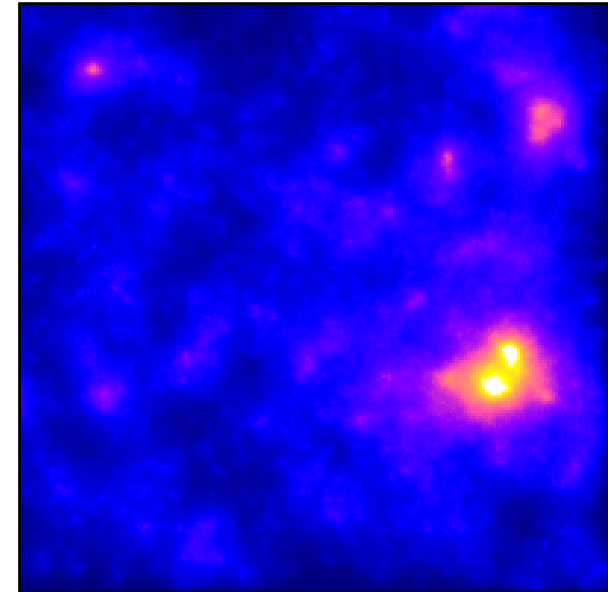
Filters



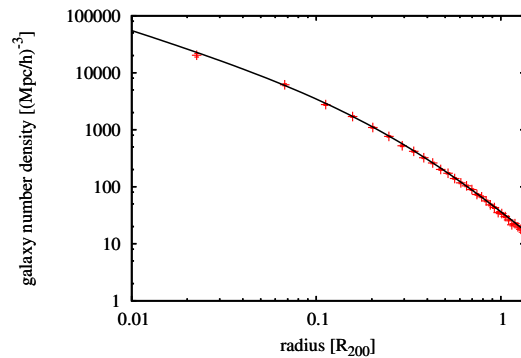
Model distributions

Schechter luminosity function,
 $f(L) \sim L^{-\alpha} \exp(-L/L_*)$, for the
cluster galaxies
[Bellagamba+18]

Map



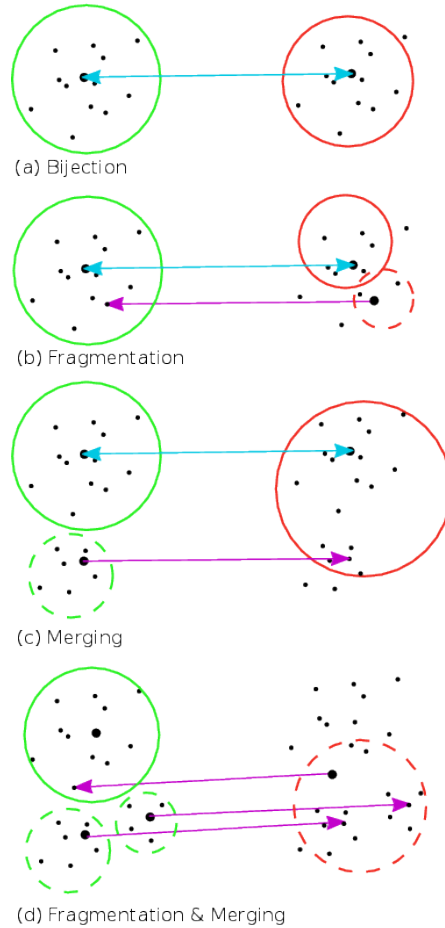
Amplitude map of $1 \times 1 \text{ deg}^2$ at $z = 0.33$
[Bellagamba+18]



NFW for radial distribution
[Bellagamba+18]

Friends of Friends

This method links together all galaxies within a chosen linking volume centered on each galaxy.

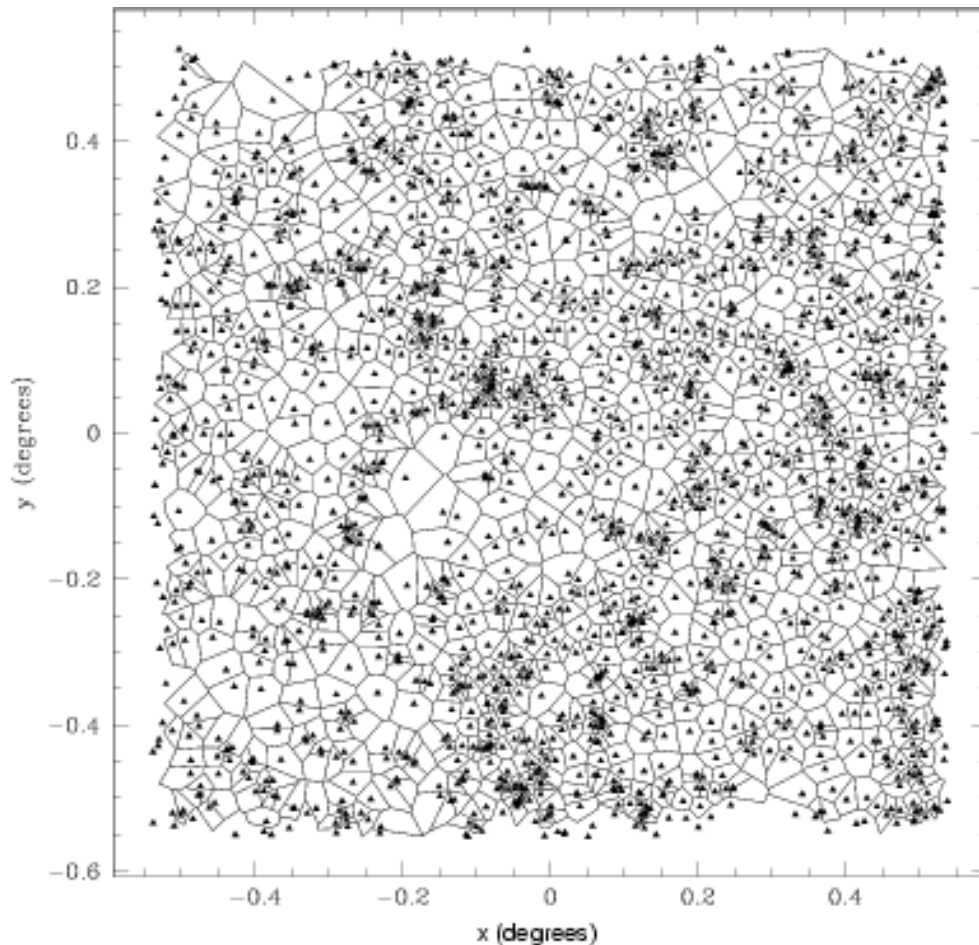


[Duarte&14]

Voronoi tessellation

With Voronoi Galaxy Cluster Finder, the projected space is divided in cells according to the Voronoi tessellation technique, each cell containing a single point (i.e. a galaxy). The inverse of the cell area defines the local galaxy density. Clusters are defined as ensembles of adjacent cells with a density above a given threshold.

The main advantages of this method is that it is nonparametric and as such it does not require a priori hypotheses on the cluster properties, such as cluster size, density profile, or shape

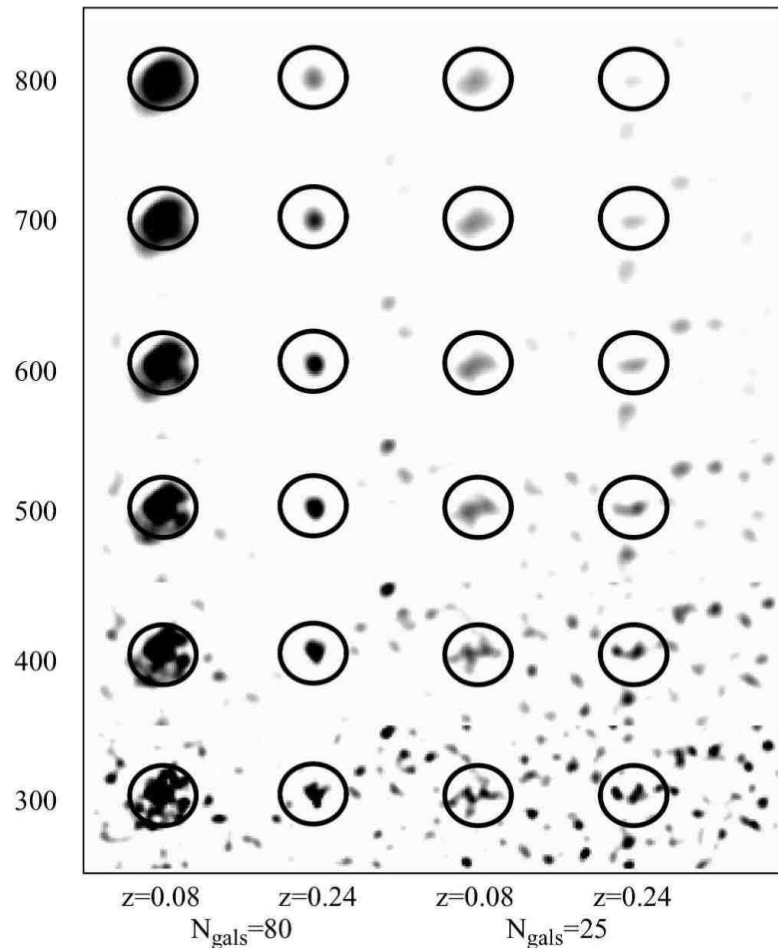


Voronoi tessellation of a galaxy field. Each triangle represents a galaxy position on the plane of the sky [Ramella+01]

Smoothed maps

A smooth density map can be generated with an [adaptive kernel](#) whose size changes as a function of the local density, with a smaller kernel at higher density or with [wavelet smoothing](#)

After cluster detection can be performed analogously to object detection in standard astronomical images.



The effect of varying the initial smoothing window for the adaptive kernel on cluster appearance. Each panel contains a simulated background with four simulated clusters, as described in the text. The smoothing kernel ranges in size from 300' to 800" in 100" increments [Gal+03].

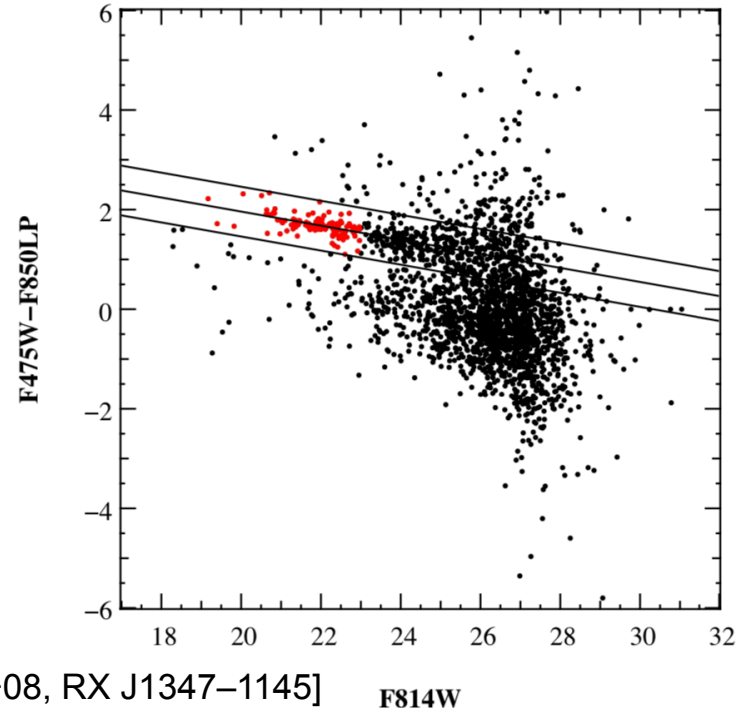
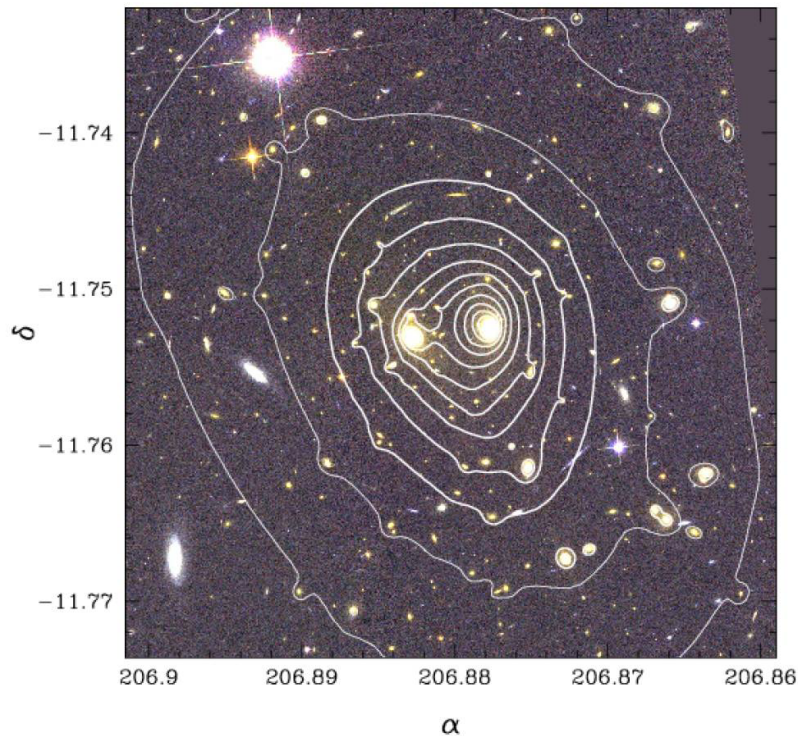
The Cluster Red Sequence method

Rich clusters, up to $z \sim 1$, have a more or less well defined red sequence of galaxies in a color–magnitude diagram, where the color is defined by two photometric bands bracketing the 4000 \AA break feature of galaxy spectra.

The method consists in slicing a given galaxy catalog in color, computing the galaxy surface density of that slice, and identifying significant overdensities

Since the 4000 \AA break is redshifted into different observational bands depending on the galaxy z , with a suitable set of filters it is possible to define color-cuts to select galaxies at a redshift close to the cluster mean redshift.

By comparison with spectrophotometric models, the CRS method also provides estimates of the mean redshifts of the detected clusters.



[Halkola+08, RX J1347-1145]

$F814W$

Mass calibration

Large number of clusters without a direct mass estimate

Unbiased scaling relations are needed to calibrate mass

Given a cheap proxy (richness, luminosity,...), we estimate the mass

conditional probability: $P(\text{mass} \mid \text{proxy})$

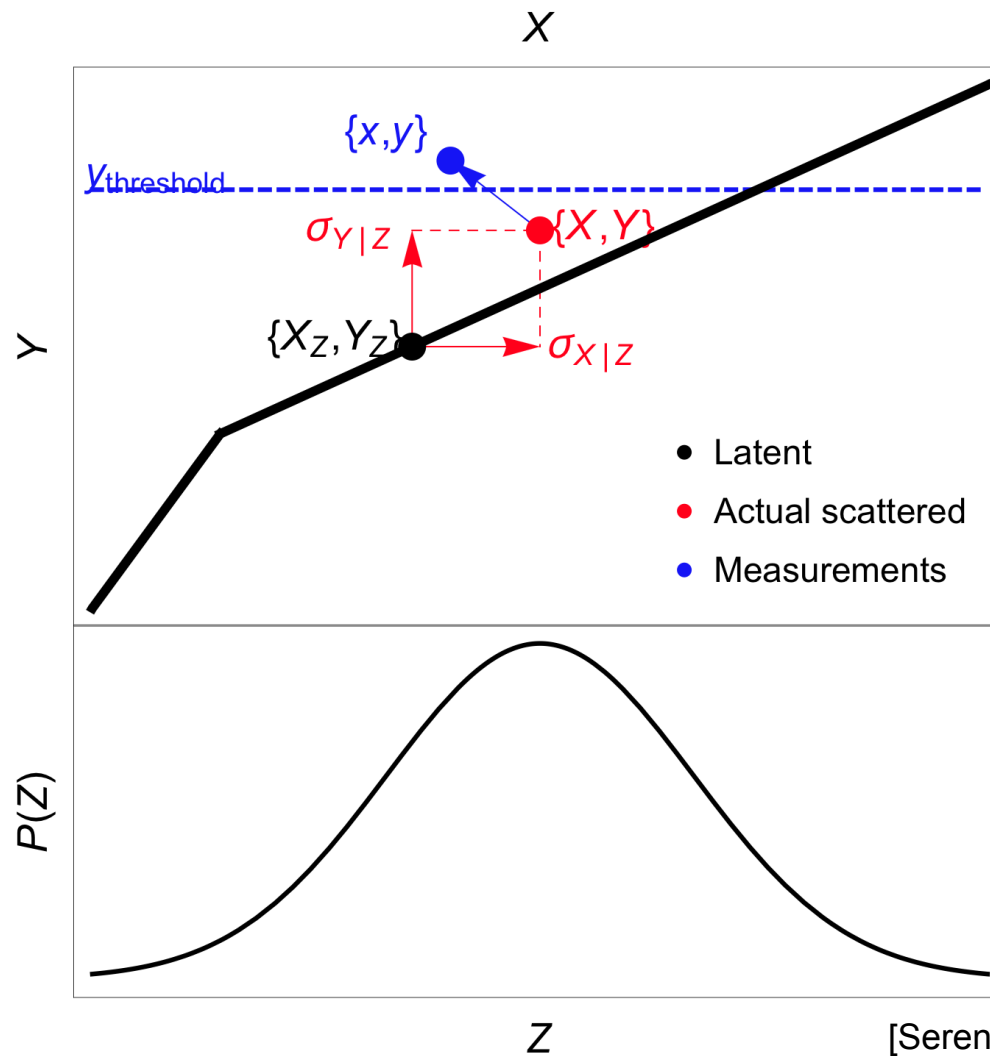
Scaling relations are approximately power-law \rightarrow linearity in log space

The intrinsic scatter is approximately log-normal

We can either:

- ❖ use a reference calibration sample with measured masses
- ❖ stack the signal of low mass halo to get average mass measurements for low SNR objects

Bayesian hierarchical regression



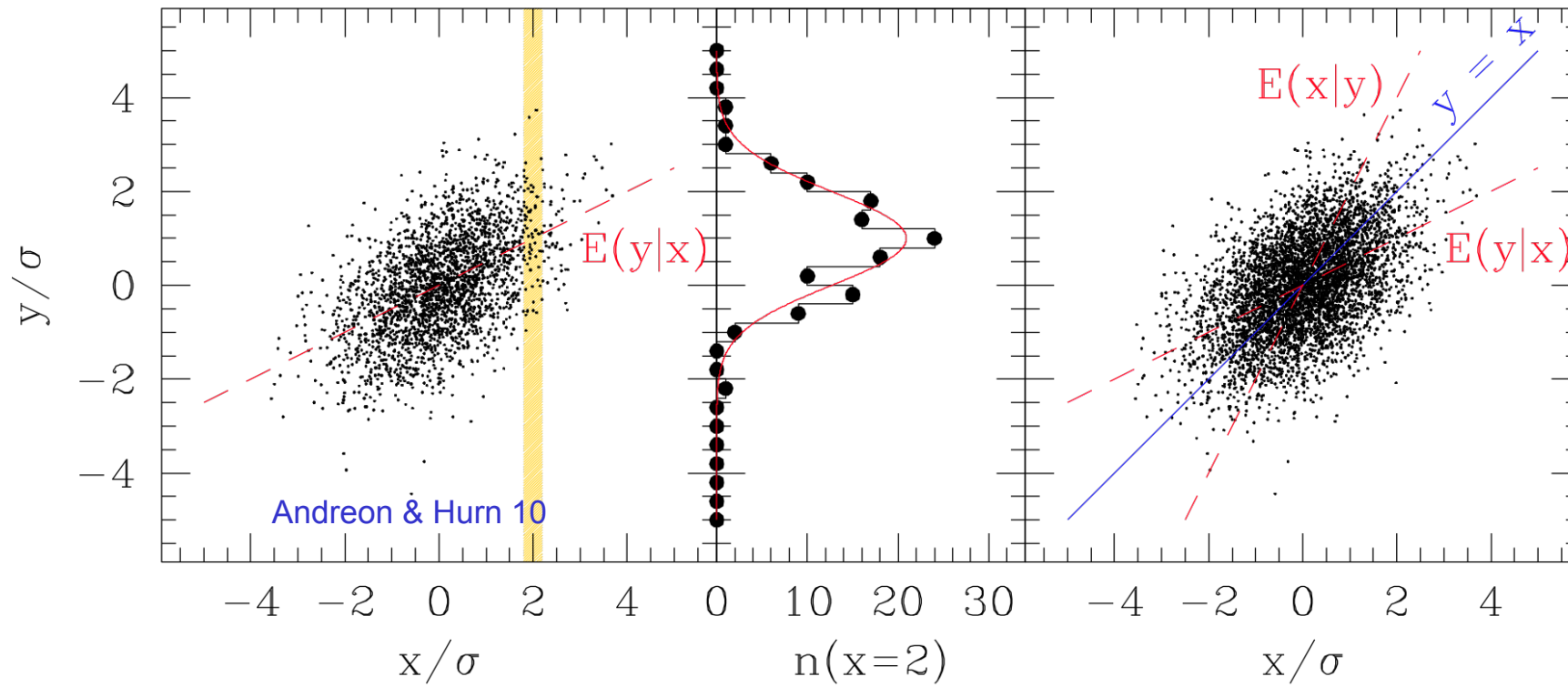
Public software:

» [linmix_err.pro](#) [Kelly2007ApJ...665.1489K]

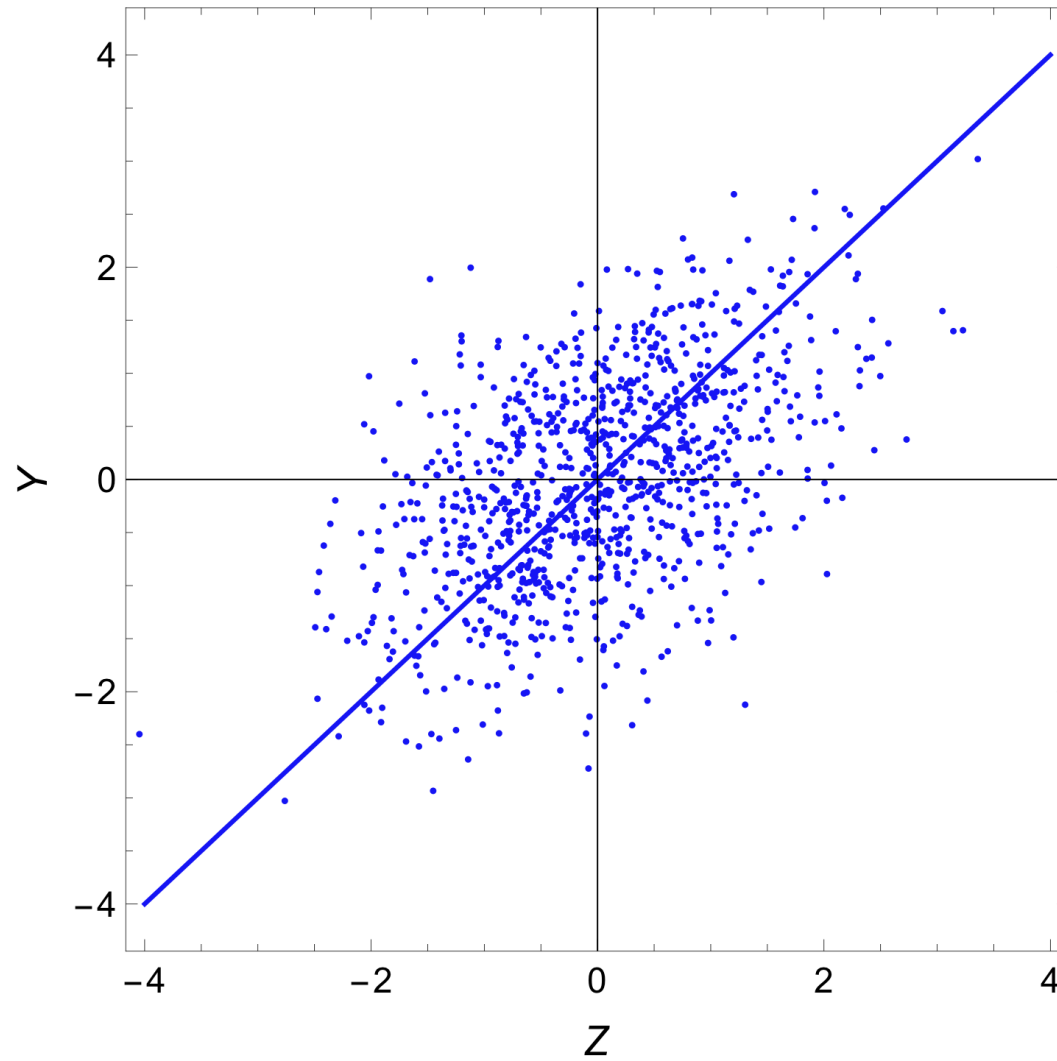
» LIRA: linear regression in Astronomy, R- package [Sereno2016MNRAS.455.2149S]

» LRGS: Linear Regression by Gibbs Sampling [Mantz2016MNRAS.457.1279M]

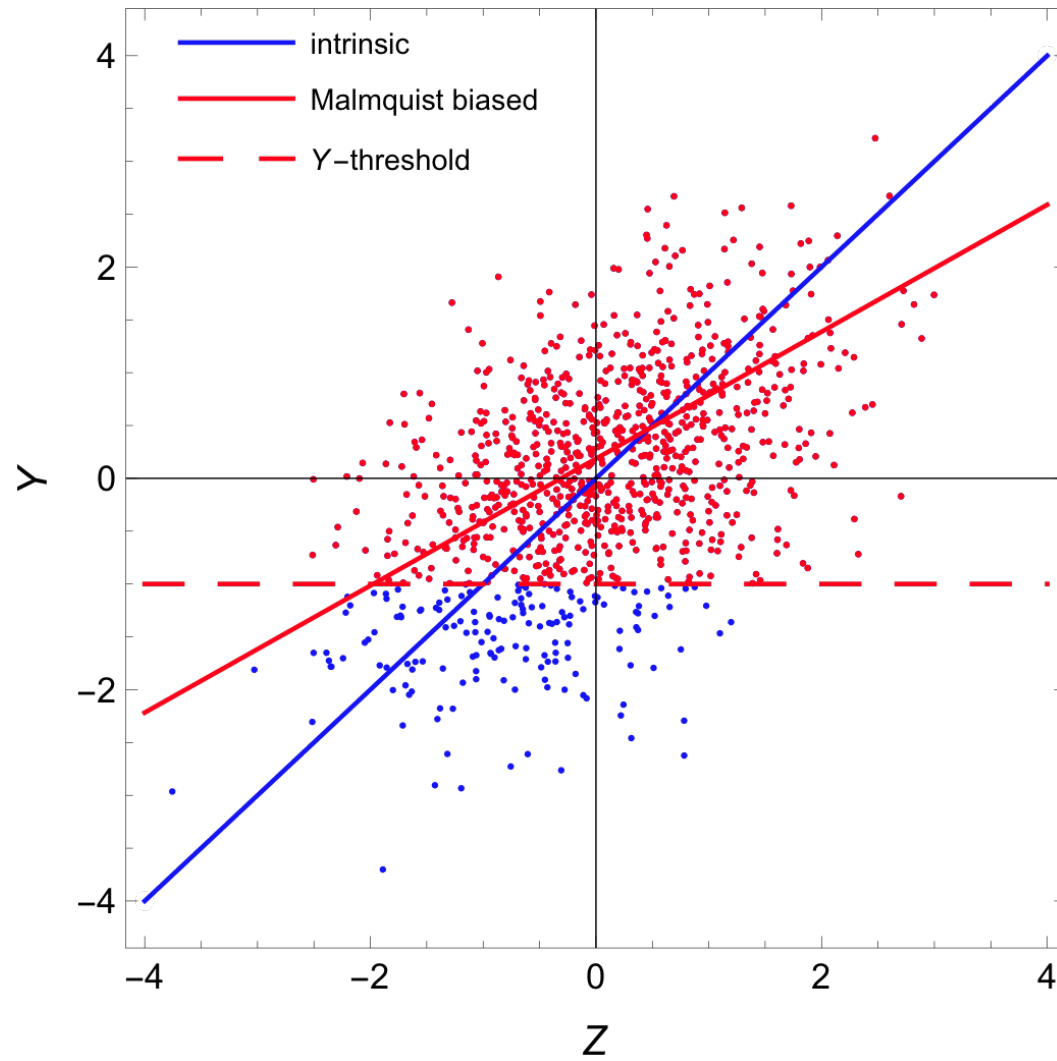
Conditional probability



Malmquist bias

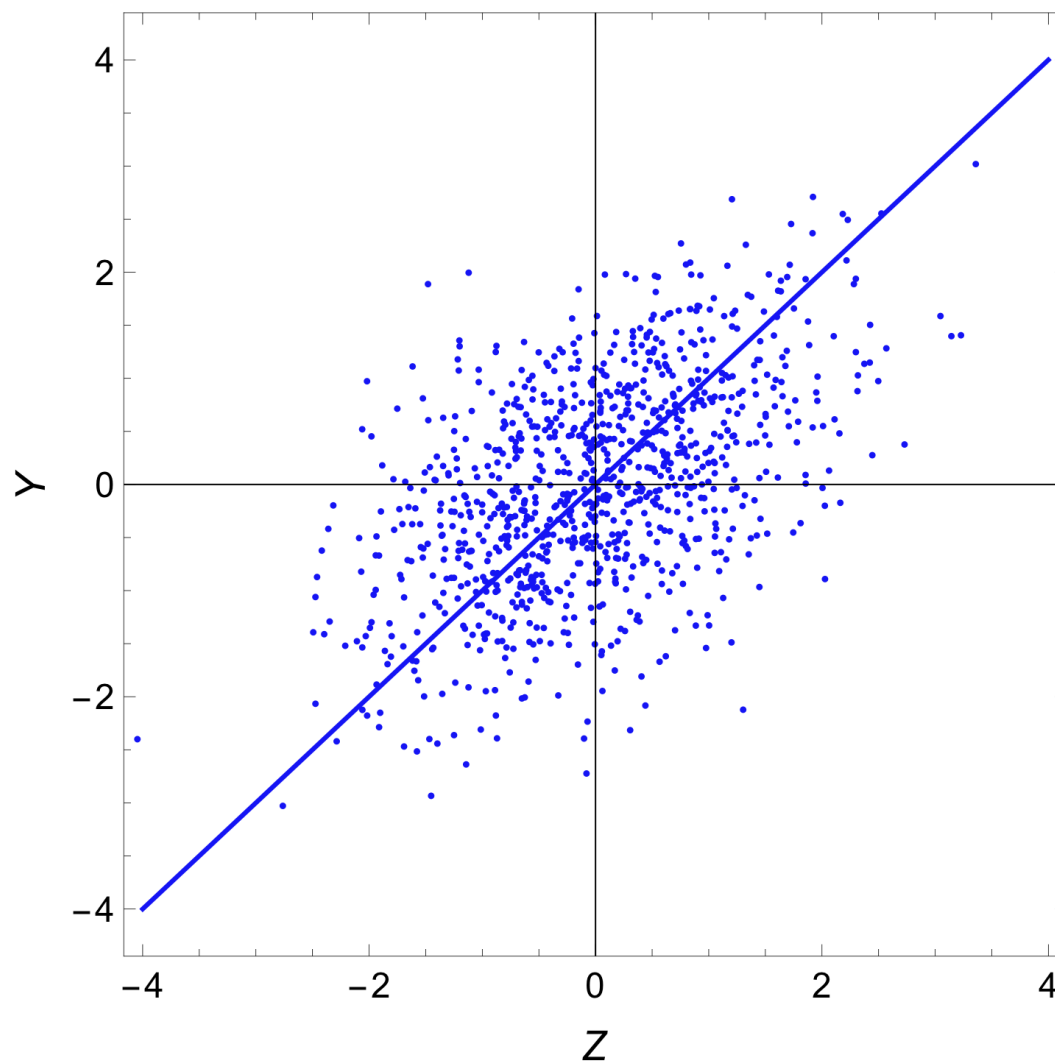


Malmquist bias



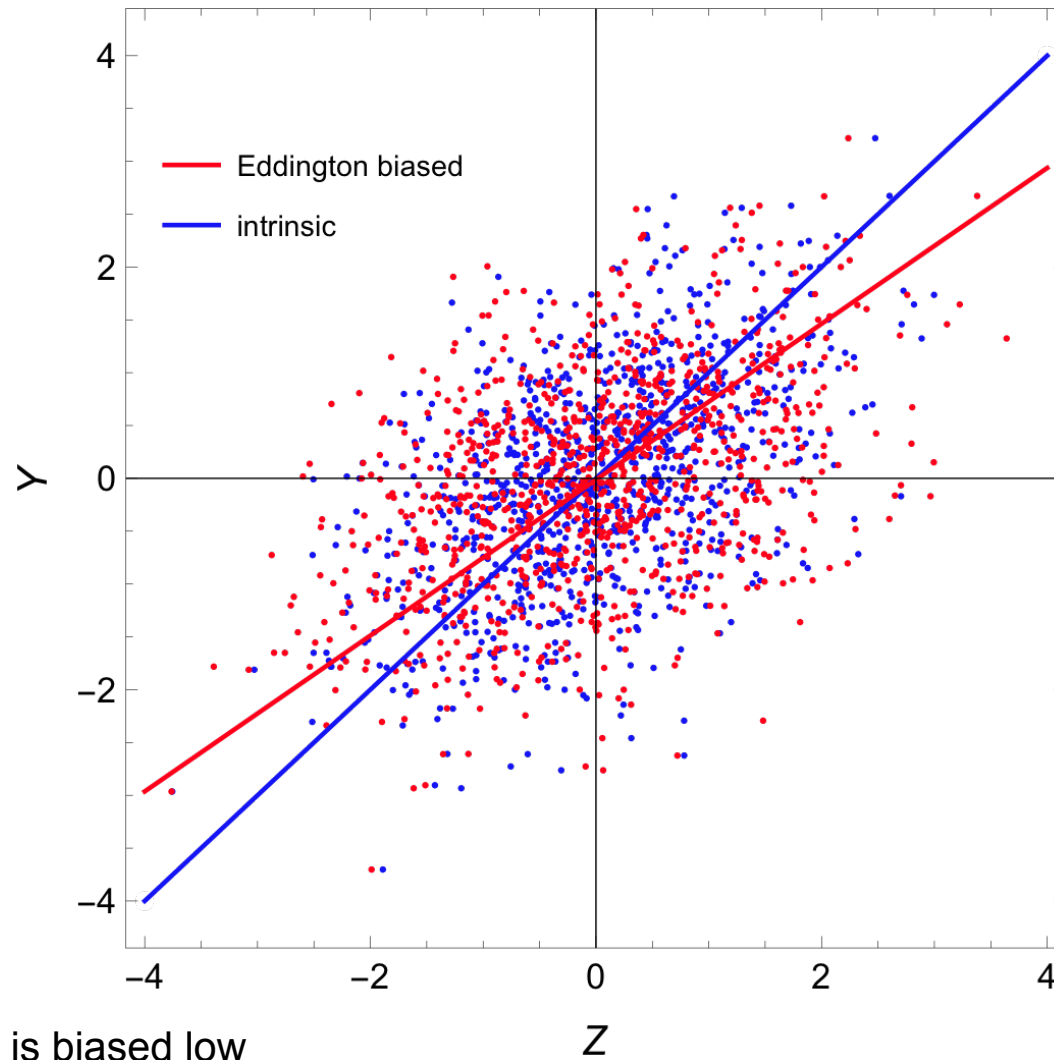
Eddington bias

Eddington (1913, 1940), Jeffreys (1938): Counts of not-uniformly distributed objects are affected by measurement errors in counting



Eddington bias

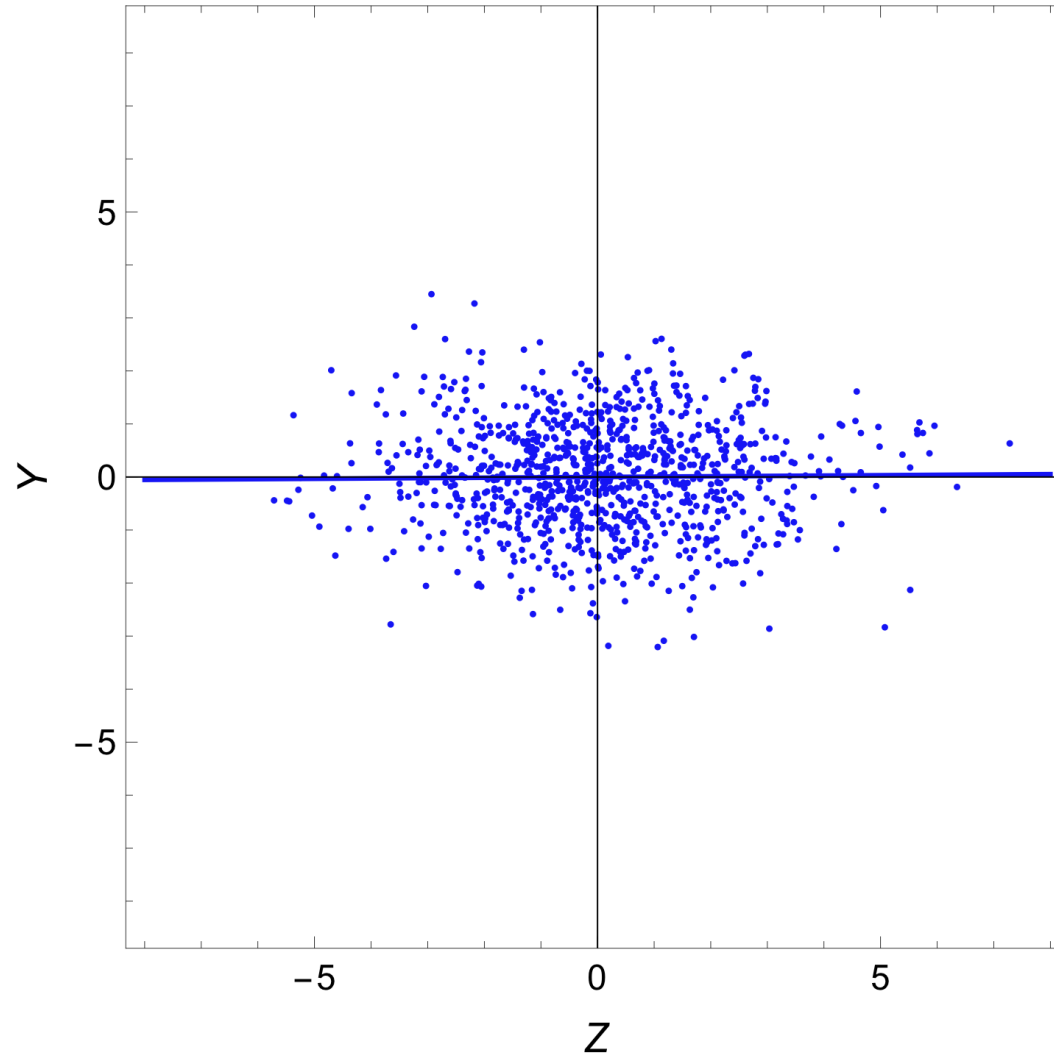
Near the border of the distribution, more objects are scattered out than scattered in. The distribution of Z flattens.



- ✓The slope $\beta(Y|Z)$ is biased low
- ✓the scatter is biased high

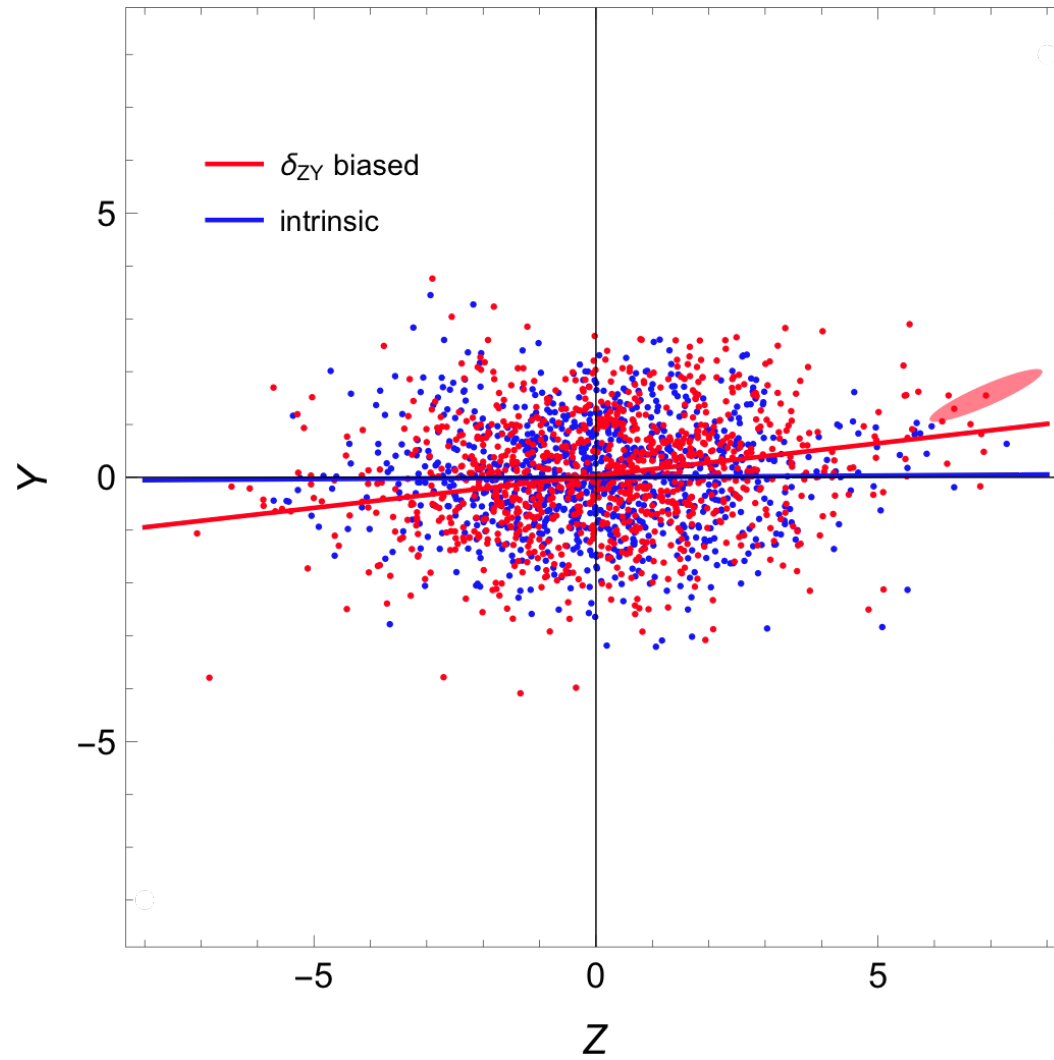
Correlated uncertainties

If measurement errors are correlated apparent



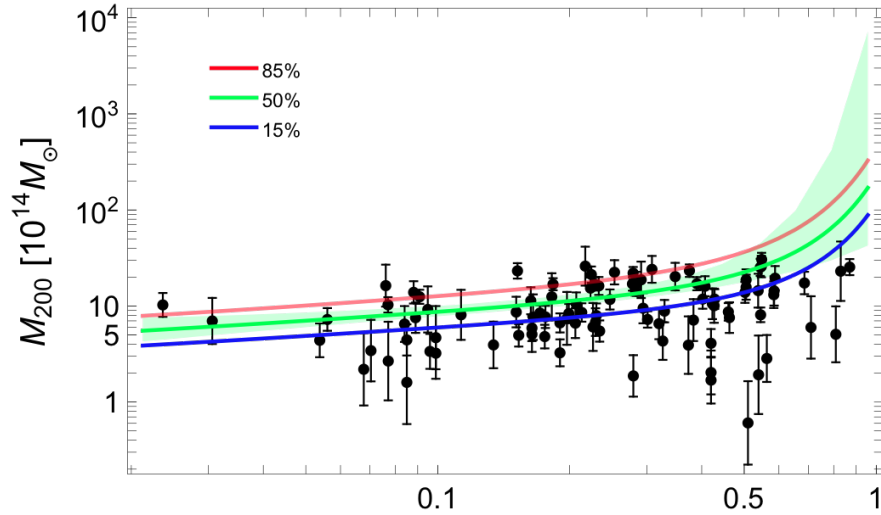
Correlated uncertainties

Apparent slope follow the uncertainty correlation

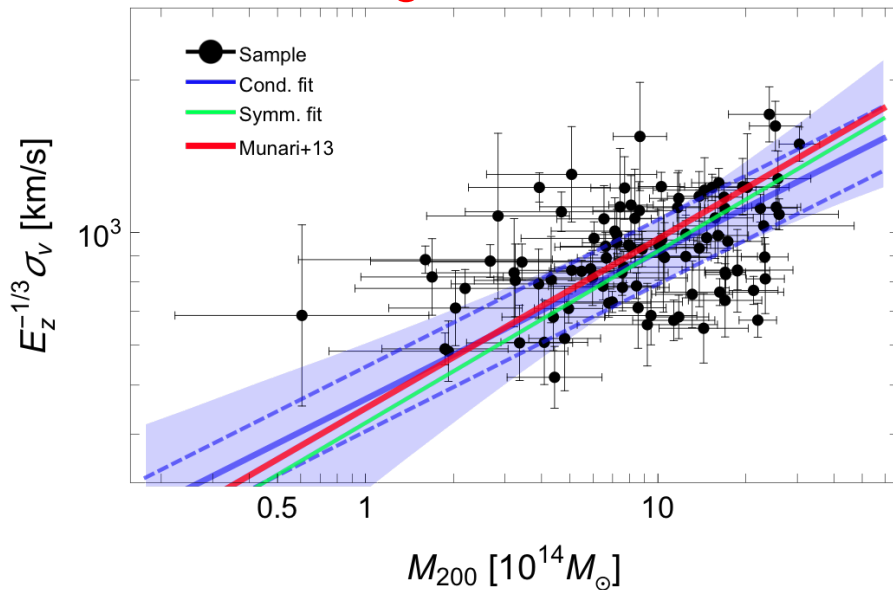


Velocity dispersion vs mass

Completeness function



Scaling



Scaling

$$E_z^{-1/3} \sigma_v \propto E_z^{\gamma_z} M_\Delta^\beta$$

97 clusters with known MWL and sigma

→ $\beta_{\gamma-z} = 0.34 \pm 0.15$ (nearly s-s, $\beta_{SS} = 1/3$),

→ $\sigma_{\gamma|z} = 14 \pm 5\%$ (small scatter)

→ $\gamma_z = -0.05 \pm 0.30$ (s-s)

✓ Observational calibration of $\sigma_v - M_\Delta$

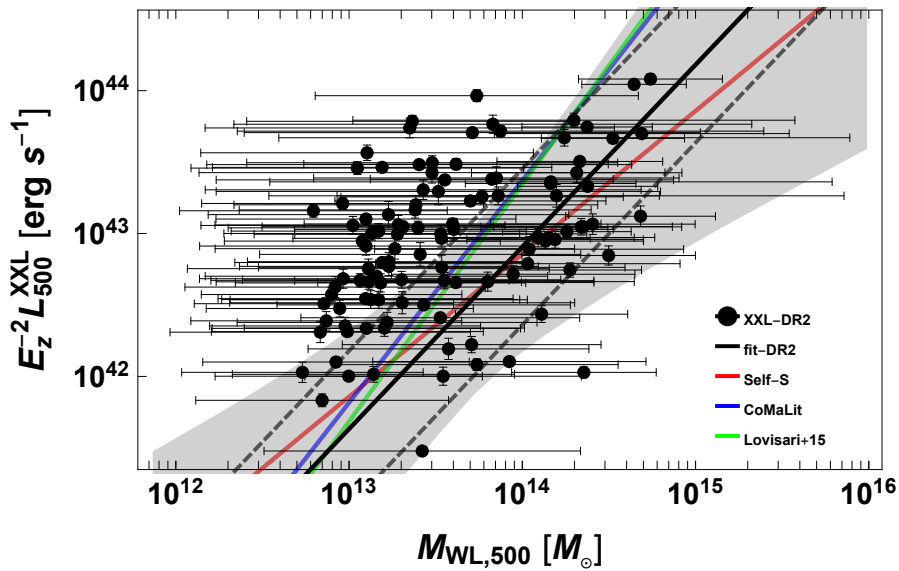
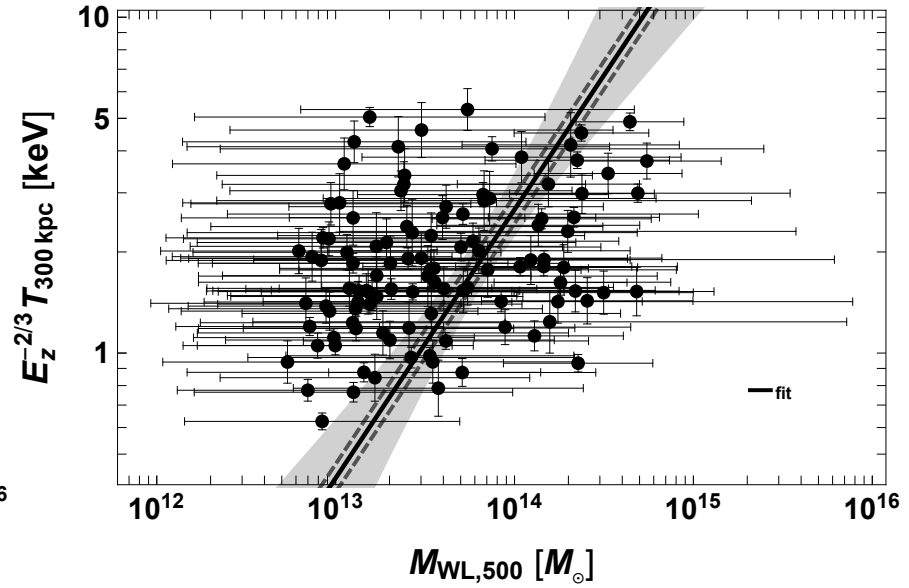
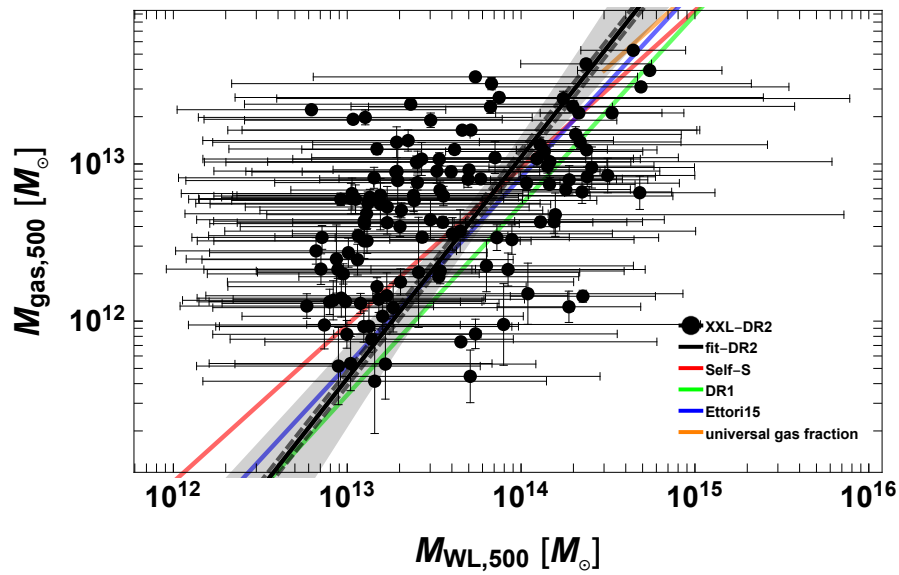
✓ Very good agreement with expectations

✓ Optimal proxy (low scatter)

✓ Completeness from $P(M_\Delta)$ assuming the MF of Tinker+08

[Sereno&2015MNRAS.450.3675S]

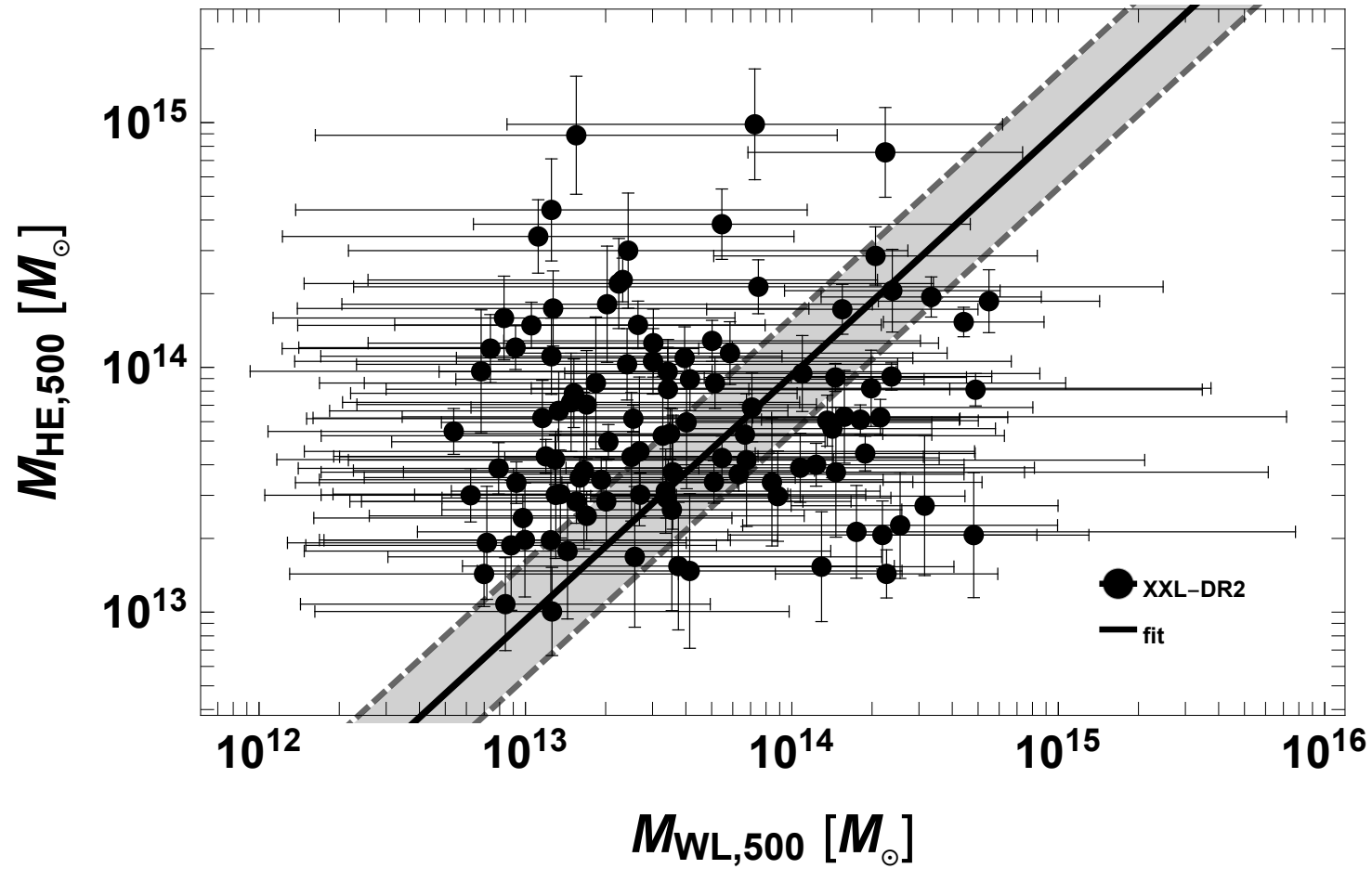
Multi-scaling relations



- ✓ steeper $M_{\text{Gas}}-M$ and L_X-M , $T-M$ nearly self-sim
- Radiative cooling regulated by AGN feedback

[Sereno+2020MNRAS.492.4528S]

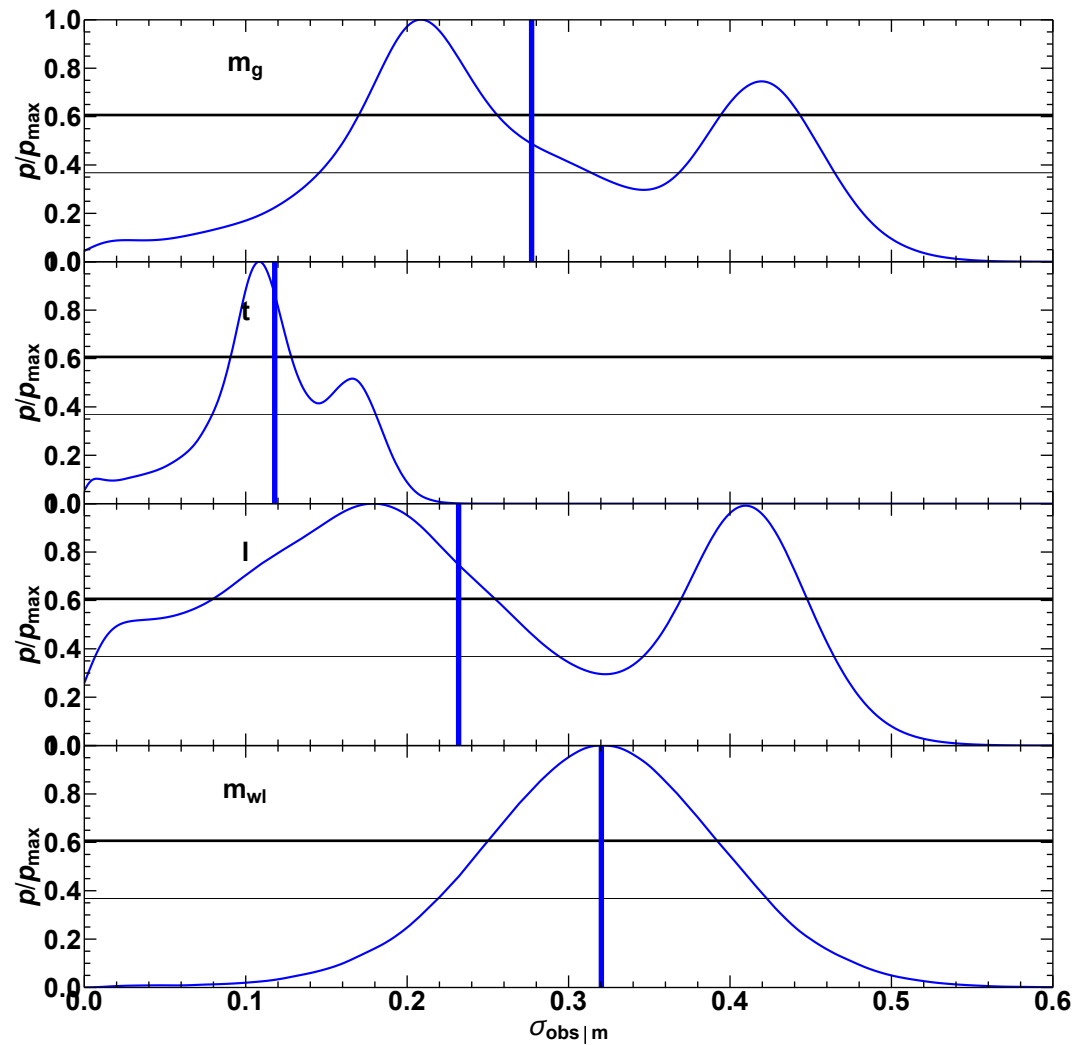
Hydrostatic bias



✓ $b_{\text{HE}} = 9 \pm 17\%$

[Sereno+2020MNRAS.492.4528S]

Intrinsic scatters

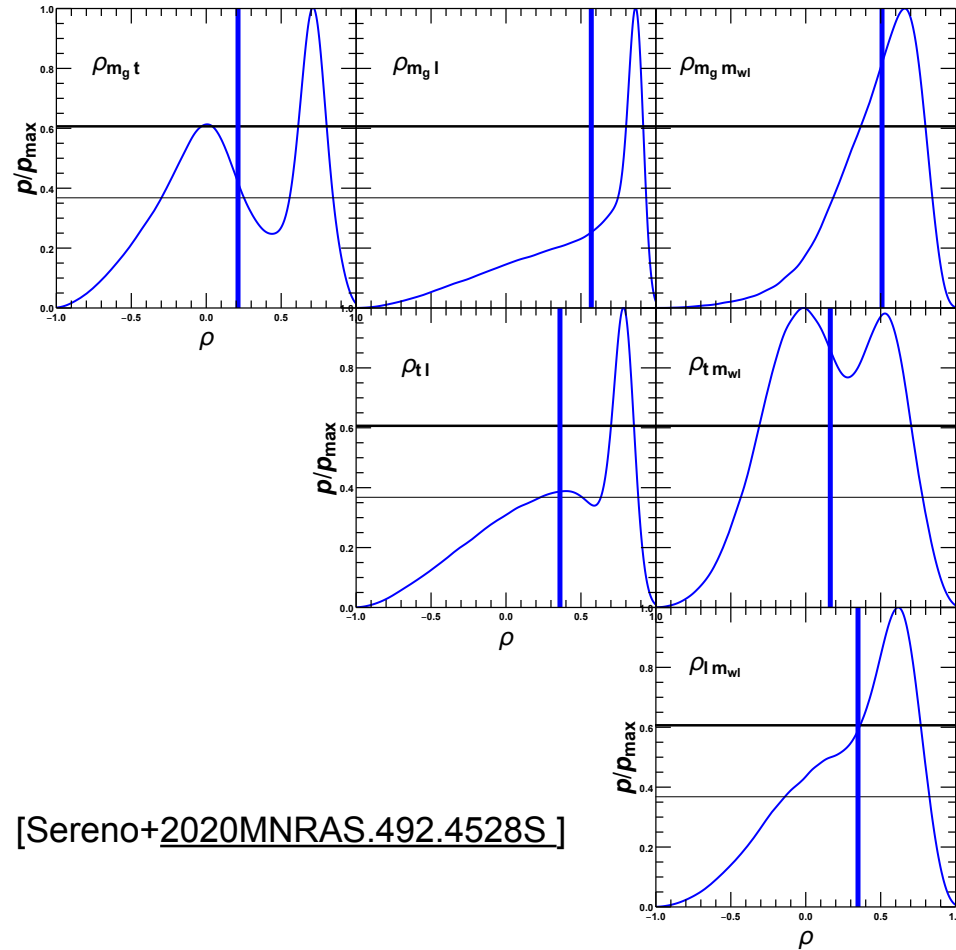


✓ scatters in M_{gas} and $T \sim 20\%$

✓ M_{gas} much more easy to measure

[Serenio+2020MNRAS.492.4528S]

Scatter correlations



[Serenio+2020MNRAS.492.4528S]

- ✓ correlated intrinsic scatters between X-observables
→ signature of coherent merging/accretion history and dynamical state
- ✓ correlated X-observables and WL mass
→ orientation effects

Mass forecasting

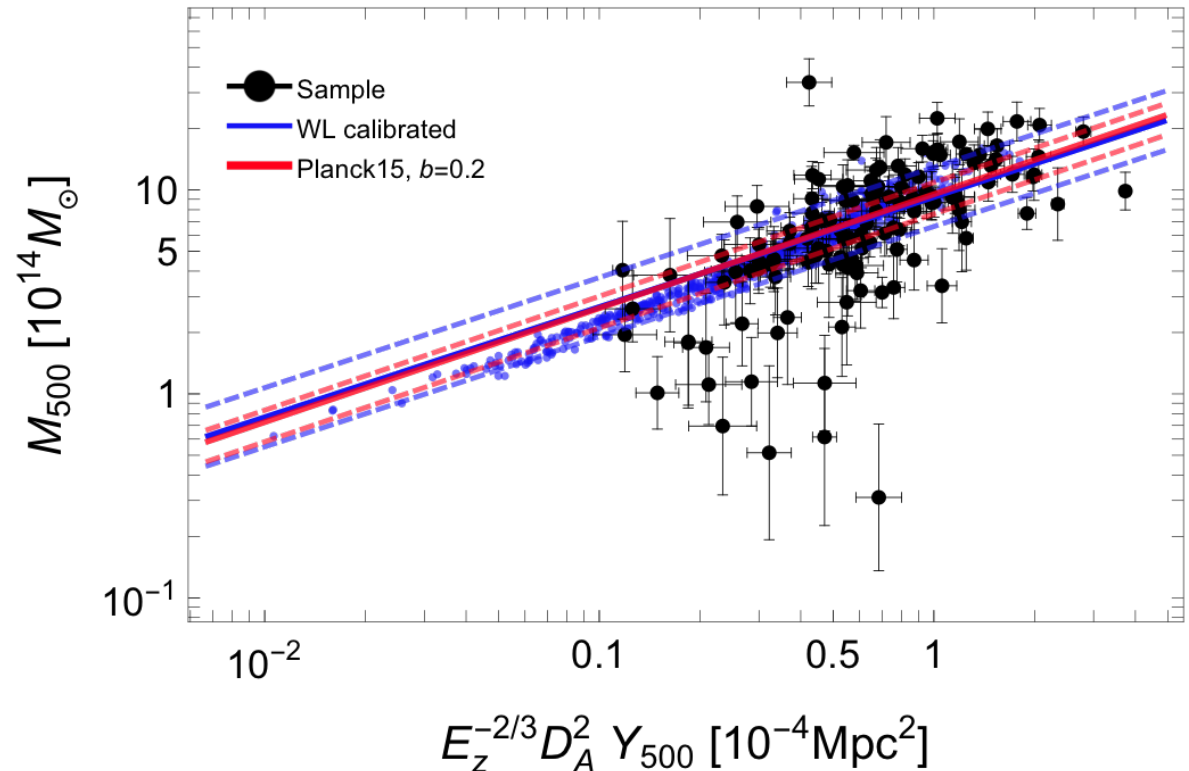
❑ Masses to be predicted are treated as missing data in the regression and are estimated together with the scaling parameters.

$$\square P = \prod_{(\text{detected clusters})} P(\lambda_{\text{euclid}} | \lambda_{\text{cl}}) P(M_{\text{euclid}} | M_{\text{cl}}) P(M_{\text{cl}} | \lambda_{\text{cl}}, \theta_{\text{SR}}) P(\lambda_{\text{cl}} | \theta_{\lambda}) P(\theta_{\text{SR}}) P(\theta_{\lambda})$$

- ✓ the full uncertainty budget (SR, intrinsic scatter, accuracy of the calibration sample)
- ✓ systematics-free (Malmquist/Eddington bias)
- ✓ time evolved SR

→ The subsample has to be representative

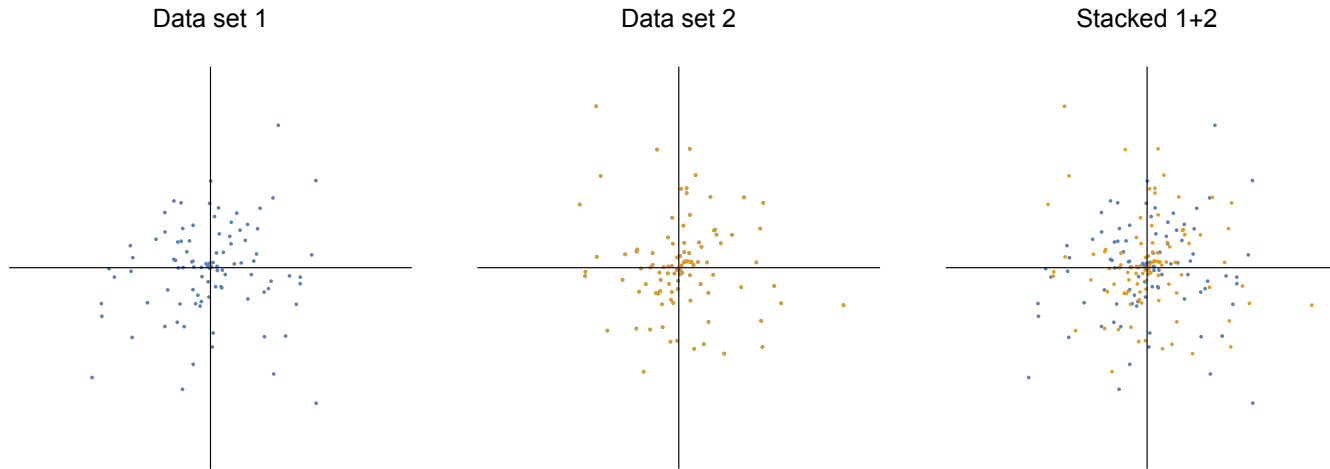
CoMaLit-V: application to RedMaPPer, PSZ2, MCXC



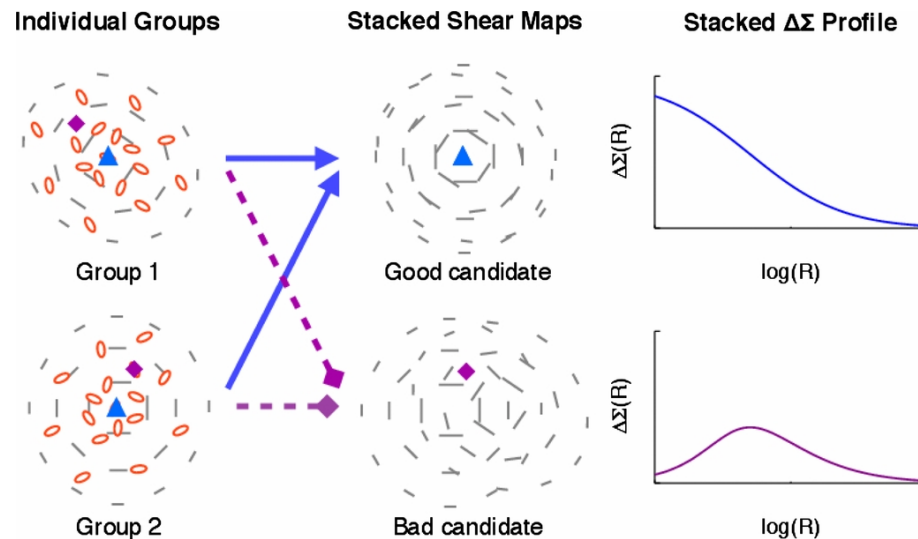
PSZ2 clusters [Sereno+2017MNRAS.468.3322S.]

Stacking

The signal of different galaxy clusters at fixed observables can be coherently added. Stacking technique allows to significantly enhance the signal of less massive halos and to measure their average mass in a range that is out of reach for analyses of individual cluster



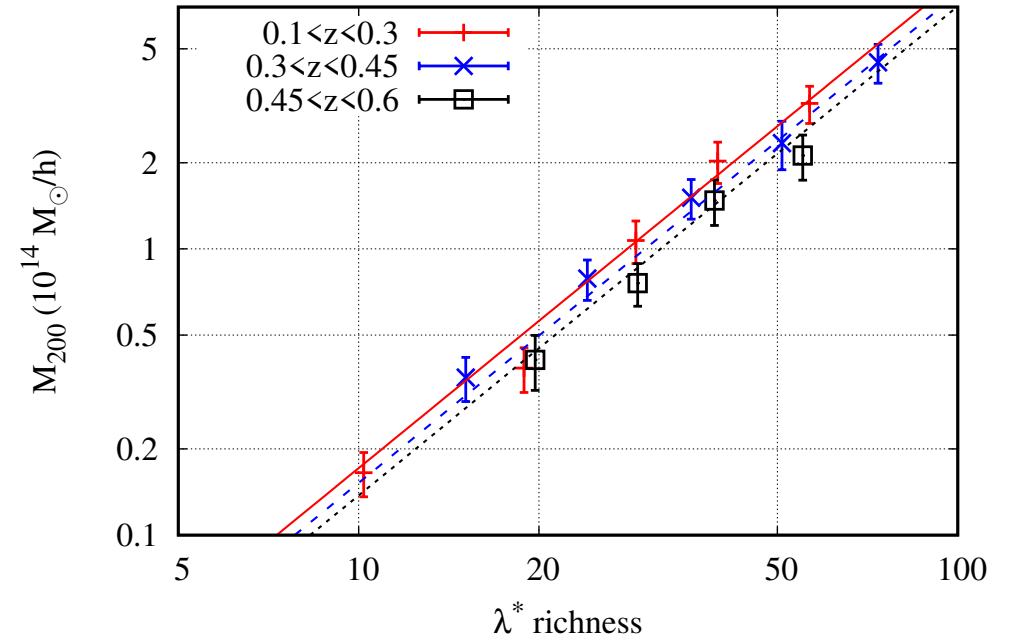
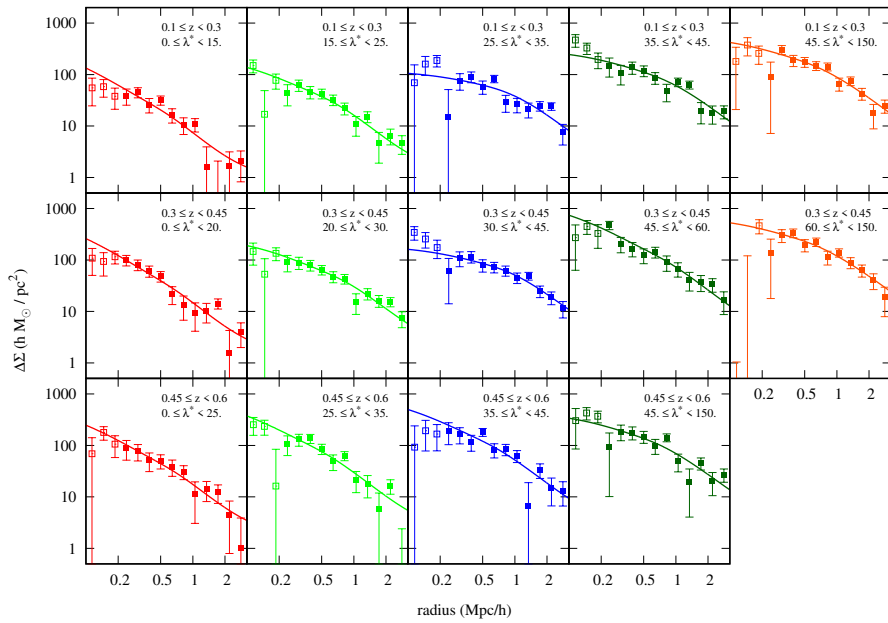
Halos have to be properly centred



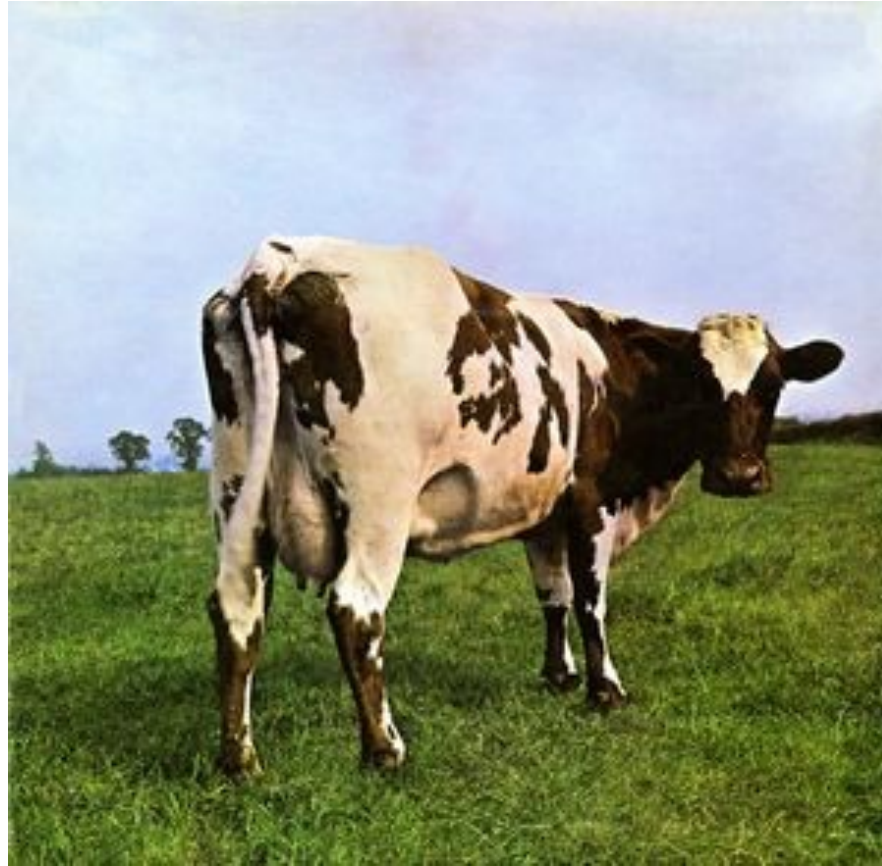
Schematic illustration of stacked lensing around different candidate centers. Candidate centers are defined in each group (left), and then shear maps are stacked around each position (middle) and azimuthally averaged to compute $\Delta\Sigma$ profiles (right) [George+2012ApJ...757....2G]

Stacking

WL mass calibration of the optically detected clusters in AMICO-KiDS-DR3 [Bellagamba+2019MNRAS.484.1598B]



Part 3



[Pink Floyd, Atom Heart Mother]

Cosmology dependence

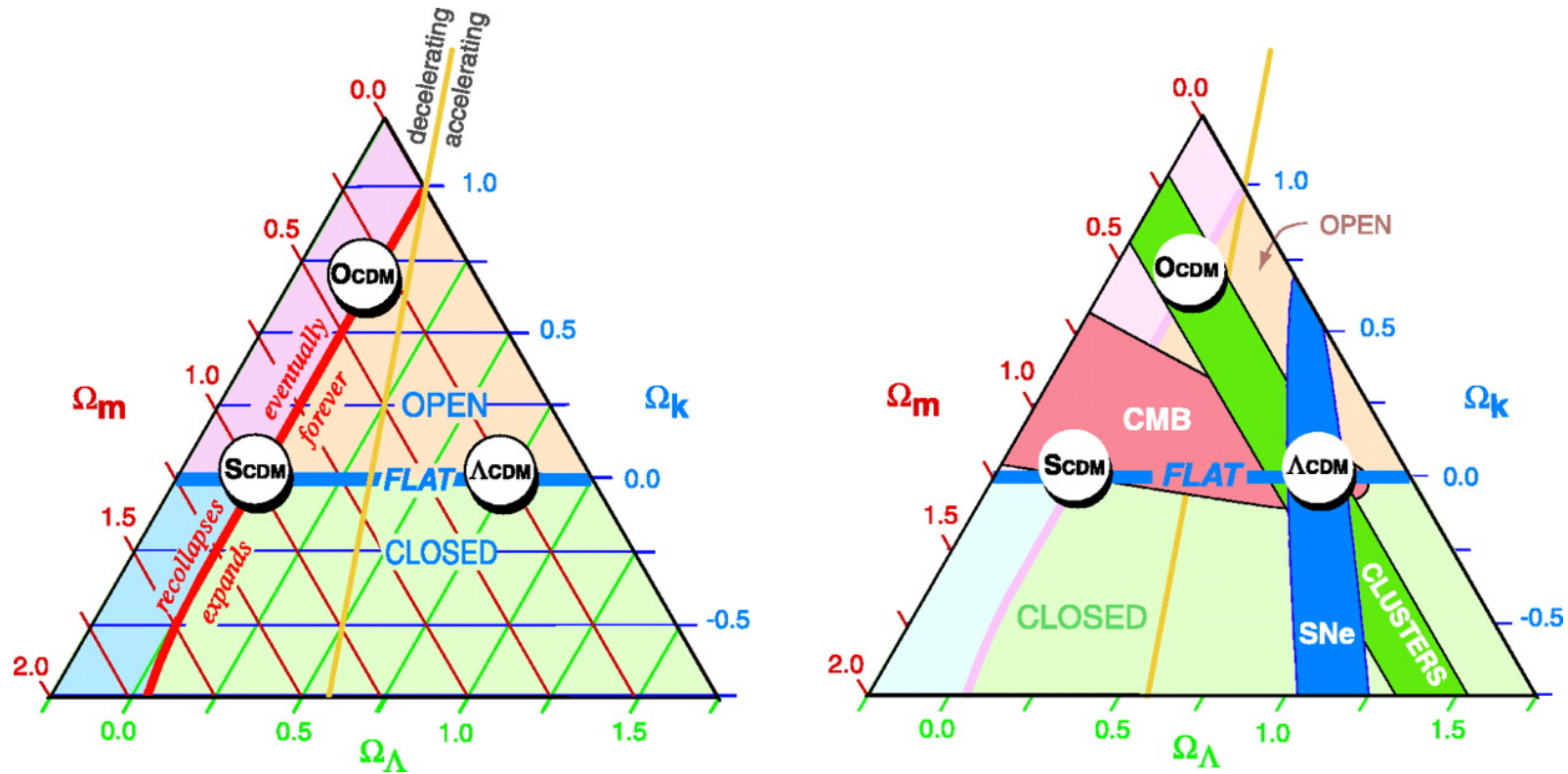
Cluster observables depends on cosmology through:

cosmological distances (H_0 , σ , Ω_M , Ω_Λ , ...)

abundance growth of halos (σ_8 , H_0 , Ω_M , Ω_Λ , ...)

Non-linear effects less prominent than in galaxy formation

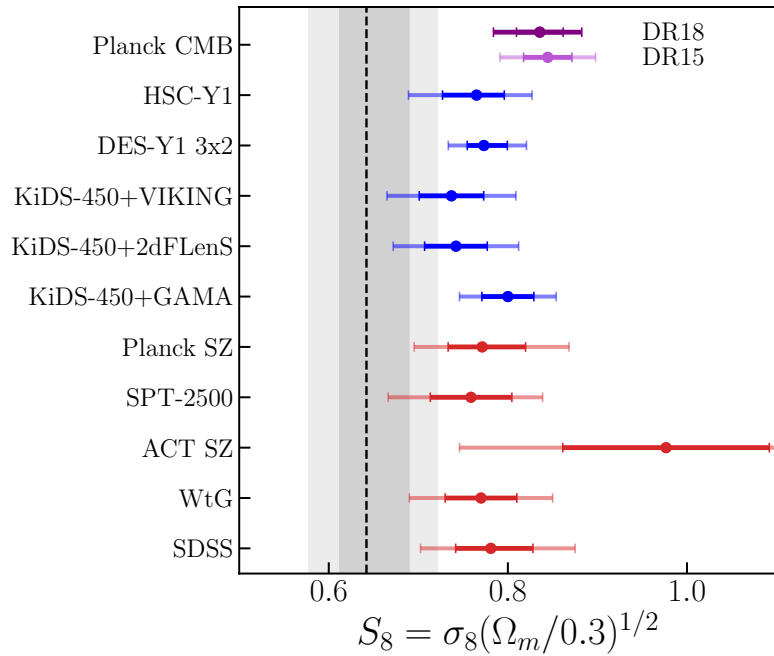
The cosmic triangle



[Bahcall+1999Sci...284.1481B]

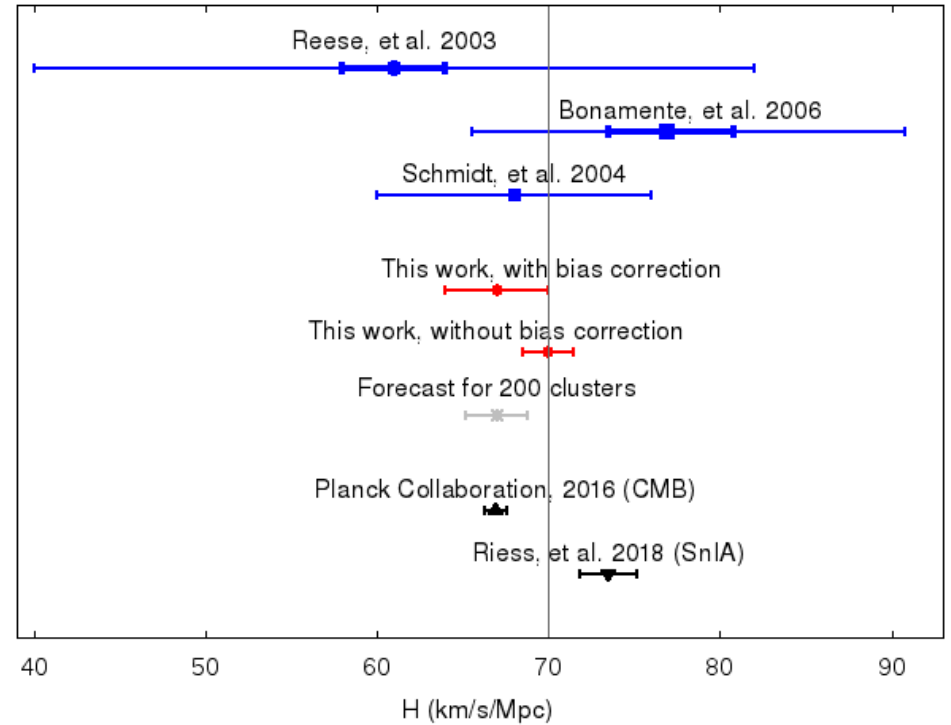
LCDM: concerns

σ_8



confidence level constraints on S_8 .
 DES-Y1-2020 number counts: shaded gray
 Red: cluster abundance analyses,
 blue: WL and galaxy clustering
 purple: CMB. [DES-Y1-2020]

H_0



Comparison on H_0 from literature
 red: XSZ from Kozmany19
 blue: XSZ clusters as a probe
 [Kozmany19]

Number counts

$$N_{\text{cl}} + N_{\text{impurity}} = \int_{\Delta z} dz \int_{\Delta \lambda} d\lambda \int dm P(I_{\text{det}} | \lambda) P(\lambda | M) \frac{dn}{dm} \frac{dV}{dz}$$

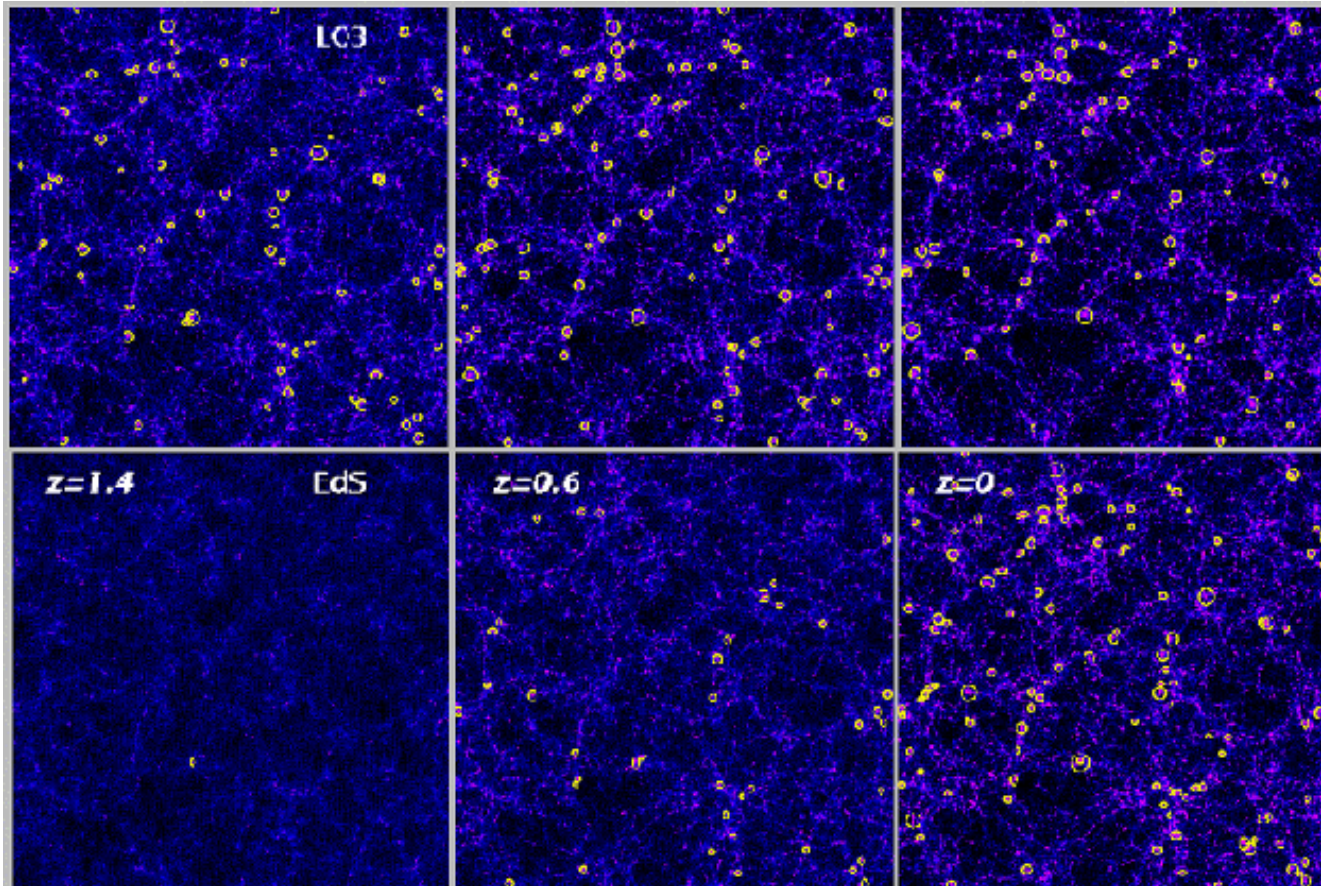
Ingredients:

- ◆ λ is a mass proxy
- ◆ N_{cl} : number of clusters in a given proxy and redshift range
- ◆ Mass calibration $P(\lambda|M)$
- ◆ completeness $P(I_{\text{det}}|\lambda)$: how many clusters we observe out of the total
- ◆ purity: N can be inflated due to not pure samples N_{impurity}

Cosmological dependence

- ❖ HMF dn/dm
- ❖ cosmic volume dV/dZ

Evolution of structures and cosmology



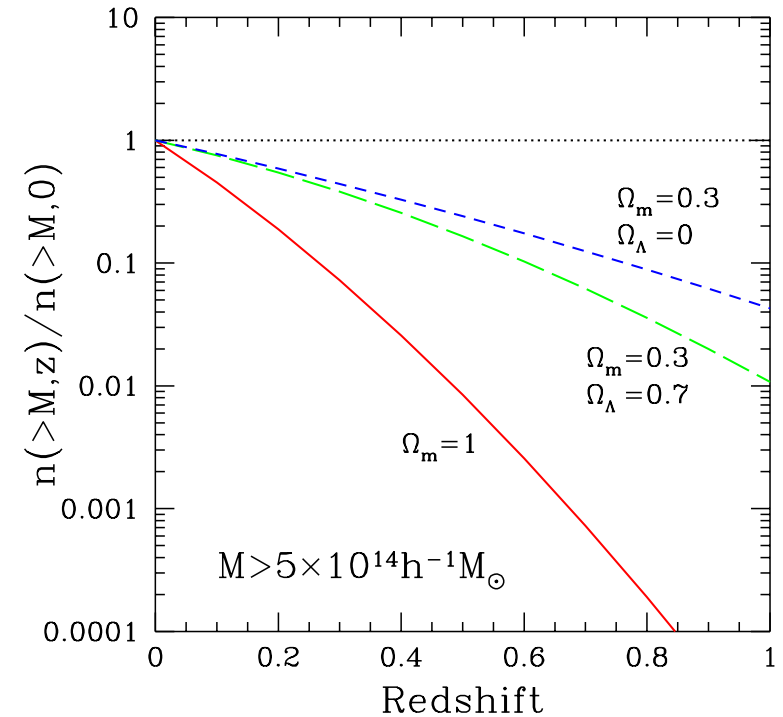
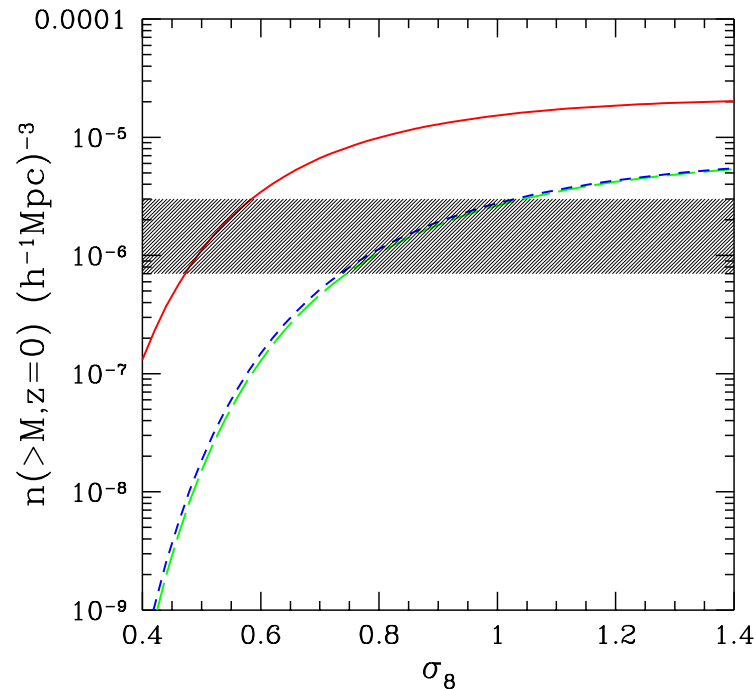
Evolution of large-scale cosmic structures simulated in N-body simulations of two cosmological models. Each of the three redshift snapshots shows a region with $250 h^{-1} \text{Mpc}$ side and $75 h^{-1} \text{Mpc}$ thick (comoving scale-lengths). Upper panels: flat LCDM with $\Omega_m = 1 - \Omega_\Lambda = 0.3$; lower panels: SCDM with $\Omega_m = 1$. In both cases the amplitude of the power spectrum is consistent with the number density of nearby galaxy clusters. Superimposed on the matter distribution, the yellow circles mark the positions of galaxy clusters that would be seen shining in X-rays with a temperature $T > 3 \text{ keV}$. The size of the circles is proportional to temperature. The difference in the evolution of cluster abundance in the two models illustrates the importance of clusters as probes of the dark matter and dark energy content of the universe. [Borgani&2001Natur.409...39B]

Number counts

At a given mass, the normalization of the mass function is $\sigma_8^2 \Omega_M^{0.5}$

The evolution of the cluster mass function, which is highly sensitive to Ω_M .

The shape as a function of M depends on Ω_M



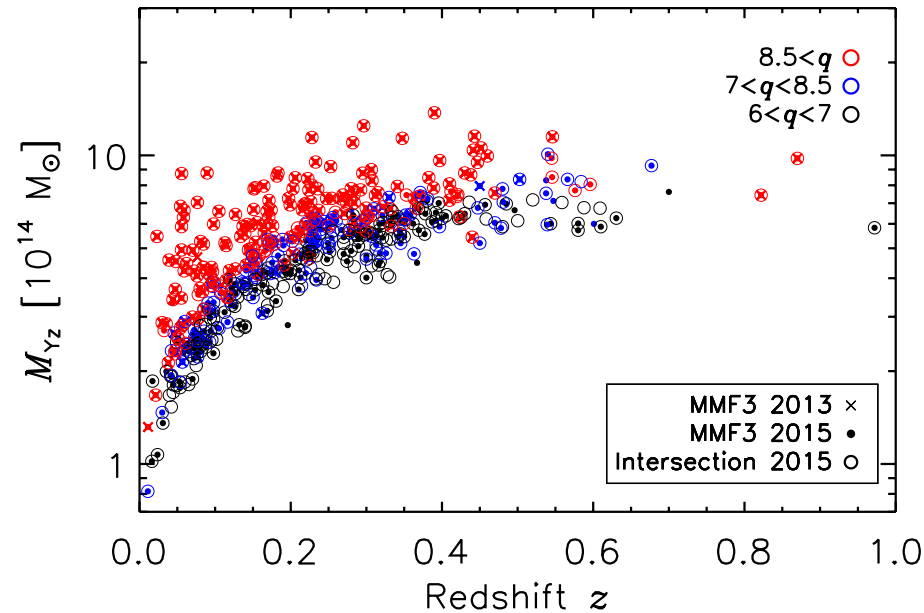
The sensitivity of the cluster mass function to cosmological models. (*Left*) The cumulative mass function at $z = 0$ for $M > 5 \times 10^{14} h^{-1} M_{\odot}$ for three cosmologies, as a function of σ_8 ; solid line, $\Omega_M = 1$; short-dashed line, $\Omega_M = 0.3$, $\Omega_{\Lambda} = 0.7$; long-dashed line, $\Omega_M = 0.3$, $\Omega_{\Lambda} = 0$. The shaded area indicates the observational uncertainty in the determination of the local cluster space density. (*Right*) Evolution of $n(>M, z)$ for the same cosmologies and the same mass-limit, with $\sigma_8 = 0.5$ for the $\Omega_M = 1$ case and $\sigma_8 = 0.8$ for the low-density models.

[Rosati+2002ARA&A..40..539R]

Planck 2015 number counts

The catalogue (PSZ2) is the largest SZ-selected sample with 1653 clusters [2016A&A...594A..27P]

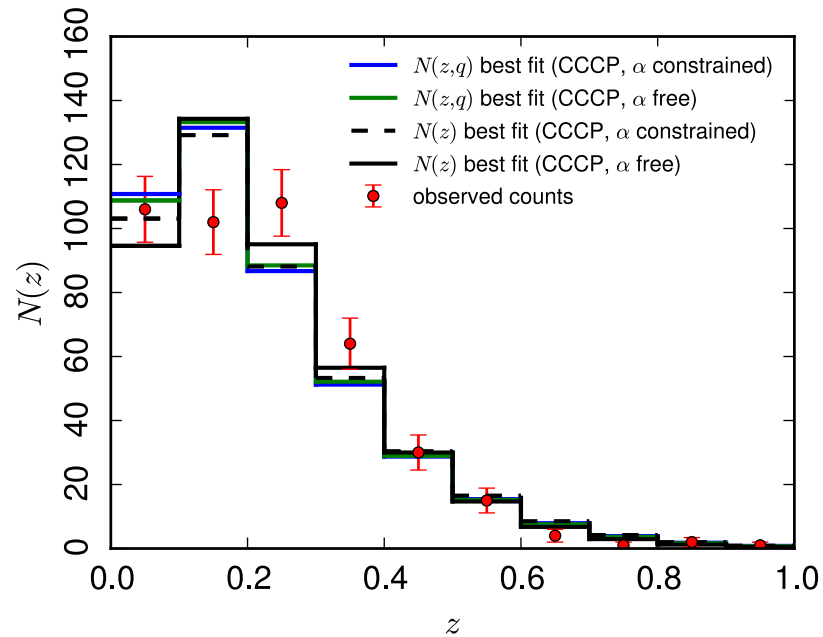
- ❖ high SNR subsample of 439 clusters for cosmology [Planck2016A&A...594A..24P]
- ❖ YSZ- M mass calibration based on a subsample of 10 relaxed X-ray clusters
- ❖ selection function based on numerical simulations



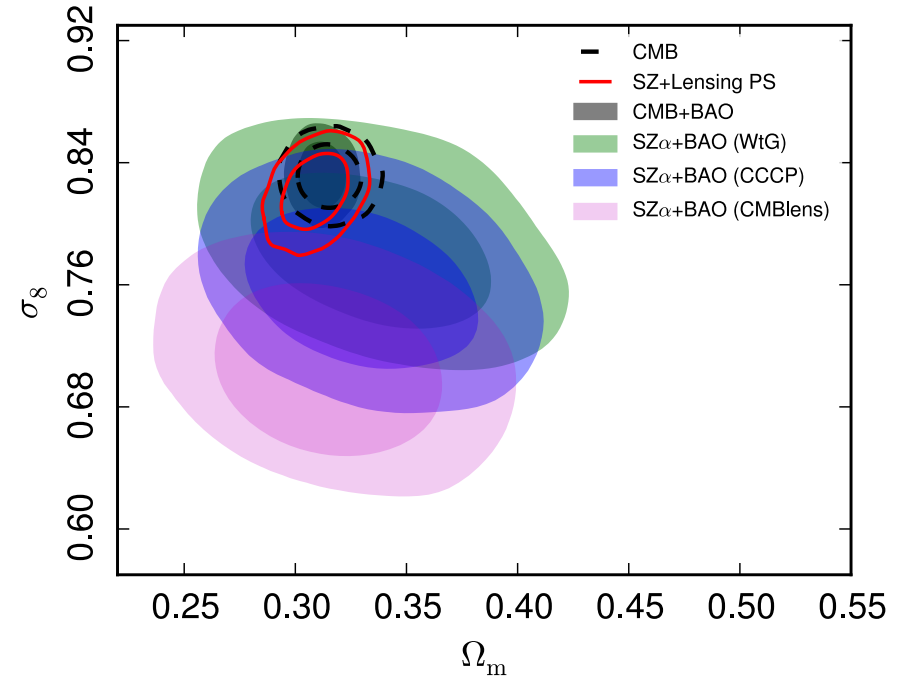
Mass-redshift distribution of the *Planck* cosmological samples colour-coded by signal-to-noise, q . The baseline cosmological sample is shown as the small filled circles. The mass M_{Yz} is the *Planck* mass proxy [Planck2016A&A...594A..24P]

Planck 2015 number counts

CMB and clusters results in disagreement at 1-4 sigma according to mass calibration



Redshift distribution of PSZ2 clusters
[Planck2016A&A...594A..24P]



CMB vs clusters in the (Ω_m, σ_8) -plane. The green, blue and violet contours give the cluster constraints (two-dimensional likelihood) at 68 and 95% for the WtG, CCCP, and CMB lensing mass calibrations. [Planck2016A&A...594A..24P]

DES Y1 number counts

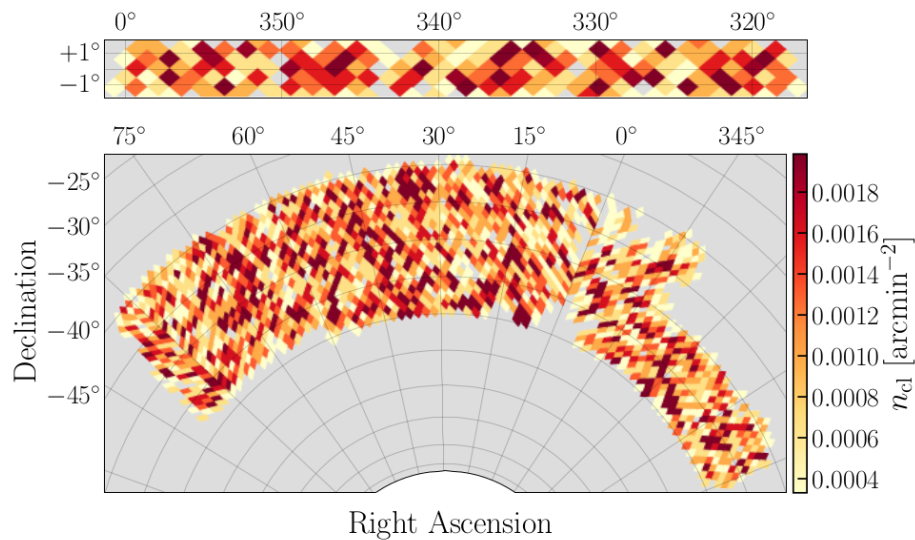
DES WL survey [DESY12020arXiv200211124D]

- ❖ 6504 optically selected clusters out to $z=0.65$
- ❖ assumed 100% completeness
- ❖ Mass calibration with stacked WL

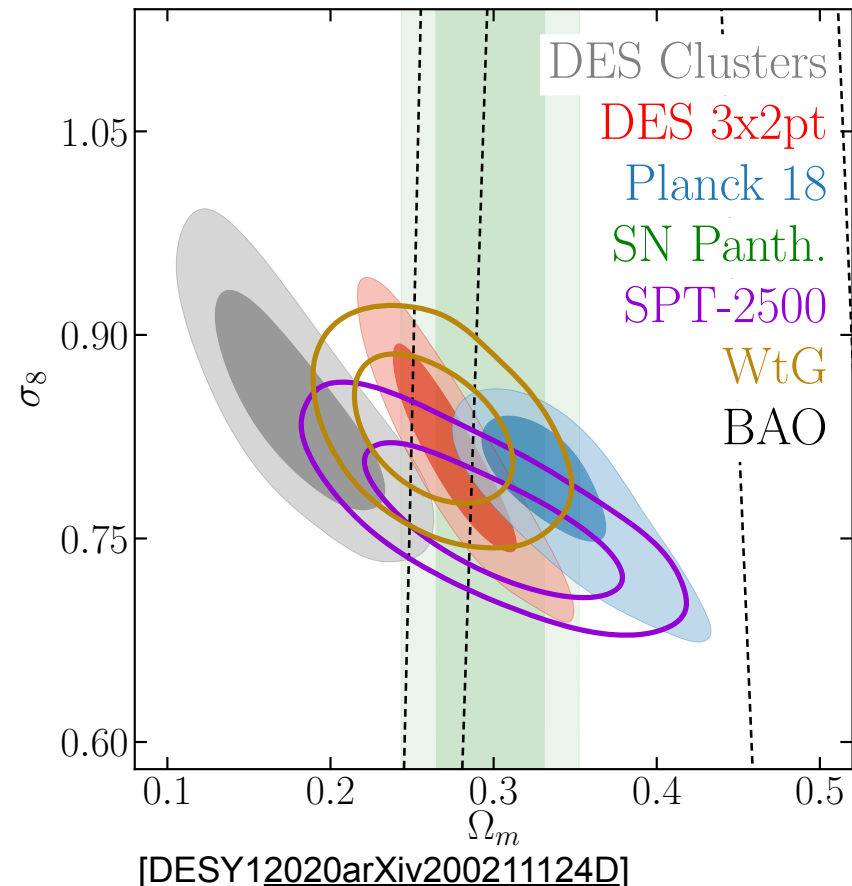
Inconclusive results:

2.4 σ tension with the DES Y1 3x2pt results,
5.6 σ with the Planck CMB analysis.

uncertain mass calibration?



The DES Y1 redMaPPer cluster density over the two non-contiguous regions of the Y1 footprint: the Stripe 82 region (116 deg² upper panel) and the SPT region (1321 deg²; lower panel) [DESY12020arXiv200211124D]



Sparsity

Mass ratio at different overdensity. Sensitive to the cluster mass accretion history:

Nearly independent of :

✓ selection effects (the dependence on total halo mass is negligible)

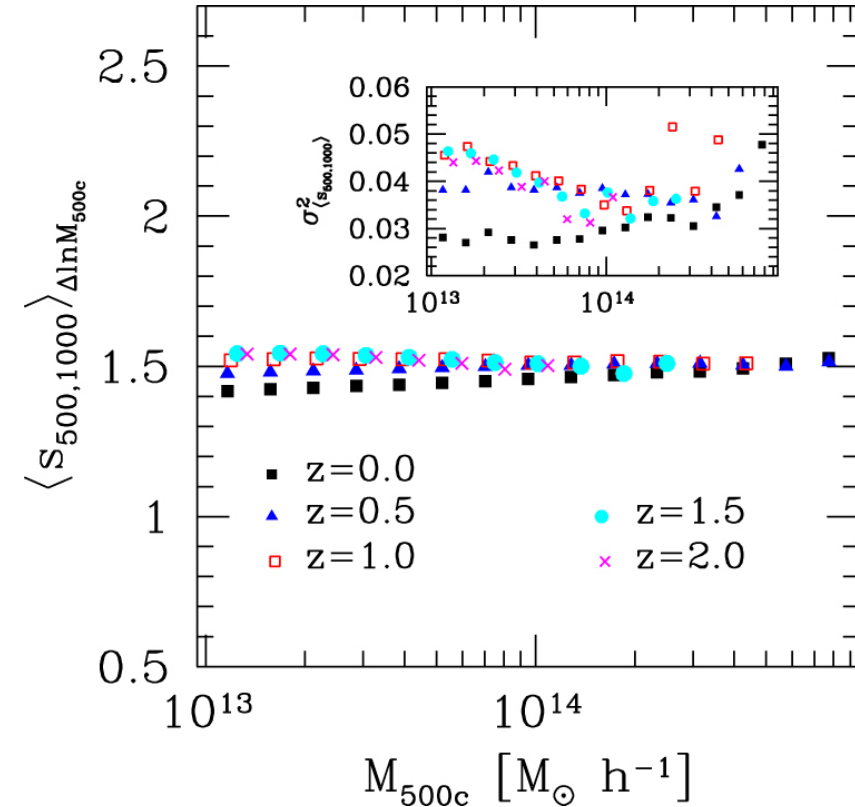
✓ mass bias (being a ratio)

$$s_{\Delta_1\Delta_1} \equiv \frac{M_{\Delta_1}}{M_{\Delta_2}}$$

How to compute the cosmo dependence

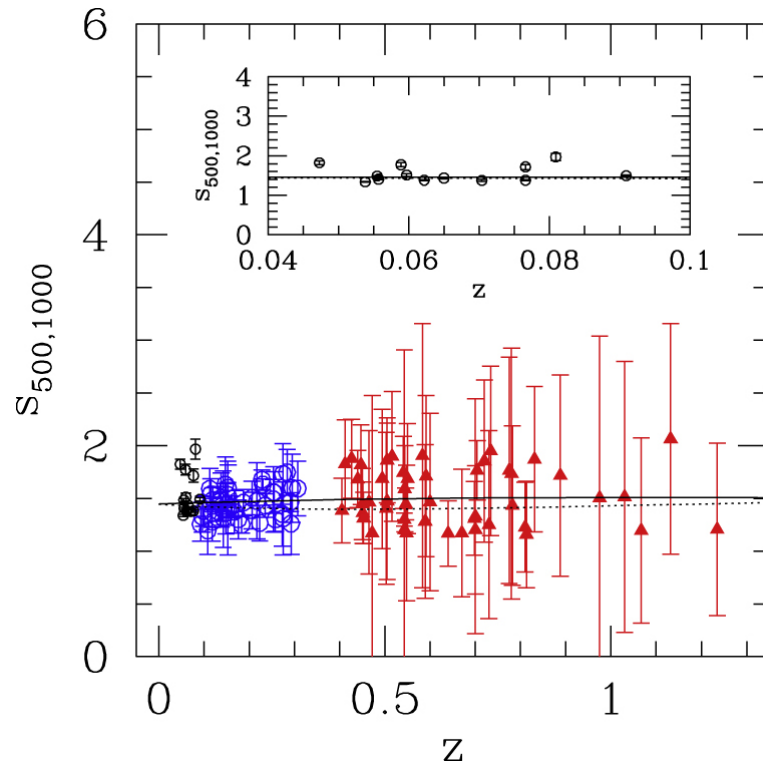
$$\frac{dn}{dM_{\Delta_2}} = \frac{dn}{dM_{\Delta_1}} \frac{dM_{\Delta_1}}{dM_{\Delta_2}} = \frac{dn}{dM_{\Delta_1}} s_{\Delta_1\Delta_2} \frac{d \ln M_{\Delta_1}}{d \ln M_{\Delta_2}}$$

$$\int_{M_{\Delta_2,\min}}^{M_{\Delta_2,\max}} \frac{dn}{dM_{\Delta_2}} d \ln M_{\Delta_2} = s_{\Delta_1\Delta_2} \int_{s_{\Delta_1\Delta_2} M_{\Delta_2,\min}}^{s_{\Delta_1\Delta_2} M_{\Delta_2,\max}} \frac{dn}{dM_{\Delta_1}} d \ln M_{\Delta_1}$$

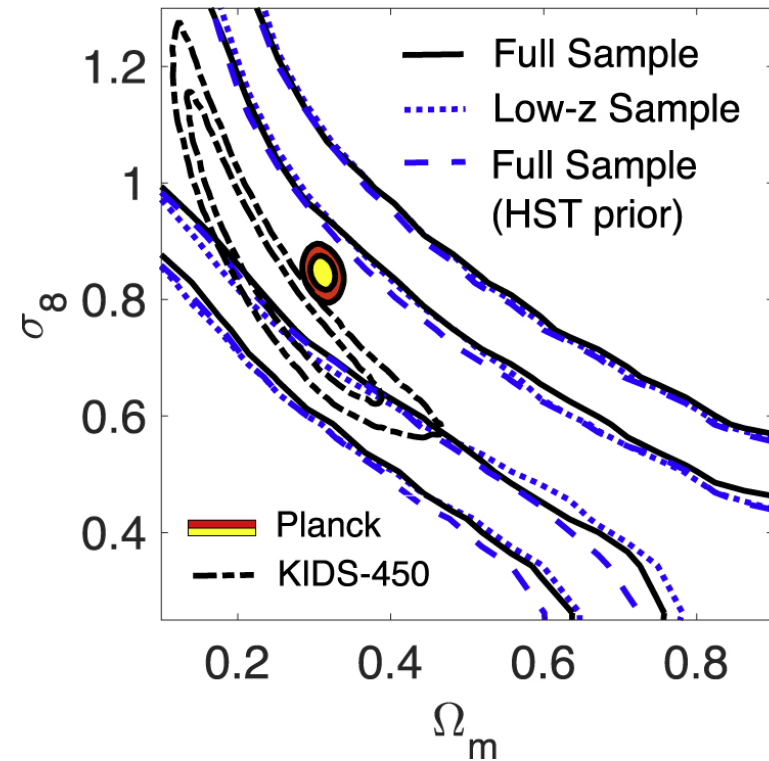


Average halo sparsity as a function of M_{500c} from N-body halo catalogs. The inset plot shows the variance of the halo sparsity in the same mass bins as a function of M_{500c} for the different redshifts. [Corasaniti+2018ApJ...862...40C]

Sparsity: first results



Sparsity of X-ray clusters. The black solid line and the black dotted line correspond to the best-fit Λ CDM models inferred assuming different mass functions [Corasaniti+2018ApJ...862...40C]



Marginalized 1σ and 2σ contours in the $\Omega_m - \sigma_8$ using the full X-ray cluster data set (black solid lines), the low- z redshift sample only (blue dotted lines), and the case of the *HST* prior on h (blue dashed lines). For comparison, contours from the *Planck* cosmological data analysis and KIDS-450 [Corasaniti+2018ApJ...862...40C]

Two point correlation function

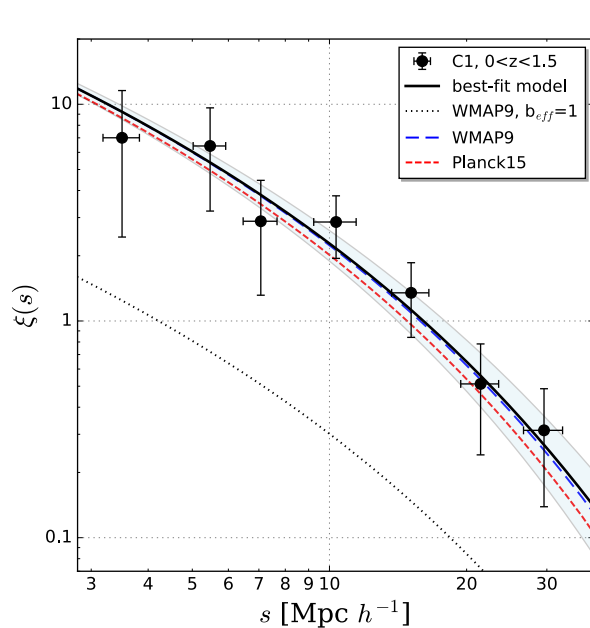
The 2PCF model in redshift space

$$\xi^m(s) = \left[(b_{\text{eff}}\sigma_8)^2 + \frac{2}{3}f\sigma_8 \cdot b_{\text{eff}}\sigma_8 + \frac{1}{5}(f\sigma_8)^2 \right] \frac{\xi_{\text{DM}}(\alpha r)}{\sigma_8^2}$$

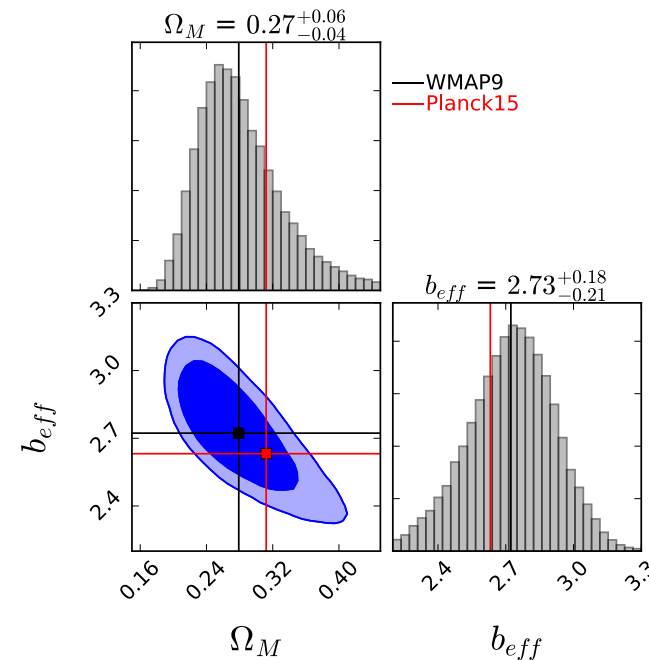
$f\sigma_8$, where growth factor $f = d \ln \delta / d \ln a \approx \Omega_M(z)^\gamma$, with $\gamma = 0.545$

$b_{\text{eff}}\sigma_8$ (since $\xi_{\text{DM}} \propto \sigma_8^2$)

α (i.e. the ratio between the test and fiducial values of the isotropic volume distance) accounts for the geometric distortions caused by an incorrect assumption of the background cosmology



Redshift-space 2PCF of the C1 XXL-DR1 clusters at $z < 1.5$ [Marulli+2018A&A...620A...1M]

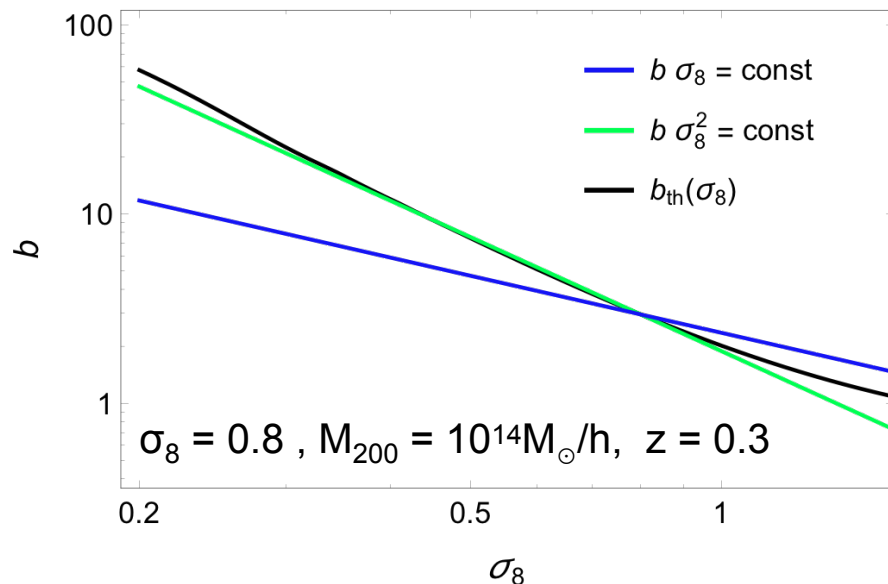


$\Omega_M - b_{\text{eff}}$ the analysis 2PCF of the C1 XXL-DR1 clusters at $z < 1.5$ [Marulli+2018A&A...620A...1M]

Lensing + Clustering

Clustering	Stacked Lensing
$\xi_{hh} = \langle \delta_h(x) \delta_h(x+r) \rangle$	$\xi_{hm} = \langle \delta_h(x) \delta_m(x+r) \rangle$
$\sim b^2 \sigma_8^2 (\xi_{mm} / \sigma_8^2)$	$\sim b \sigma_8^2 (\xi_{mm} / \sigma_8^2)$

- Clusters and large scales:
 - bias is linear
- Same population for both clustering and lensing
 - no need to model the bias

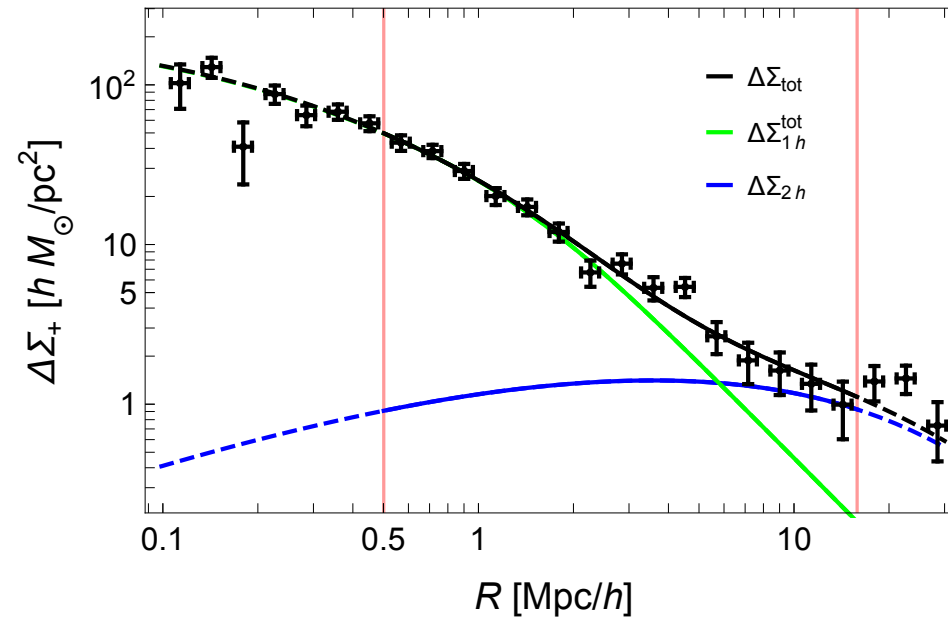


$$b(M_{\text{eff}}, z) = \int b(M_{200}, z) f_{\text{sel}}(M_{200}) dM_{200}$$

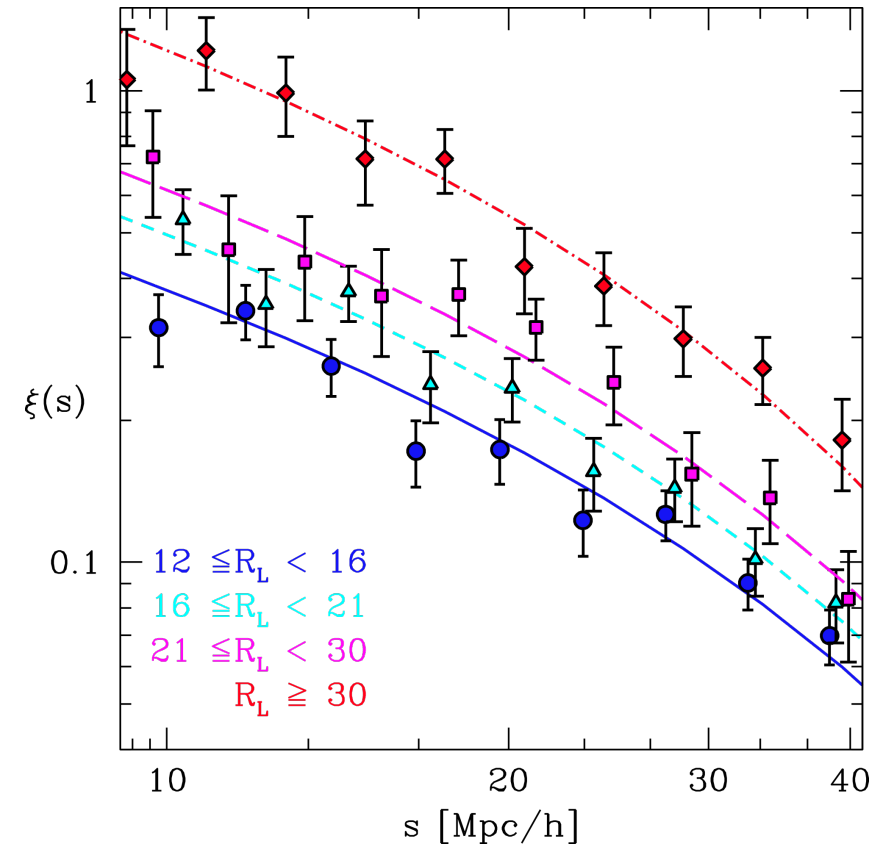
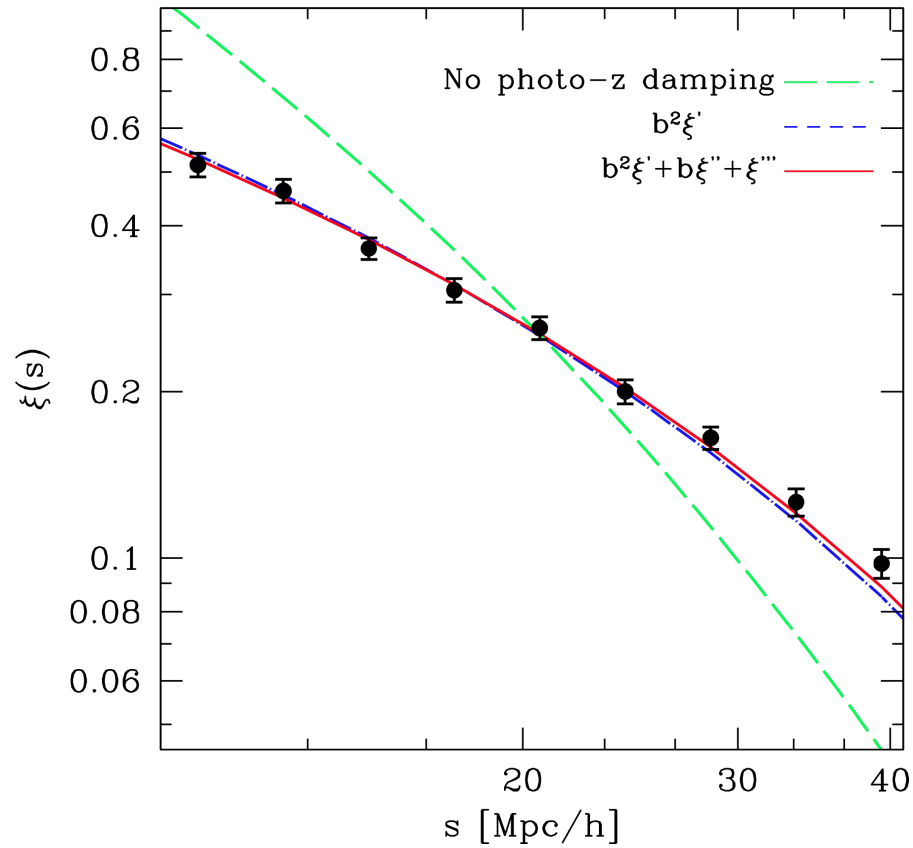
$$f_{\text{sel}}(M_{200}) = \int_{R_{L^*}^{\min}}^{R_{L^*}^{\max}} P(M_{200} | R_{L^*}) n(R_{L^*}) dR_{L^*}$$

Stacked lensing of galaxy clusters

Stacked lensing signal behind the WHL clusters in the CFHTLenS fields
[\[Sereno+2015MNRAS.449.4147S\]](#)



The redshift-space correlation function

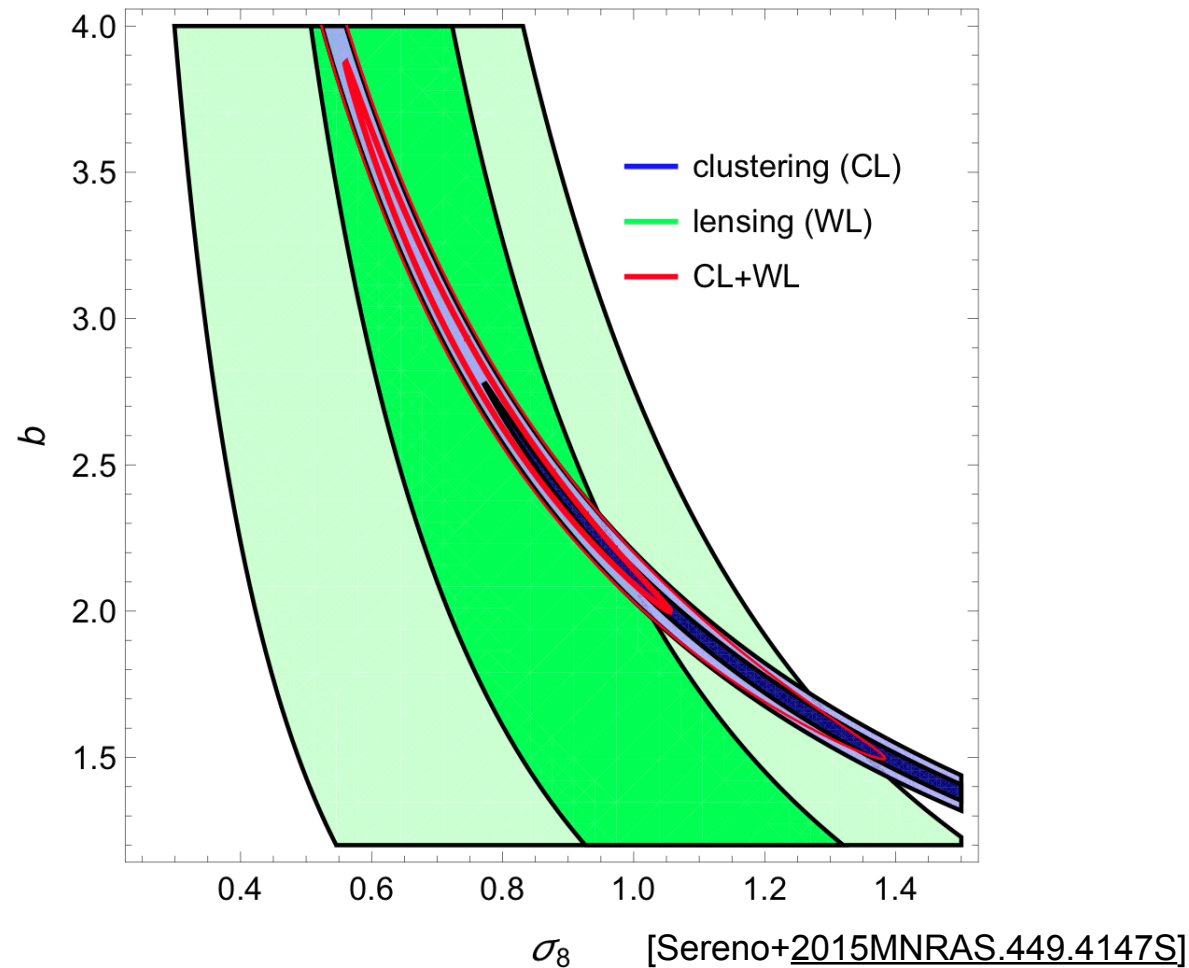


[Serenio+2015MNRAS.449.4147S]

Cosmological parameters

➤ $\sigma_8 = 0.78 \pm 0.17$

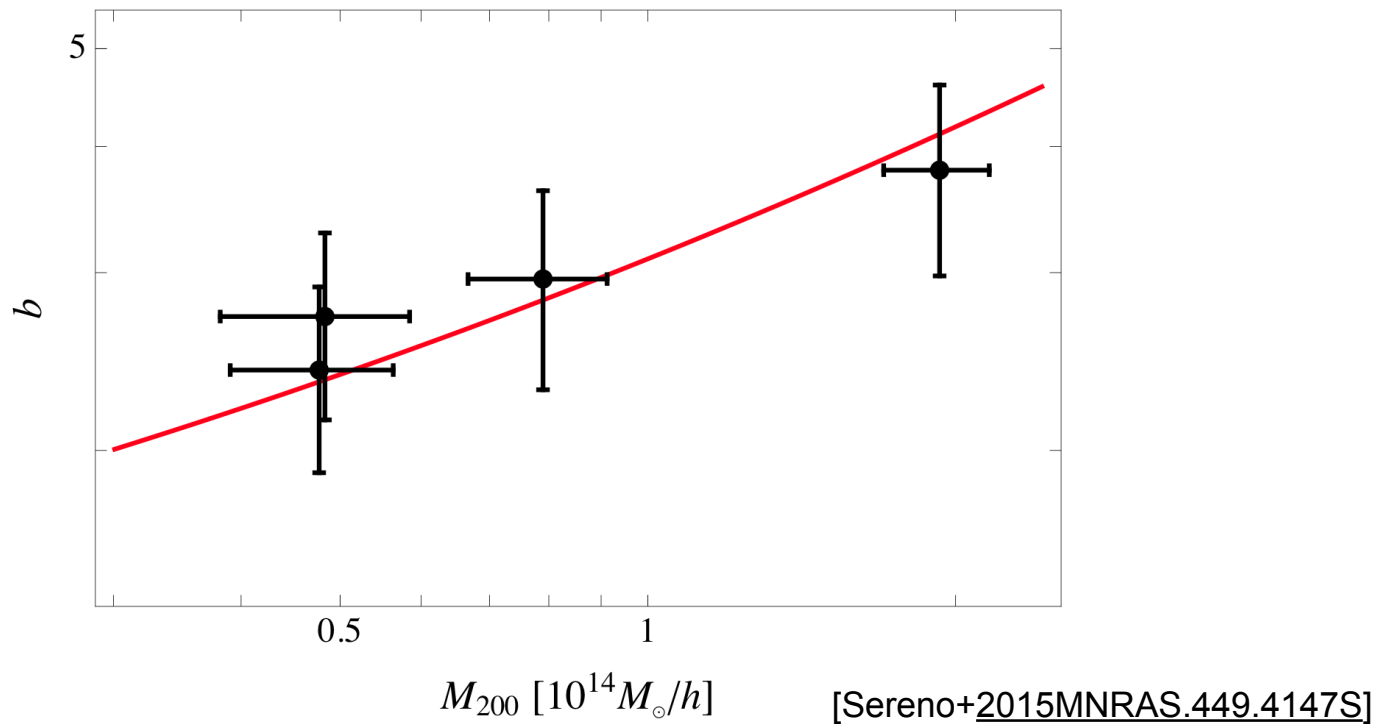
➤ $\sigma_8 = 0.80 \pm 0.10$ with priors on $b(M200)$



Halo bias

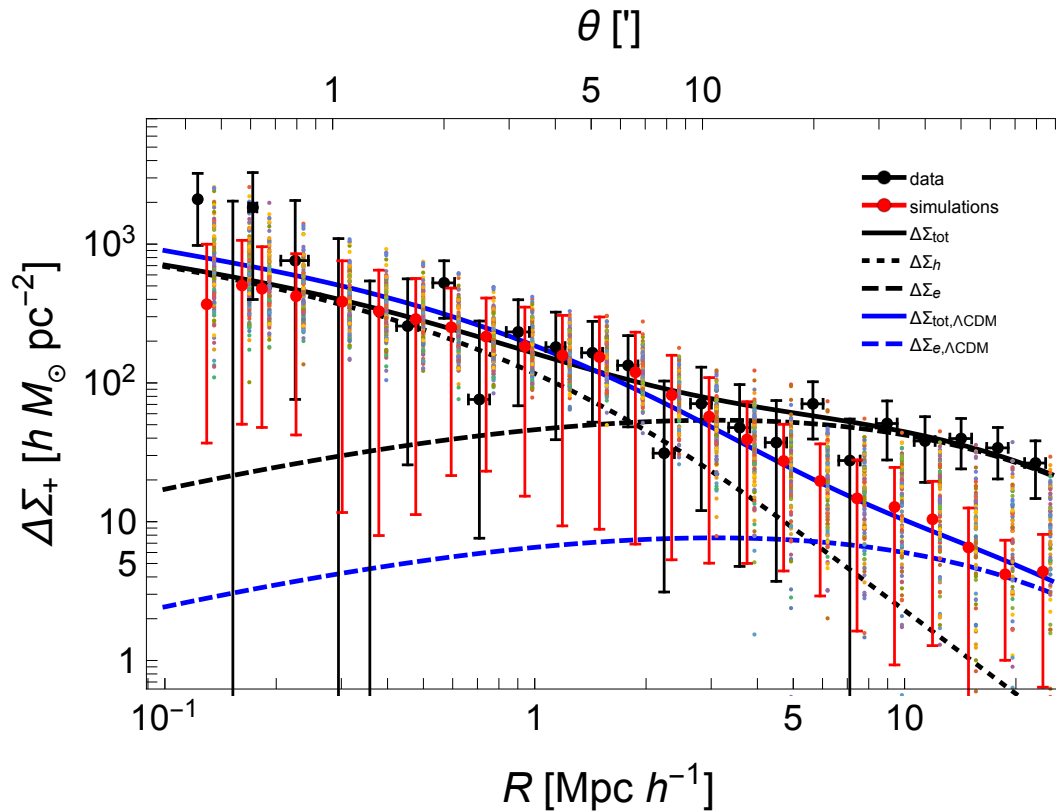
Direct measurement of the halo bias after combining with clustering of galaxy clusters

- ✓ stacked lensing can directly probe the bias as a function of mass
- ✓ close agreement with Λ CDM predictions



Detection of the matter environment

Detection of the environment bias around PSZ2 G099.86+58.45



Measurements
MOKA Simulation
Bias-halo model

[Serenio+2018NatAs...2..744S]

✓ The measured lensing signal in the range $10 < R < 25.1$ [Mpc/h] is $\Delta\Sigma_{\text{obs}} = 32.1 \pm 4.5(\text{stat.}) \pm 8.1(\text{LSS}) \pm 2.1(\text{sys.}) M_{\odot} h \text{ pc}^{-2}$.

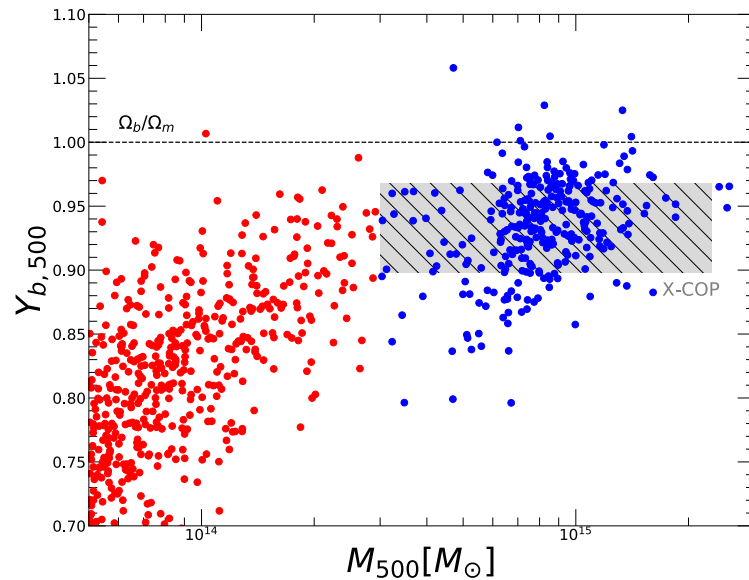
✓ The signal-to-noise ratio is $\text{SNR} \approx 3.4$

✓ The signal is ~ 5.6 times larger than expected in ΛCDM . The probability that the signal is over-estimated due to statistical or systematic uncertainties or LSS is $\sim 0.5\%$

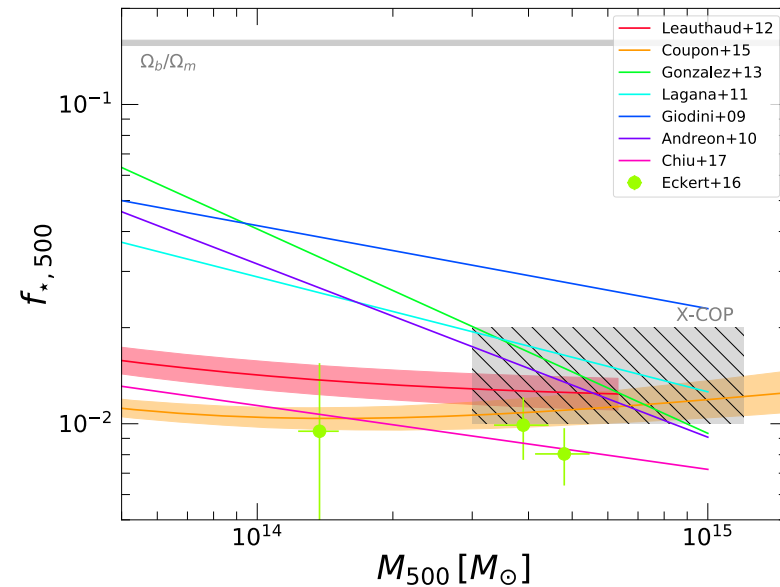
Gas fraction

Gas fractions as a proxy of the cosmo baryonic fraction

$$f_{\text{gas}}(R_{\Delta}) = \frac{M_{\text{gas}}(< R_{\Delta})}{M_{\text{tot}}(< R_{\Delta})} = Y_b \frac{\Omega_b}{\Omega_m} - f_{\text{star}}$$



Baryon depletion factor Y_b at R_{500} for The300 simulation (filled circles). Y_b flattens at $M_{500} > 3 \times 10^{14} M_{\odot}$. [Eckert+2019A&A...621A..40E]

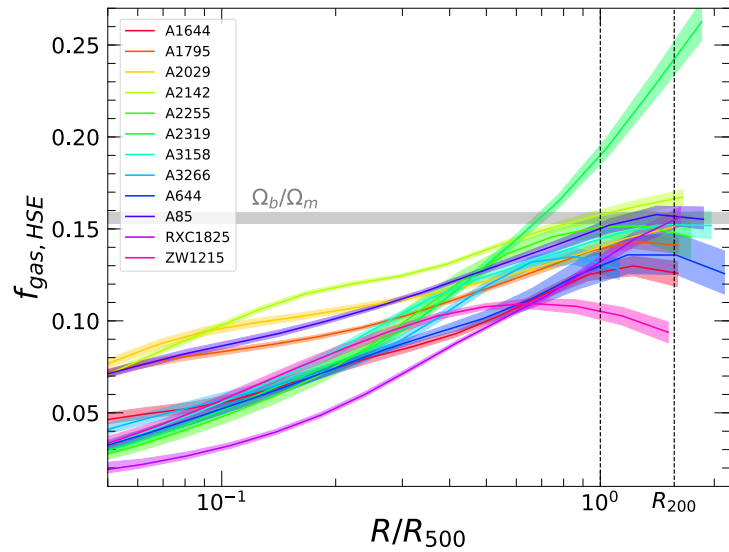


Stellar fraction within R_{500} [Eckert+2019A&A...621A..40E]

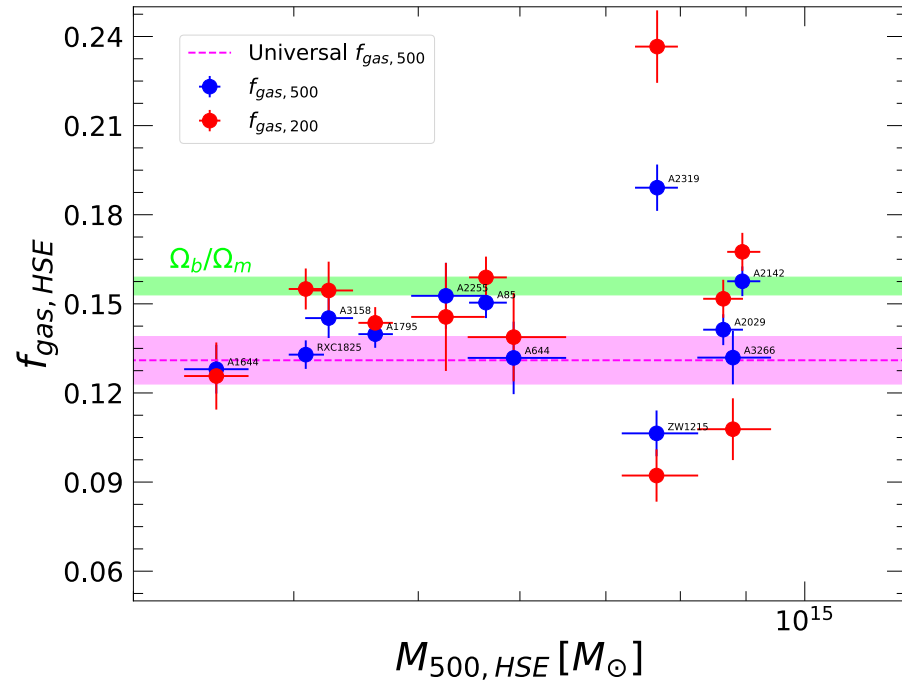
Gas fraction

XMM-Newton cluster outskirts project (X-COP) : sample of 12 SZ-Planck selected nearby clusters
 [Eckert+2019A&A...621A..40E]

The fraction value is nearly universal at r500



Hydrostatic gas fraction profiles $f_{\text{gas},HSE}(R)$ for the X-COP clusters. The gray area shows the *Planck -2015-XIII* baryon fraction [Eckert+2019A&A...621A..40E]



Hydrostatic gas fractions at $R_{500,HS E}$ (blue points) and $R_{200,HS E}$ (red points) obtained as a function of cluster mass. The dashed magenta line and shaded area represent the universal gas fraction at R_{500} . The green shaded area indicates the cosmic baryon fraction [Eckert+2019A&A...621A..40E]

Gas fraction and distances

Gas fraction at a fixed radius $R=\theta*d_A$

$$f_{\text{gas}} = \frac{M_{\text{gas}}}{M_{\text{tot}}}$$

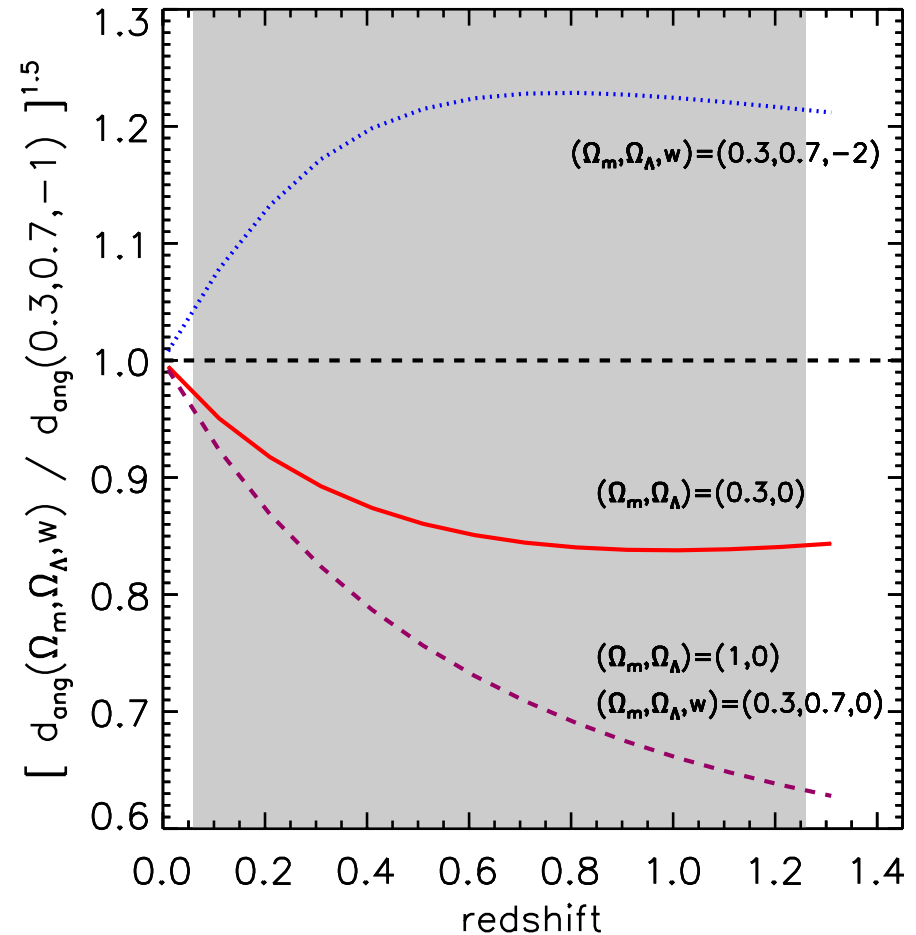
$$M_{\text{tot}} \propto T_{\text{gas}} R \propto d_A$$

$$L_X \sim n_{\text{gas}}^2 \Lambda(T_{\text{gas}}) R^3 \propto \frac{M_{\text{gas}}^2}{R^3}$$

$$S_X = \frac{L_X}{(1+z)^4 4\pi d_A^2} \propto \frac{M_{\text{gas}}^2}{d_A^5}$$

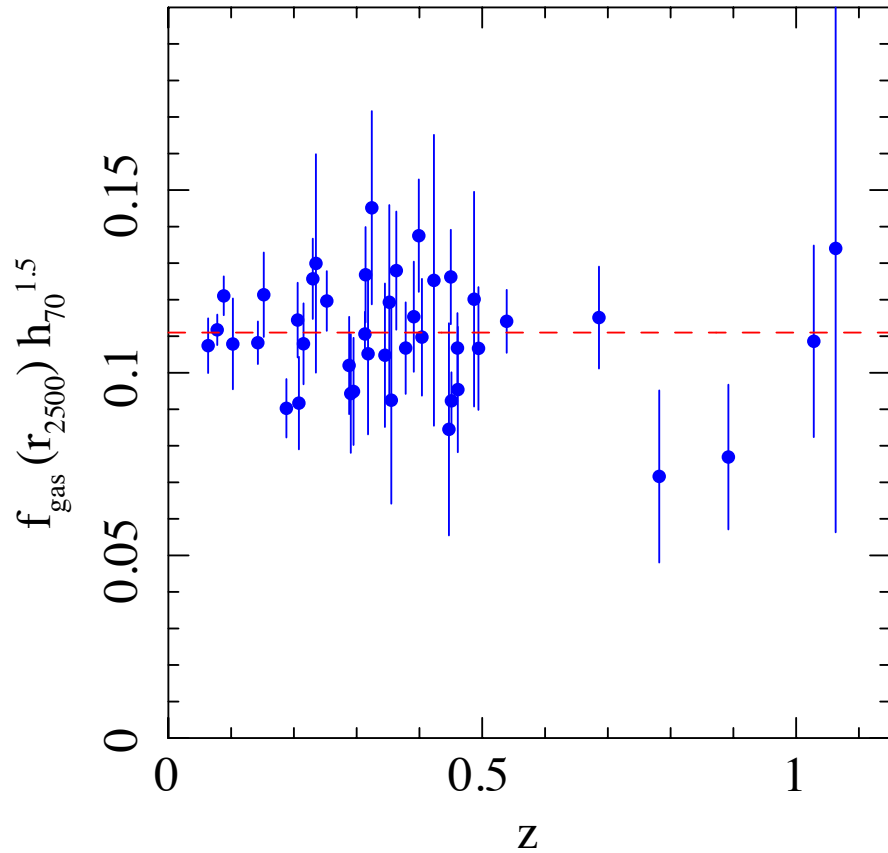
$$M_{\text{gas}} \propto d_A^{5/2}$$

$$f_{\text{gas}} = \frac{M_{\text{gas}}}{M_{\text{tot}}} \propto d_A^{3/2}$$

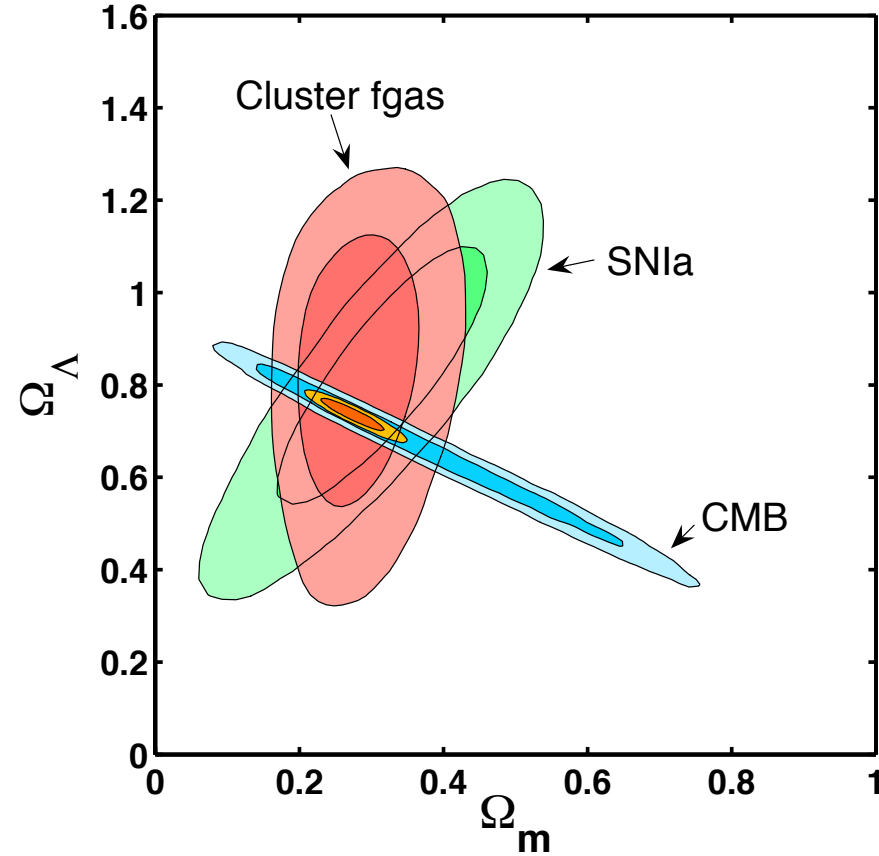


[Sensitivity of the cluster baryon fraction method to the variation of the cosmological parameters. Etti+2009A%26A...501...61E]

Gas fraction: results



$f_{\text{gas}}(z)$ measurements for relaxed clusters are compared for a flat LCDM model (consistent with the expectation of no evolution) [Allen+2011ARA%26A..49..409A]



Joint 68.3% and 95.4% confidence regions on Λ CDM models with curvature from cluster f_{gas} data at $z < 1.1$, compared to those from cosmic microwave background (CMB) data (Spergel et al. 2007) and SNIa (Davis et al. 2007). Inner, gold contours show results from the combination of these data [Allen+2011ARA%26A..49..409A]

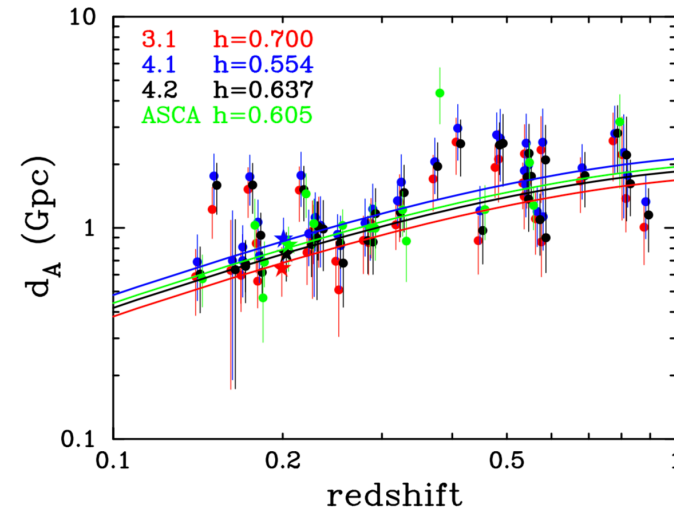
X-SZ distance

X-ray and SZ measurements can be combined to determine distances to clusters [Silk&1978ApJ...226L.103S] SZE/X-ray measurements depend differently on the ICM density

$$S_X(\Delta E) = \frac{1}{4\pi(1+z)^4} \int_{l.o.s.} n_e^2 \Lambda_{eH}(T, Z) dl \propto n_{e,0}^2 \Lambda_{eH}(T, Z) \theta_c d_A$$

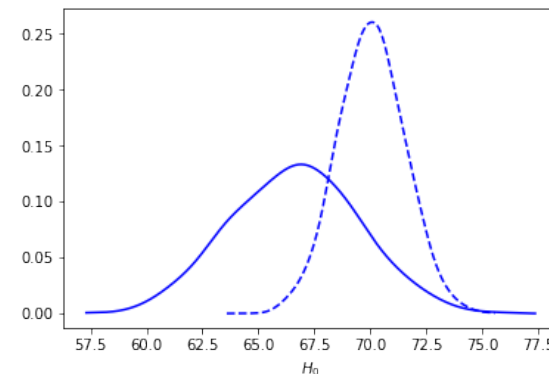
$$\Delta T_{SZ} = f_{SZ}(\nu, T) T_{CMB} \frac{\sigma_T k_B}{m_e c^2} \int_{\parallel} n_e T_e dl \propto f_{SZ} T_{gas} n_{e,0} \theta_c d_A$$

$$d_A \propto \frac{\Delta T_{SZ}}{S_X} \frac{\Lambda(T_{gas})}{(k_B T_{gas})^2 f^2(\nu, T_{gas})} \frac{1}{\theta_c}$$



Distances for different Chandra calibrations for 38 clusters. Points are slightly offset. $\Omega_m = 0.27$ and $\Omega_\Lambda = 0.73$ [Reese+2010ApJ...721..653R+19]

- ✓ independent of the extragalactic distance ladder
- ✓ do not rely on standard candles or rulers
- Galactic NH
- Cluster asphericity
- SZE point sources
- Kinetic SZE effect
- CMB anisotropy
- X-ray background
- Presence of radio halo
- X-ray absolute flux calibration (SX)
- X-ray temperature calibration (Te)
- SZE calibration



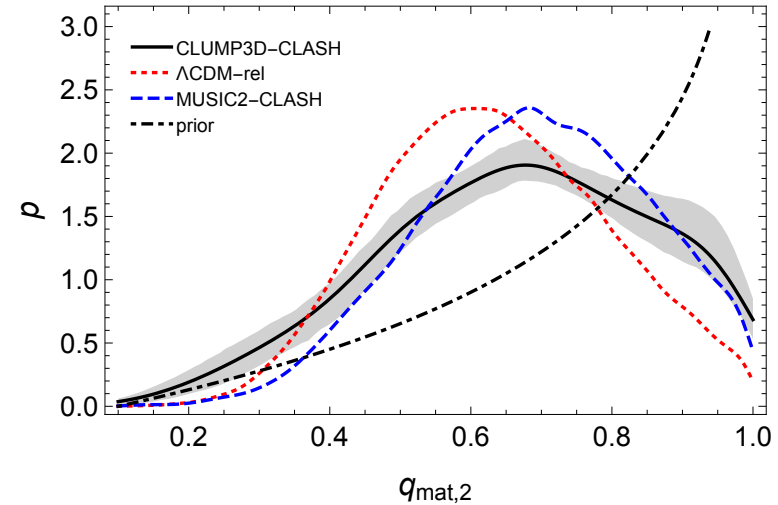
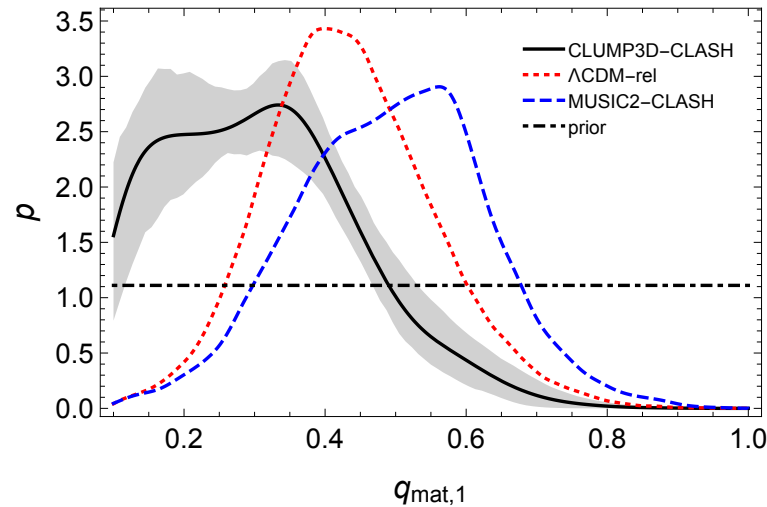
H_0 for a flat Λ CDM universe. Cluster triaxiality and clumpiness can be corrected with informed priors. Sample of 61 galaxy clusters up to $z < 0.5$ observed with *Planck* and *XMM-Newton*: $h = 0.67 \pm 0.03$. The dashed line is the value of H_0 when the bias correction is not applied. [Kozmany+2019A&A...621A..34K]

3D shape

X vs SZ. Since their different dependencies on the gas density, comparing X-ray and SZ pressures enable us to directly infer the elongation of the gas distribution if you trust H_0 measurements [deFilippis+03,MS+05]

$$e_{\parallel} = \frac{1}{D_d} \frac{\Delta T_{\text{SZ},0}^2}{\text{SB}_0} \frac{\Lambda}{T^2}$$

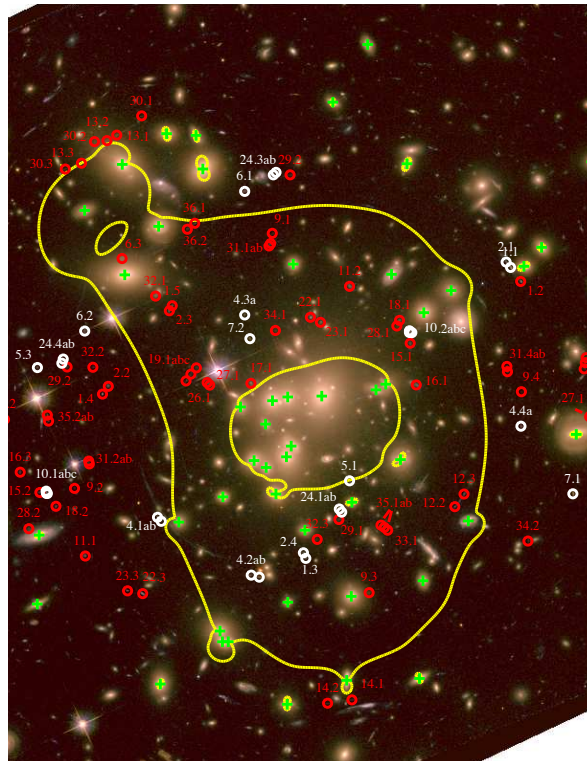
Analysis of 16 CLASH X-ray regular clusters. Geometric test to probe structure formation scenario. Shape are in line with LCDM predictions [Serenio+2018ApJ...860L...4S]



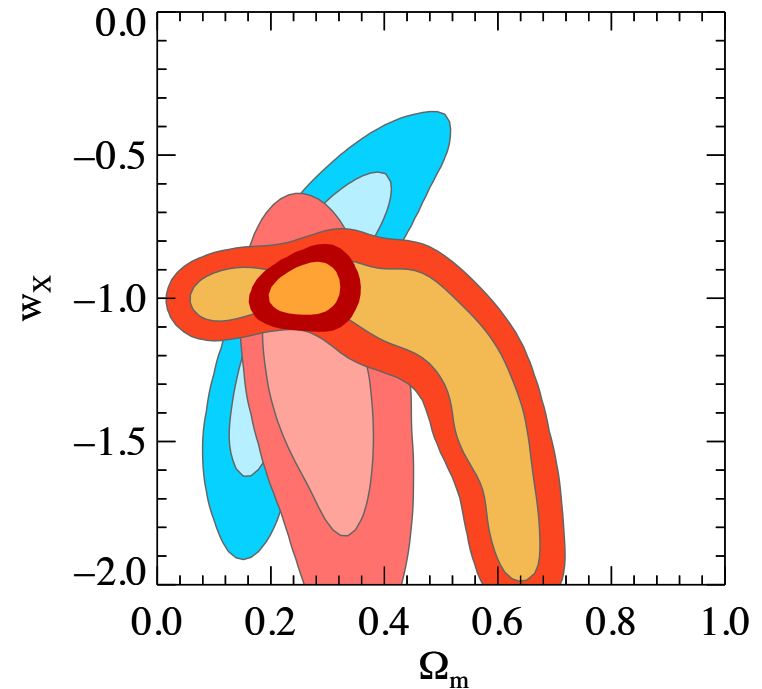
SL multiple images

Ratio of distances can be inferred from image positions. A very accurate mass modelling is required

$$D_d \frac{D_{ds}}{D_s} = \frac{4\pi G}{c^2} \frac{M_{\text{cyl}}(< \theta_E)}{\theta_E^2}$$

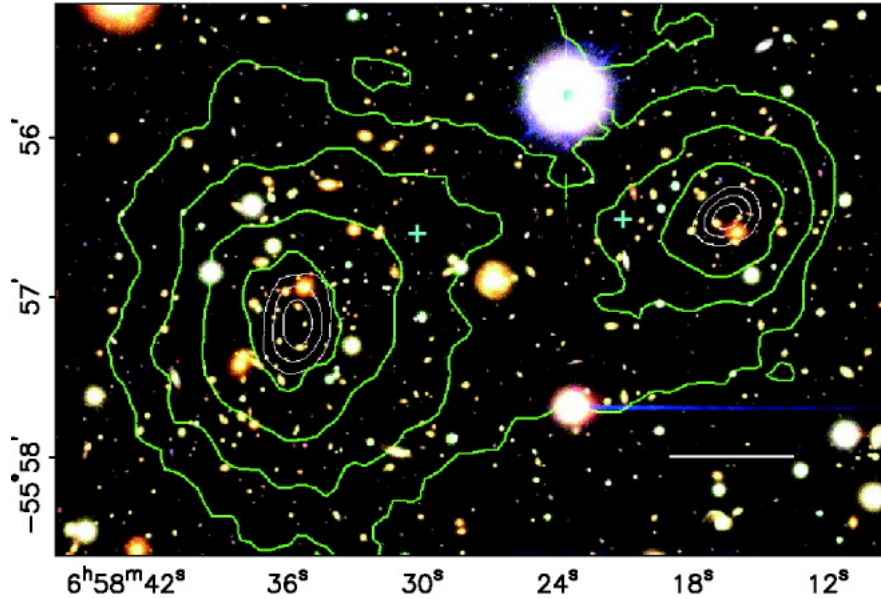


HST-ACS image of Abell 1689. The lensing mass model includes two large-scale clumps, the BCG, and 58 galaxies [green]. yellow: critical lines for a source at $z = 3$. white: 28 multiple images arising from 12 families. red: rejected images [Jullo+2010Sci...329..924J]



Results for Abell 1689. blue: WMAP5; pink: x-ray clusters; orange: cluster SL [Jullo+2010Sci...329..924J]

DM cross section



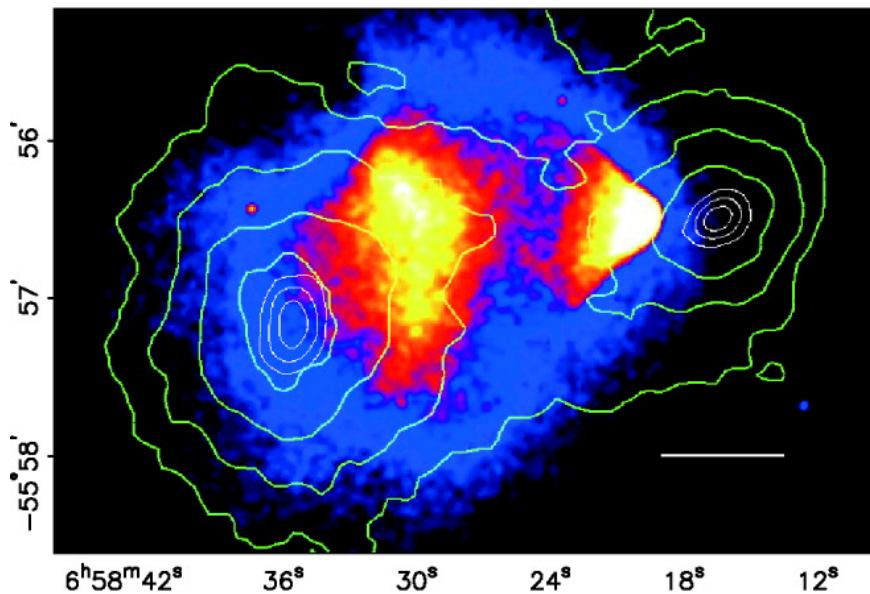
1E 0657-558, collision of two clusters
[Clowe+2004ApJ...604..596C]

There is dark matter:

- ✓ the dissipationless stellar component and the fluid-like X-ray-emitting plasma are spatially segregated
- ✓ the mass traces the distribution of galaxies
- ✓ the gravitational potential does not trace the plasma distribution

The dark matter is dissipationless:

- ✓ Spatial offset of the center of the total mass from the center of the baryonic mass peaks



References

These slides are only meant as support for the lessons. They should not be used as stand-alone material. Please consult the references in the following or cited in the text

General

Voit, G. Mark, Tracing cosmic evolution with clusters of galaxies , 2005RvMP...77..207V

Optical

Biviano, A., Galaxy systems in the optical and infrared, 2008arXiv0811.3535B

X-ray

Arnaud M. X-ray observations of clusters of galaxies, 2005bmri.conf...77A

Rosati P, Borgani S, Norman C, The Evolution of X-ray Clusters of Galaxies, 2002ARA&A..40..539R

SZE

Birkinshaw M., The Sunyaev-Zel'dovich effect, 1999PhR...310...97B

Thermodynamics

Kravtsov, Andrey V., Borgani, Stefano, Formation of Galaxy Clusters, 2012ARA&A..50..353K

GL

Bartelmann, M., Schneider, P., Weak gravitatalional lensing, 2001PhR...340..291B

Cosmology

J. A. Peacock, Cosmological Physics, 1998, Cambridge University Press

Peacock J.A. Large-scale surveys and cosmic structure, 2003astro.ph..9240P

Cosmological tests

Allen S.W., Evrard A.E., Mantz, A.B., Cosmological Parameters from Observations of Galaxy Clusters , 2011ARA&A..49..409A

Scaling relations and self-similar model

Giodini, S., Lovisari, L., Pointecouteau, E., Ettori, S., Reiprich, T. H., Hoekstra, H., Scaling Relations for Galaxy Clusters: Properties and Evolution, 2013SSRv..177..247G

The Euclid Mission



<http://www.euclid-ec.org>

- Medium-class ESA mission
- 1.2m primary
- Optical imaging
- NIR imaging
- NIR slitless spectroscopy
- Ground-based optical bands (photo-z)
- **Launch 2022**, Orbit L2
- Mission duration 7 years
- 15000 deg²
- **Cosmology**
 - **Cosmic shear**
 - **BAO & RSD**
 - **Galaxy Clusters**
 - ISW, Strong Lensing, ...
- **Legacy Science**

XMM-Heritage: Witnessing the culmination of structure formation in the Universe

- ★ 118 Planck clusters
- ★ 3Ms (largest XMM program ever)
- ★ X-ray mass profiles up to r_{500} at 15%
- ★ multi-wave length coverage

